

UC San Diego

UC San Diego Electronic Theses and Dissertations

Title

AC Electrokinetic separation and detection of nanoparticles and DNA nanoparticulates under high conductance conditions

Permalink

<https://escholarship.org/uc/item/4s1392pg>

Author

Krishnan, Rajaram

Publication Date

2010

Peer reviewed|Thesis/dissertation

UNIVERSITY OF CALIFORNIA, SAN DIEGO

**AC Electrokinetic Separation and Detection of Nanoparticles and DNA
Nanoparticulates under High Conductance Conditions**

A dissertation submitted in partial satisfaction of the requirements for the degree
of Doctor of Philosophy

in

Bioengineering

by

Rajaram Krishnan

Committee in charge:

Professor Michael J. Heller, Chair
Professor Sadik C. Esener
Professor Xiaohua Huang
Professor Mark Mercola
Professor John T. Watson

2010

©

Rajaram Krishnan, 2010

All rights reserved.

The Dissertation of Rajaram Krishnan is approved, and it is acceptable in quality and form for publication on microfilm and electronically:

Chair

University of California, San Diego

2010

DEDICATION

To Mom, Dad, Hari, and DC,
I couldn't have come this far without you guys.

We still got a long ways to go.
But now's where the fun begins...

EPIGRAPH

“The only constant is change”

- Narayan Krishnan

TABLE OF CONTENTS

SIGNATURE PAGE	iii
DEDICATION	iv
EPIGRAPH.....	v
TABLE OF CONTENTS	vi
LIST OF ABBREVIATIONS.....	x
LIST OF FIGURES.....	xi
ACKNOWLEDGEMENTS	xiii
VITA	xvii
ABSTRACT OF THE DISSERTATION	xix
Chapter 1: INTRODUCTION.....	1
1.1: Introduction.....	1
1.2: DEP as a useful tool for cancer detection	2
1.3: Background on DEP.....	3
1.4: Background on Cancer Biomarkers	7
Chapter 2: AC ELECTROKINETIC SEPARATION AND DETECTION OF DNA NANOPARTICLES IN HIGH-CONDUCTANCE SOLUTIONS	10
2.1: Introduction	10
2.2: Materials and Methods	13
2.2.1: Buffers and Conductivity Measurements	13

2.2.2: Particles, Nanoparticles and DNA Derivatization.....	14
2.2.3: DEP Microelectrode array device	17
2.2.4: Experimental Setup and Measurements.....	18
2.3: Results.....	21
2.3.1: Low conductivity DEP experiments	21
2.3.2: High conductivity experiments	24
2.4: Discussion	30
 Chapter 3: AN AC ELECTROKINETIC METHOD FOR ENHANCED DETECTION OF DNA NANOPARTICLES	 36
3.1: Introduction	36
3.2: Materials and Methods	39
3.2.1: Buffers and Conductivity Measurements	39
3.2.2: Particles, Cells, Nanoparticles and DNA Derivatization.....	39
3.2.3: High Molecular Weight (hmw) DNA	40
3.2.4: DEP microelectrode array device	41
3.2.5: Experimental Setup and Measurements.....	42
3.3: Results and Discussion	44
3.3.1: Low conductivity and Cell Experiments	44
3.3.2: Fluorescence Analysis and High Conductivity Experiments	48
3.4: Conclusions	52

Chapter 4: INTERACTION OF NANOPARTICLES AT THE DEP

MICROELECTRODE INTERFACE UNDER HIGH CONDUCTANCE

CONDITIONS.....	54
4.1: Introduction	54
4.2: Experimental Section	56
4.3: Results and Discussion	59
4.3.1: High Conductivity Experiments.....	59
4.3.2: Electrochemical effects at microelectrode surface	62
4.4: Conclusions.....	65

Chapter 5: ISOLATION AND DETECTION OF DNA NANOPARTICULATES

DIRECTLY FROM BLOOD	67
5.1: Introduction	67
5.2: Experimental	70
5.2.1: DEP Microelectrode Array and Nanoparticle Separation Process.....	70
5.2.2: Buffers, Blood Samples, Microparticles and Conductivity Measurements	73
5.2.3: High Molecular Weight (hmw) and Low Molecular Weight (lmw) DNA	73
5.2.4: Experimental Setup and Measurements.....	75
5.3: Results.....	78
5.3.1: Separation of High Molecular Weight (hmw) Single-Stranded (ss) DNA in Whole Blood.....	78

5.3.2: Separation of High Molecular Weight (hmw) Double-Stranded (ds) DNA in Buffy Coat Blood	81
5.3.3: Post-Staining and Low Molecular Weight (lmw) DNA Experiments...	83
5.4: Discussion and Conclusions	86
Chapter 6: SEPARATION OF NANOPARTICLES DIRECTLY FROM BLOOD FOR NANOMEDICINE APPLICATIONS	
6.1: Introduction	89
6.2: Materials and Methods	94
6.2.1: DEP Device	94
6.2.2: Buffy Coat Blood and Whole Blood	97
6.3: Results and Discussion	100
6.4: Conclusions	105
Chapter 7: OVERALL CONCLUSIONS AND FUTURE WORK.....	107
REFERENCES.....	108

ABBREVIATIONS

DEP.....Dielectrophoresis
AC Electrokinetics.....Alternating Current Electrokinetics
hmw DNA.....high molecular weight DNA
lmw DNA.....low molecular weight DNA
cfc hmw DNA.....cell free circulating high molecular weight DNA
PCR.....polymerase chain reaction

LIST OF FIGURES

Figure 1.1.	DEP Spectra and microelectrode array.....	5
Figure 2.1.	DEP microarray – overall view, magnified view and setup.....	16
Figure 2.2.	DEP separation at low conductivity for 60nm DNA nanoparticles..	20
Figure 2.3.	DEP separation of 200nm nanoparticles in high conductance.....	23
Figure 2.4.	3D Fluorescence peak images for 60nm DNA nanoparticles.....	27
Figure 2.5.	Red and 3D Fluorescence images of 60nm particles in 1xPBS....	28
Figure 2.6.	Fluorescence intensity graphs versus time.....	29
Figure 2.7.	Graph of real part of $K(w)$ versus conductance.....	33
Figure 3.1.	Epifluorescent microscope and setup.....	38
Figure 3.2.	DEP separation of 40nm red nanoparticles from Jurkat cells.....	43
Figure 3.3.	DEP separation in 0.01x TBE of 40 and 200nm nanoparticles.....	46
Figure 3.4.	Fluorescence analysis using polar coordinates of the electrode...	47
Figure 3.5.	Area of concentration of 40nm and 200nm nanoparticles.....	50
Figure 3.6.	DEP separation of hmw DNA and 10 μ m spheres in 1x TBE.....	51
Figure 4.1.	DEP Experimental setup pictures.....	55
Figure 4.2.	DEP Separation of 200nm nanoparticles with and without gels...	58
Figure 4.3.	Microscope and SEM images of microelectrodes in 1xPBS.....	61
Figure 4.4.	SEM images of control and activated electrodes in 1xPBS.....	64
Figure 5.1.	Microarray device and flow diagram for DNA separation.....	72
Figure 5.2.	Separation and detection of hmw ss DNA in whole blood.....	77
Figure 5.3.	Separation and detection of hmw ds DNA in whole blood.....	80

Figure 5.4.	Post staining of hmw ss DNA after DEP.....	82
Figure 5.5.	DEP of fluorescent low molecular weight DNA.....	85
Figure 6.1.	Microarray device and flow diagram.....	92
Figure 6.2.	Separation and detection 40nm nanoparticles in buffy coat blood.....	93
Figure 6.3.	Separation and detection 40nm nanoparticles in whole blood.....	96
Figure 6.4.	Detection levels of nanoparticles in buffy coat blood.....	99
Figure 6.5.	Detection levels for red 40nm nanoparticles in 1xTBE buffer.....	104

ACKNOWLEDGEMENTS

First and foremost, I would like to acknowledge Professor Michael J. Heller for his support as chair of my committee. His incredible vision and amazing insight into the intricacies of Dielectrophoresis and AC Electrokinetics as well as his mentorship have been invaluable. It has been a privilege to work with a true pioneer with far reaching ideas for early cancer detection. It is my hope that future lab students achieve the same appreciation for his genius that I did during my dissertation research under his guidance.

For Dr. Esener and Dr. Watson, it has been a true joy to work with you and bounce ideas off of you as well as follow your advice during my dissertation. Your ideas and accomplishments have been a true inspiration during my work at UCSD.

For Dr. Huang, I would like to express my most sincere gratitude for your help during my dissertation and for challenging my ideas and methodologies while also encouraging me to strive ever higher to achieve my goals.

For Dr. Mercola, I owe you a debt of gratitude for allowing me to work with you and in your lab at Burnham even though I walked out of the blue and into your office one day with merely an idea for using AC Electrokinetics for heart disease research. Your support allowed me to learn so much more than I ever could have by focusing on cancer alone and expanded my worldview and knowledge base.

Financial Support from UCSD during my first two years and the NIH Center of Excellence of Nanotechnology for Treatment, Understanding and Monitoring of Cancer (U54 CA119335) for my last four years is gratefully acknowledged.

To Ben Sullivan, one of my coworkers and mentors, thanks for the invaluable insight into our various discussion and theories. You are truly the smartest man I've ever met, and an incredible compendium of knowledge. I still am better at movie trivia though. It was a privilege to work with you and learn from you, my only regret is that those enjoyable days didn't last longer.

To Dietrich Dehlinger, for your unique perspective and many hours of discussion on AC Electrokinetics, I am forever grateful. Dr. Greg Gemmen and Dr. Jennifer Marciniak, thank you for your contributions and your help and advice. Alex Hsiao, Robert Mifflin, Sara Zare, Dr. Stuart Ibsen, Lucas Kumosa, Adam Strobl, Dr. Adam Wright, Dr. Gene Hsiao, Dr. Karen Christman, Dr. Jennifer Singleyn, Jennifer Young, Jennifer Park, Eun Hee Han, Terrell Green, Dr. Peter Chen, Dr. Adam Feist, Nicole Justis Truitt, Dr. Shankar Subramanian, Dr. Jeff Hasty, Dr. Michael Ferry, Lili Peng, Martin Kolnik, Ying-Ja Chen, Eric Roller, Aric Joneja, Kristopher Barbee, Sergio Sandoval, Thomas Cohen, Alice Kiselyuk, Jason Steiner, Emmanuel Ruidiaz, Iveta Kalcheva, Dr. Bradley Messmer, Dr. Stephen Flaim, Dr. Andrew Kummel, Edward R. Truitt III Esq., Dr. Paul Swanson, Dr. Sangeeta Bhatia, Dr. Shu Chien, Dr. YC Fung, Dr. Schmid-Schoenbein and to all the graduate students from my year (2004).

To my fellow workers at the Burnham Institute for Medical Research (aka. Sanford Burnham Medical Research Institute): Karen April Wei, Joaquim Teixeira, Dr. Masanao Tsuda, Tina Kiffer, Dr. Ramon Diaz-Trelles, Denise Carroll, Dr. Behrad Azimi and Dr. Ramses Agustin, keep up the good work.

To my muse: you are my inspiration, my love, my joy and the reason I wake up in the morning to work so hard. You give me hope, and strength as well as incredible ideas in brand new areas, which I would have never thought of if not for you. I can only humbly acknowledge your profound affect on my life and way of thinking with mere words of gratitude. I hope they suffice. I will always be there for you no matter what.

To my best friends David Charlot and Roy Lefkowitz, thank you immensely for your feedback and for your hard work. We had a tremendous amount of fun but there's lots more to come.

To my grandmother, your death opened my eyes to the weaknesses in heart disease diagnostics. I will strive to come up with a solution.

To Kian Win Ong and Alicia Gamez, thanks for being the best roommates, I could ever hope for, and for listening to all my shenanigans. To Sheelo, thanks for being such an awesome dog.

To the Krishnan family: mom, dad and hari, much love and thanks.

Chapter 2, in full, is a reprint of the material as it appears in Electrophoresis: Krishnan R, Sullivan BD, Mifflin RL, Esener SC, Heller MJ. Alternating current electrokinetic separation and detection of DNA nanoparticles

in high-conductance solutions. *Electrophoresis* 2008, 29(9): 1765-1774. The dissertation author was the primary investigator and author of this paper.

Chapter 3, in full, is a reprint of the material as it appears in *Journal of Biophotonics*: Krishnan R, Heller MJ. An AC electrokinetic method for enhanced detection of DNA nanoparticles. *J. Biophoton.* 2009, 2(4): 253-261. The dissertation author was the primary investigator and author of this paper.

Chapter 4, in full, is a reprint of the material as it appears in *Electrochemistry Communications*: Krishnan R, Dehlinger DA, Gemmen GJ, Mifflin RL, Esener SC, Heller MJ. Interaction of nanoparticles at the DEP microelectrode interface under high conductance conditions. *Electrochem. Comm.* 2009, 11(8): 1661-1666. The dissertation author was the primary investigator and author of this paper.

Chapter 5, in full, is currently being prepared for submission for publication of the material: Krishnan R, Marciniak JY, Sonnenberg AV, Carson DA, Esener SC, Heller MJ. Isolation and detection of DNA nanoparticulates directly from blood. The dissertation author was the primary investigator and author of this paper.

Chapter 6, in full, is currently being prepared for submission for publication of the material: Krishnan R, Marciniak JY, Sonnenberg AV, Carson DA, Esener SC, Heller MJ. Separation of nanoparticles directly from blood for Nanomedicine Applications. The dissertation author was the primary investigator and author of this paper.

VITA

2000	Diploma, Leland High School, San Jose, CA
2004	Bachelor of Science Electrical Engineering, Cum Laude, University of California, Los Angeles
2004-2006	Teaching Assistant, Department of Bioengineering, University of California, San Diego
2006	Master of Science Bioengineering, University of California, San Diego
2006-Present	Chief Executive Officer and President, Biological Dynamics, Inc.
2010	Doctor of Philosophy, University of California, San Diego

PUBLICATIONS

Krishnan R, Sullivan BD, Mifflin RL, Esener SC, Heller MJ. Alternating current electrokinetic separation and detection of DNA nanoparticles in high-conductance solutions. *Electrophoresis* 2008, 29(9), 2008: 1765-1774.

Krishnan R, Heller MJ. An AC electrokinetic method for enhanced detection of DNA nanoparticles. *J. Biophoton.* 2009, 2(4): 253-261.

Krishnan R, Dehlinger DA, Gemmen GJ, Mifflin RL, Esener SC, Heller MJ. Interaction of nanoparticles at the DEP microelectrode interface under high conductance conditions. *Electrochem. Comm.* 2009, 11(8): 1661-1666.

PATENTS

PCT/US09/039565, Ex-Vivo System for Separation, Isolation of Cells, Nanoparticles, Biomarkers, ((Lab-On-A-Chip, Point of Care Systems and Sample to Answer Systems) – Patent Pending

ABSTRACTS

Heller MJ, Sullivan B, Krishnan R. DEP system for cancer cell, DNA nanoparticulate and therapeutic nanoparticle detection. *Nanomedicine*, 2007, 3(4): 337-338.

Heller MJ, Krishnan R, Sullivan B, Mifflin R, Esener S. Electrokinetic Separation and Detection of DNA Nanoparticles and Cancer BioMarkers. *NSTI*, 2008.

AWARDS

- | | |
|------|--|
| 2009 | 1 st Place Poster All-Grad Symposium |
| 2009 | 1 st Place Business Plan Competition \$80,000 UCSD Entrepreneurship Challenge |
| 2009 | 1 st Place Poster Bioengineering Symposium |
| 2009 | 1 st Place Podium Award UC Systemwide Symposium |
| 2009 | Winner of Best Pitch award at 2009 3 rd annual Tech Coast Angel QuickPitch Competition |
| 2009 | Grand Prize Poster Jacobs School of Engineering Exposition |
| 2009 | 1 st Place Poster Nanoengineering Jacobs School of Engineering Exposition |
| 2009 | Science and Engineering Library Award for Best use of Literature Jacobs School of Engineering Exposition |
| 2009 | Finalist DFJ-Cisco \$250K Global Business Plan Challenge |
| 2008 | 2 nd Place Poster Bioengineering Symposium |
| 2008 | 1 st Place Poster All-Grad Symposium |
| 2008 | 3 rd Place Podium Award UC Systemwide Symposium |

FIELDS OF STUDY

Major Field: Engineering (Bioengineering)

Studies in Biomedical Engineering
Professor Carlo Montemagno, University of California, Los Angeles

ABSTRACT OF THE DISSERTATION

AC Electrokinetic Separation and Detection of Nanoparticles and DNA
Nanoparticulates under High Conductance Conditions

by

Rajaram Krishnan

Doctor of Philosophy in Bioengineering

University of California, San Diego, 2010

Professor Michael J. Heller, Chair

In biomedical research and diagnostics, it is a significant challenge to directly isolate and identify rare cells and potential biomarkers in blood, plasma and other clinical samples. Additionally, the advent of bio-nanotechnology is leading to numerous drug delivery approaches that involve encapsulation of drugs and imaging agents within nanoparticles, which now will also have to be identified and separated from blood and plasma. AC electrokinetic techniques

such as dielectrophoresis (DEP) offer a particularly attractive mechanism for the separation of cells and nanoparticles. Unfortunately, present DEP techniques require the dilution of blood/plasma, thus making the technology less suitable for clinical sample preparation. The current dissertation explores methods and techniques of overcoming the high conductivity barrier in AC Electrokinetics to isolate nanoparticles. It further explores the various applications of isolating nanoparticles from complex physiological solutions. Using array devices with microelectrodes over-coated with porous hydrogel layers, AC electric field conditions have been found which allow the separation of DNA nanoparticles to be achieved under high conductance (ionic strength) conditions. At AC frequencies in 3000Hz to 10,000Hz range and 10 volts peak-to-peak, the separation of 10 micron polystyrene particles into low field regions, and 60nm DNA derivatized nanoparticles and 200nm nanoparticles into high field regions was carried out in 149mM 1xPBS buffer (1.68S/m). Furthermore, SYBR-Green fluorescent-stained hmw-DNA was separated from whole undiluted blood, at a level of <260ng/ml. While this DEP process concentrates hmw-DNA (>10kb) in high-field areas and cells into the low-field areas, very low molecular weight DNA <100bp and small protein molecules are only minimally affected by the process. These results may allow AC electrokinetic systems to now be developed, which can be used as seamless sample-to-answer systems for point-of-care diagnostics based on detection of early disease biomarkers directly from whole blood.

Chapter 1: INTRODUCTION

1.1 Introduction

In cancer research and clinical diagnostics it is a significant challenge to separate and identify exfoliated rare cancer cells and low levels of clinically relevant biomarkers (DNA, RNA, antibodies, other proteins) from complex samples like blood, plasma, serum, saliva and urine [1] Additionally, the advent of bionanotechnology is leading to numerous drug delivery approaches that involve encapsulation of drugs and imaging agents within nanovesicles and nanoparticles, which may also need to be identified and/or separated from blood. A variety of physical and electronic techniques are now used for sample preparation and the isolation of specific cells, nanovesicles and biomolecules from complex samples like blood and plasma. These include centrifugation, gel filtration, affinity binding, magnetic bead separation, electrophoresis and various combinations incorporated into lab-on-a-chip, microfluidic devices and sample to answer systems, as well as flow cytometry (FACS) cell sorting. More classical cell separations of whole blood have been used to perform complete blood counts (CBC) [2], to isolate metastasizing cancer cells [3], to identify cell free circulating DNA for the purposes of cancer detection [4-13], as well as isolate high molecular DNA fragments to monitor chemotherapy effectiveness [14]. However such current separation methods are largely constrained by the amount of blood required [15-16], sample preparation time, significant loss of analyte

during preparation steps, inefficient rare cell separation efficiency as well as low throughput. Many of these conventional techniques (or combinations) are relatively time consuming, expensive and often lead to significant loss of the desired analyte [17-19]. These procedures may also cause considerable degradation of the sample. Additionally, rare cell and biomarker detection may also be limited by sample size; i.e., only a relatively small amount of blood may be drawn from very ill patients, the elderly and infants. Thus, sample preparation processes that are inefficient or require high dilution of the original sample often fail or are unreliable for isolating cells and other disease related markers at lower concentration ranges. This in particular is a problem for early detection of cancer and for residual disease monitoring.

1.2 DEP as a useful tool for cancer detection

Alternating current electrokinetic techniques which involve the use of AC fields to manipulate particles offers some attractive advantages for the separation of cells [20-23], high molecular weight DNA and protein biomarkers [24-27] and ultimately for drug delivery nanovesicles [28]. In particular is the fact that the analytes (cells, DNA, nanoparticles, etc.) do not have to be labeled during the separation process i.e., at specific DEP AC frequencies the entities are directed and isolated at known locations on device, and labeling for final identification or quantification can be carried out after the separation process. While DEP techniques have been established for separating cancer and other cells from

blood, they require dilution and low conductivity conditions, i.e. 1-500 mS/m [21-23], whereas whole blood has conductivity of 108 mS/m [29]. DEP methods for isolating DNA also exist, but require polynomial or castellated design electrodes, low ionic strength conditions and do work well for cells and larger entities [30-32]. In general electrokinetic techniques can be broken down into three distinct phenomena: 1) AC electroosmosis, which is surface fluid flow due to the surface charge on the electrode; 2) Electrothermal flow, which is bulk flow in solution due to thermal gradients produced by the electric fields; and 3) Dielectrophoresis (DEP), which is an induced motion of particles produced by the dielectric differences between the particles and media in an AC electric field [33]. In particular, the use of dielectrophoresis (DEP) to separate cells has long been proposed as a noninvasive method for extracting pathogenic, cancer, or stem cells from a complex biological sample [20-23].

1.3 Background on DEP

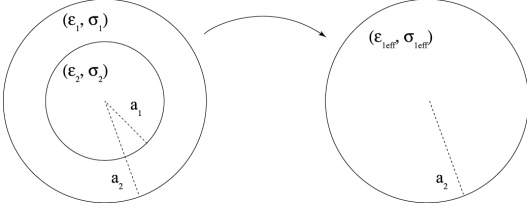
Dielectrophoretic forces are well described by the following equation:

$$F_{DEP} = 4\pi a^3 \epsilon_0 \epsilon_c^* \operatorname{Re}[f_{CM}] \nabla E_{RMS}^2, \text{ (eq.1), where: } f_{CM} = \left(\frac{\epsilon_p^* - \epsilon_c^*}{\epsilon_p^* + 2\epsilon_c^*} \right), \text{ and: } \epsilon^* = \epsilon - j \frac{\sigma}{f}$$

(eq.1)

where a is the particle radius, ϵ_c is the permittivity of the medium, $\epsilon_0 = 8.85 \times 10^{-12}$ F/m, E is the electric field, ϵ_p^* is the complex permittivity of the particle and ϵ_c^* is the complex permittivity of the medium. ϵ is the permittivity, σ is the conductivity

and f is the frequency of the applied AC field. Dielectrophoresis works on a simple principle whereby microscopic particulates travel to either the high field or low field region in solution in a non-uniform AC electric field based off of their polarization in relation to that of the media. As can be seen, dielectrophoresis relies heavily on the real part of the Clausius Mossoti factor [f_{CM}] as well as the radius of the particle, when separating two sets of particles, because the medium conductivity and the electric field will be constant for all. [53]. Using a spherical shell model [4,54] we can express a “cell-like” entity with a lipid bilayer outer ring as shown in Eq. 2. Replacing the particle permittivity with ϵ_{1eff} in f_{CM} , gives the characteristic Clausius-Mosotti curve in Figure 1.1.

$$\epsilon_{1eff} = \frac{\left(\frac{a_2}{a_1}\right)^3 + \frac{(\epsilon_1^* - \epsilon_2^*)}{(\epsilon_1^* + 2\epsilon_2^*)}}{\left(\frac{a_2}{a_1}\right)^3 - \frac{(\epsilon_1^* - \epsilon_2^*)}{(\epsilon_1^* + 2\epsilon_2^*)}}$$


(Eq. 2)

DEP separation relies upon the fact that different cell types cross over the 0 line at different AC frequencies. By setting the applied field to oscillate between these crossover points, cell types with positive f_{CM} will go toward the high field region (positive DEP), and others will go towards the low field region (negative DEP). Given the gross (sometimes orders of magnitude) difference between crossover frequencies of differing cell types, i.e., between *E. Coli* and lymphocytes, DEP is able to readily distinguish between the species.

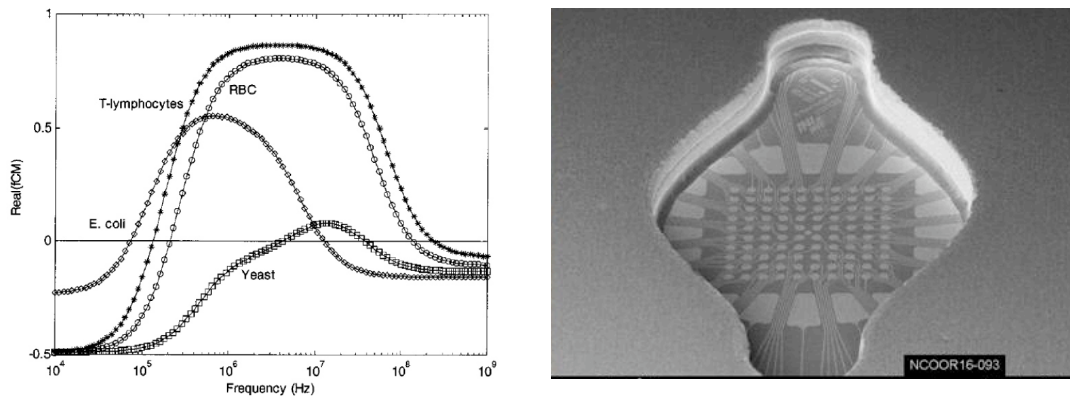


Figure 1.1. (left) shows the DEP spectra for 4 different kinds of cells, E. Coli, Yeast, red blood cells and lymphocytes. (right) 100 site microelectrode array (80 um micron electrodes) on which DEP is performed.

In the case of closely related cells, however, crossover frequencies converge. Traditional dielectrophoretic separations then become susceptible to random variations within subpopulations, where these variations may supersede the mean differences between phenotypes. In keeping with the classification terminology, dielectrophoretic crossover separation would therefore correspond to a single frequency.

It is important to note that most traditional DEP devices have a separation efficiency of roughly around 1 in a 100-1000 cells [20-23]. While higher ratios are sometimes claimed, generally the process does not translate to clinical relevancy, and it is always carried out on a significantly diluted or processed sample. In almost all cases, efficient DEP separations in terms of speed and control of selectivity have to be carried out at relatively low ionic strength (conductance $<10-100\text{mS/m}$) [20-23, 33]. More specifically, the ability to isolate certain desired entities such as DNA biomarkers or nanoparticles in the DEP high field regions (at the electrodes) becomes more difficult as the ionic strength increases and the conductance becomes greater than 10 mS/m . Thus, biological samples such as blood that have ionic strengths in the $100-200\text{ mM}$ range must be diluted and/or processed before DEP separations can be carried out. This alone often limits the usefulness of DEP for clinical diagnostics involving the detection of rare cells or low numbers of biomarkers. In cases where a sample (one ml blood) has to be diluted 100 to 1000 fold, this now means that a very large sample volume must be processed which can be very time consuming. If

cells are first concentrated by physical mechanisms such as centrifugation or filtration and then diluted into low conductance buffers, these processes are not only time consuming, but also costly and cause considerable perturbation to the sample.

1.4 Background on Cancer Biomarkers

The key to early screening cancer diagnostics is the creation of a low cost system that can provide immediate prognostic and diagnostic information on cancer through detection and analysis of cell-free circulating high molecular weight (CFC-HMW) DNA. Early detection (during stage 1) and treatment of cancer can significantly reduce morbidity and mortality for even the most lethal types of cancer. Tumor biomarkers currently used for the management of cancer are most often proteins secreted by the tumor, such as CA-125 [34] and prostate specific antigen [35], or cell surface receptors that can predict response to targeted treatments such as HER2 for breast cancer [36]. Unfortunately, current tumor markers lack sufficient sensitivity and specificity for early disease diagnosis. CFC-HMW DNA in blood may provide enhanced specificity and sensitivity [37] for early detection of malignant diseases. CFC-HMW DNA based biomarkers may be a far more attractive option than either tumor sample based biomarkers, which require biopsies from tumors that are often inaccessible, or RNA and protein based biomarkers, which are far more unstable and degrade rapidly at room temperature [38]. Some low molecular weight cell free circulating

DNA is found in small amounts in the plasma of healthy individuals. However, there can be more than four times the amount of CFC-HMW DNA in the plasma of patients with cancer. Early studies have also indicated the existence of higher levels of circulating DNA in the serum of patients with metastatic disease compared to localized disease [39]. Moreover, there is a correlation between circulating DNA levels and prognosis in a number of tumor types [40]. Occurrence of alterations in DNA, and increase in the overall level of DNA, is not restricted to any particular tumor site, type or grade and has been proven for a variety of hematological cancers (AML, ALL, myeloma, etc.) as well as for solid tumors (in the lung, bladder, liver, cervix, esophagus) [41]. The source of this DNA remains unknown, though it is thought to be released from either malignant circulating cancer cell lysis or necrotic cell death [38]. Most of the CFC-HMW DNA is double stranded and in the form of a nucleoprotein complex [42]. Therefore, CFC-HMW DNA has a more three-dimensional shape and is of relatively high molecular weight. Depending on the study, the amount of cell-free DNA in healthy patients varies greatly from 1ng/mL to ~57 ng/mL [37,41]. The amount of cell-free DNA in cancer patients also varied from 75ng/mL to >100 ng/mL [37,41]. The reason for the large variations is very likely due to the highly involved protocols used for blood processing, and the time between blood drawing and the DNA separation and analysis. These findings indicate that rapid processing of plasma or serum is critical before storage at -20°C or lower [42]. This indicates the absolute necessity of performing diagnostics as quickly as possible on the sample before natural degradation of the cells in the blood make

subsequent genotyping of the DNA inaccurate. The different protocols for extraction of the DNA include phenol/chloroform or using commercial kits based on ion exchange binding of DNA, which can also produce varying results [43] and can lead to a loss of 65% or more of the DNA isolated from blood [44].

Chapter 2: AC ELECTROKINETIC SEPARATION AND DETECTION OF DNA NANOPARTICLES IN HIGH CONDUCTANCE SOLUTIONS

Reprinted from: Electrophoresis (2008)

2.1 Introduction

In clinical diagnostics and many areas of biomedical research it is both important and frequently a challenge to separate and identify rare cells (cancer), low numbers of bacteria and virus; low concentrations of DNA biomarkers, antibodies and other entities in complex samples like blood [1], plasma [2], serum [3], saliva [4] and urine [5]. Additionally, the advent of bionanotechnology is leading to numerous drug delivery approaches that involve encapsulation of drugs and imaging agents within nanovesicles and nanoparticles [6]. Thus, it will now also be important to identify and monitor residual nanovesicles and nanoparticles that remain in the blood.

A variety of physical, electronic and biological methods and techniques can be used for the isolation of cells, biomarkers and nanoparticles from complex samples like blood. These include centrifugation, gel filtration, affinity binding, magnetic beads, electrophoresis, flow cytometry and various combinations thereof incorporated into lab-on-a-chip, microfluidic devices and sample to answer systems [7,8]. Nevertheless, many of these techniques still remain relatively time consuming processes that are not without problems and limitations. Alternating current electrokinetic techniques which involve the use of AC fields to manipulate particles offers a particularly attractive mechanism for

rapid separation and analysis of cells [9-11], biomarkers such as cell free circulating high molecular weight DNA [12-15] and proteins [16], and ultimately drug delivery nanoparticles. These techniques can be broken down into three distinct phenomena: 1) AC Electroosmosis, which is surface fluid flow due to the surface charge on the electrode; 2) Electrothermal flow, which is bulk flow in solution due to thermal gradients produced by the electric fields; and 3) Dielectrophoresis (DEP), which is an induced motion of particles produced by the dielectric differences between the particles and media in an AC electric field [17]. For spherical particles, movement to the high or low field regions of the electrodes is given by [18]:

$$\text{Re}(K(\omega)) = \text{Re}((\epsilon_p^* - \epsilon_m^*)/(\epsilon_p^* + 2\epsilon_m^*)) \quad (1)$$

where ϵ_p^* and ϵ_m^* are the complex dielectric permittivities of the particle and medium respectively, defined by $\epsilon^* = \epsilon - j\sigma/\omega$, where $j^2 = -1$, ϵ is the dielectric constant and σ is the conductivity. If a particle has a positive $\text{Re}(K(\omega))$, it will migrate to the high field regions, and if it has a negative $\text{Re}(K(\omega))$, it will migrate to the low field regions. Equation (1) shows that in high conductance media ($>100\text{mS/m}$), $\text{Re}(K(\omega))$ will always be negative. Most conventional forms of DEP and related electrokinetic effects have problems that limit the technologies' usefulness for clinical sample preparation and diagnostic applications. The most relevant problem to biological sample analysis is that efficient DEP separations in terms of speed and size selectivity requires relatively low ionic strength conditions (conductance $<10\text{-}100\text{mS/m}$) [19]. More specifically, the ability to isolate sub-micron sized entities such as nanoparticles and high molecular

weight DNA biomarkers into the DEP high field regions (at the electrodes), while micron-sized or cell size entities are kept in low field regions becomes more difficult as the ionic strength increases and the conductance becomes greater than 100 mS/m. Thus, biological samples such as blood or plasma that have ionic strengths in the 100-150 mM ($\sim 1\text{S/m}$) [20] range must be diluted and/or processed before DEP separation and analysis can be carried out. This alone often limits the usefulness of DEP for clinical diagnostics involving the detection of rare cells or low numbers nanoparticles or DNA biomarkers. In cases where a sample (one ml blood) has to be diluted 10 to 100 fold, now means that a very large sample volume must be processed which can be prohibitively time consuming. By way of more specific examples, the isolation of low concentrations of DNA, RNA and protein biomarkers from blood will be extremely important for future clinical diagnostics, in particular for monitoring cancer chemotherapy [21], residual disease [22] and early detection of cancer [23]. While DEP has been used for the isolation of DNA and proteins, problems and limitations do exist in using DEP to carry out the detection of DNA in blood. The primary limitation is again the need to dilute and/or process the blood sample before DEP analysis. In the case of clinically relevant DNA markers in blood, finding and measuring the small amounts of DNA, its fragment size and base composition (for cancer related mutations) is very important [24, 25]. Sample processing that involves or requires centrifugation, filtration and washing procedures can cause the release of DNA molecules from normal cells that are damaged or lysed in the process, as well as shear the clinically relevant high

molecular weight DNA into smaller fragments. The release of extraneous DNA fragments and processing damage to the clinically relevant DNA greatly compromises and limits the diagnostic value of using such procedures. Such sample processing is also highly inefficient, and up to 65% or more of the DNA and RNA in the blood can be lost during the procedure [26].

Thus, the development of new AC electrokinetic devices and techniques which allows samples such as blood, plasma and serum to be rapidly and directly analyzed for rare cells, DNA biomarkers and drug delivery nanoparticles would represent a major advance for biomedical research and clinical diagnostic applications. We have now shown that under certain conditions it is possible to separate nanoparticles in high conductance solutions.

2.2 Materials and Methods

2.2.1 Buffers and Conductivity Measurements

Concentrated 5x Tris Borate EDTA (TBE) buffer solution was obtained from USB Corporation (USB, Cleveland, Ohio, USA), and was diluted using deionized Milli-Q Ultrapure water (55 nS/cm) to the following concentrations: 0.01x TBE, 0.1x TBE and 1x TBE. Dulbecco's Phosphate Buffer Saline (1x PBS) solution was obtained from Invitrogen (Invitrogen, Carlsbad, CA, USA) and was diluted using Milli-Q water to 0.1x PBS. Conductivity measurements were made with an Accumet Research AR-50 Conductivity meter (Fisher Scientific, Fair

Lawn, NJ, USA) using a 2 cell (range: 10-2000 μS) and a 4 cell (range: 1-200 mS) electrode and was adjusted with proper conductivity standards. The following buffer conductivities were measured: 0.01x TBE – 18.1 $\mu\text{S}/\text{cm}$; 0.1x TBE – 125 $\mu\text{S}/\text{cm}$; 1x TBE – 1.09 mS/cm; 0.1x PBS – 1.77 mS/cm; and 1x PBS – 16.8 mS/cm.

2.2.2 Particles, Nanoparticles and DNA Derivatization

Fluorescent polystyrene nanoparticles (FluoSpheres) with NeutrAvidin coated surfaces were purchased from Invitrogen (Invitrogen, San Diego, CA, USA). The nanoparticle diameters were 0.04 μm (40nm) and 0.2 μm (200nm). The 40nm polystyrene nanoparticles were red fluorescent (ex:585/em:605) and the 200nm polystyrene nanoparticles were yellow-green fluorescent (ex:505/em:515). Larger 10.14 μm carboxylated polystyrene particles were obtained from Bangs Labs (Bangs Labs, Fishers, IN, USA). Biotinylated DNA oligonucleotide sequences were obtained from Trilink Bio Technologies (Trilink, San Diego, CA, USA). The single-stranded 51mer DNA oligonucleotide used to derivatize the 40nm nanoparticles had the sequence – [5]'-Biotin- TCA GGG CCT CAC CAC CTA CTT CAT CCA CGT TCA CTC AGG GCC TCA CCA CCT [3]'. A second single-stranded 23mer DNA oligonucleotide used had the sequence – [5]'-Biotin- GTA CGG CTG TCA TCA CTT AGA CC [3]'. The derivatization of the 40nm NeutrAvidin nanoparticles with the biotinylated DNA oligonucleotides was carried out by first suspending the nanoparticles in different concentrations of Tris Borate EDTA (0.01x, 0.1x, 1x TBE) or Phosphate Buffered Saline (0.1x, 1x

PBS) buffers. The ss-DNA oligonucleotide was added to the mixtures in the amounts of 400:1 (DNA:40nm nanoparticles) ratio for the 51mer ss-DNA sequence, and 6500:1 (DNA:40 nm nanoparticle) ratio for the 23mer ss-DNA sequence. Once the DNA was added, the solution was vortexed at high speed for 20 seconds and then allowed to react for about 20 minutes. For the 40nm DNA derivatized nanoparticle experiments, the DNA nanoparticle mixture was made by adding 0.5 μ L of the stock solution into 299 μ L of the appropriate buffer. For the 200nm nanoparticle experiments, 0.5 μ L of the stock solution was added to 299 μ L of the appropriate buffer. Finally, 1 μ L of the 10.14 μ m polystyrene particle stock solution was added to the samples, the samples were then slowly mixed for about 10 seconds. The samples were now ready to be applied to the microarray cartridge device.

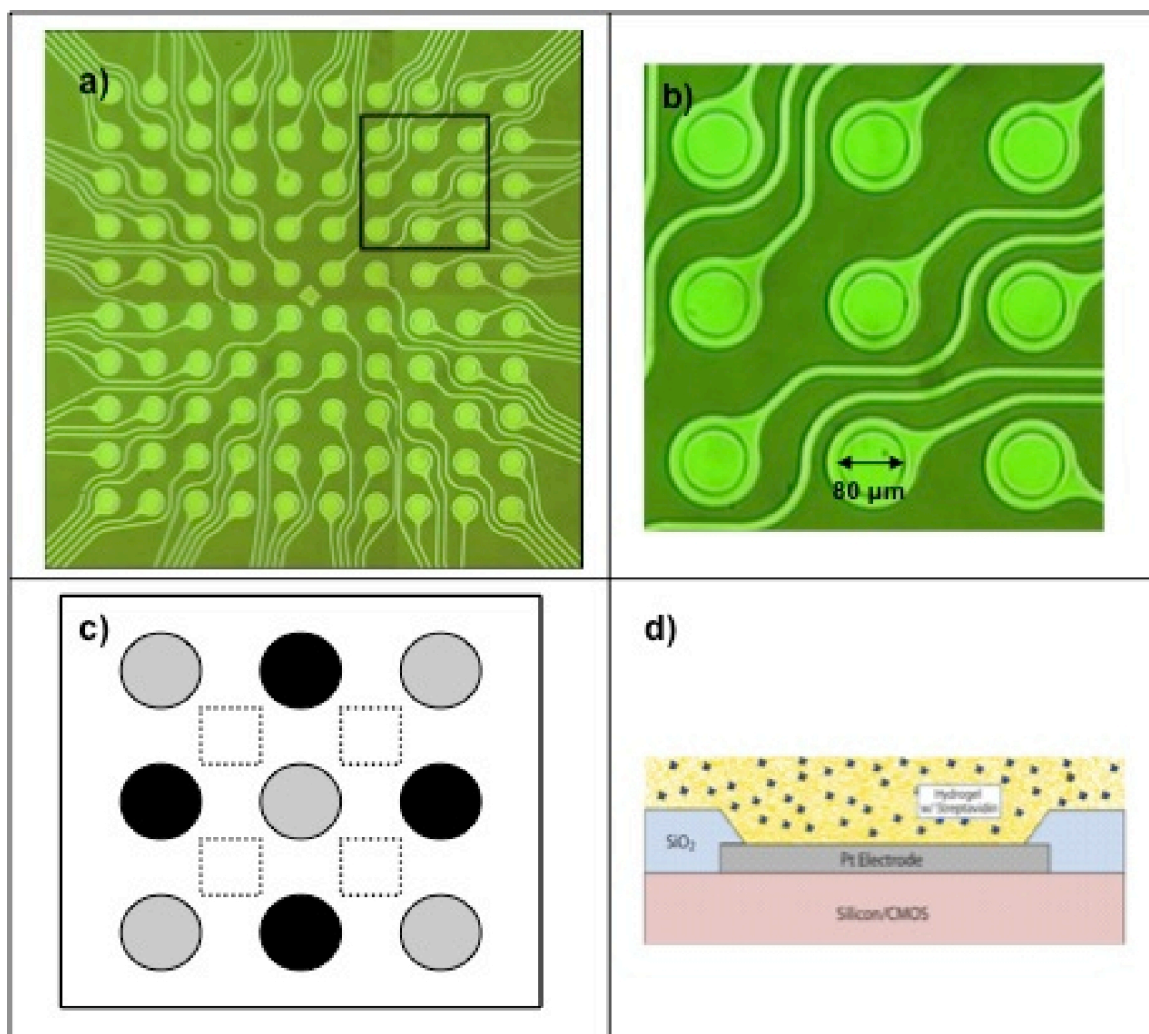


Figure 2.1. DEP Microarray. a) An overall view of the microelectrode array device. b) A 10x magnified view of the 3x3 matrix of nine microelectrodes used to carry out DEP. c) Black and gray colors indicate the relative AC polarity biased on each microelectrode in a checkerboard geometry setup. The dotted squares between the microelectrodes indicate the negative DEP low field areas, the positive DEP high field areas are on the microelectrodes. d) A cross-sectional diagram of the microelectrode array identifying the different components (Note: diagram is not to scale)

2.2.3 DEP microelectrode array device

The microelectrode array devices used for these studies were obtained from Nanogen (San Diego, CA, USA, NanoChip® 100 Cartridges). Figure 2.1a shows an image of the 100 microelectrode array used in the experiments. The circular microelectrodes on the array are 80 μ m in diameter and made of platinum. The microarray is over-coated with 10 μ m thick porous polyacrylamide hydrogel layer. The microarrays are enclosed in a microfluidic cartridge which forms a 20 μ L sample chamber over the array that is covered with a glass window. Electrical connections to each individual microelectrode are pinned out to the bottom of the cartridge. Only a 3x3 subset of nine microelectrodes was used to carry out DEP (see Figure 2.1b). Alternating current (AC) electric fields were applied to the nine microelectrodes in a checkerboard-addressing pattern. In this checkerboard pattern of addressing, each microelectrode has the opposite bias of its nearest neighbor. The corresponding computer model for the asymmetric electric field distribution created by this pattern has been discussed previously [27]. This model indicates that the positive DEP field maxima (high field regions) exist at (on) the microelectrodes and the negative DEP field minima (low field regions) exist in the areas between the electrodes (see Figure 2.1c). In general, for DEP in low conductance solutions the 60nm DNA and 200nm nanoparticles are expected to concentrate in the positive or high field regions over the microelectrodes [28] and the 10 micron particles concentrate in the negative or low field DEP regions [29] between the microelectrodes (see Figure 2.7). Figure 2.1d shows a cross-sectional view of the microelectrode array for

one electrode and indicates the general structure of the array, including the hydrogel layer above the platinum electrode. The computations from the previous model were performed for a 5x5 microelectrode set [27]. However, since a 3x3 set of microelectrodes was used to carry out the experiments, the model was modified and indicated that the electrodes marked in **black** in Figure 2.1c will have higher electric field strengths than the other microelectrodes (**gray**). As a result, these microelectrodes (**black**) will concentrate nanoparticles faster than the other microelectrodes. Before each experiment, the microarray cartridge is flushed 10 times with 200 μ L of the appropriate buffer, over a span of 5 minutes. The cartridge is allowed to sit for 5 minutes, and is then washed two more times with 200 μ L of buffer. A total of 150 μ L of the sample solution containing the nanoparticle mixture is then slowly injected into the cartridge, a final sample volume of about 20 μ L remains in the cartridge.

2.2.4 Experimental Setup and Measurements

The microarray devices were controlled using a custom made switching system (designed and constructed in our lab) that allows for individual control over the voltage being applied to each of the 100 microelectrodes. The microelectrodes were set to the proper AC frequency and voltages using an Agilent 33120A Arbitrary Function Generator (Agilent, Santa Clara, CA, USA). AC frequencies ranged from 1000Hz to 10,000Hz, at 10 volts peak to peak (pk-pk). The wave form used for all experiments was sinusoidal. The experiments were visualized using a 10x PL Fluotar objective in a JenaLumar epifluorescent

microscope (Zeiss, Jena, Germany) employing the appropriate excitation and emission filters (green fluorescence Ex 505nm, Em 515nm; red fluorescence Ex 585nm, Em 605nm. Both back lighted and the fluorescent images were captured using an Optronics 24-bit RGB CCD camera (Optronics, Goleta, CA, USA). The image data was processed using a Canopus ADVC-55 video capture card (Canopus, San Jose, CA, USA) connected to a laptop computer using either Adobe Premiere Pro (Adobe Systems Inc, San Jose, CA, USA) or Windows Movie Maker. The final fluorescence data was analyzed by inputting individual fluorescent image frames of the video into MATLAB (Mathworks, Natick, MA, USA) at 0 minutes, 30 seconds, 1 minute, 2 minutes, 4 minutes, 8 minutes, 16 minutes, and 20 minutes time points. The graphs in Figure 2.6a and Figure 2.6b were created using Excel from data gathered through MATLAB analysis of fluorescence intensity readings across the microelectrode. Figure 7 was created using MATLAB. Figure 2.7 used the following data to create the graph: σ_p (for 200nm)= 18mS, σ_p (for 40nm+DNA)= 50mS $K_s=0.9nS$, $\epsilon_p=2.55\epsilon_0$. $r = 30nm$ & $r = 100nm$. $f=3kHz$.

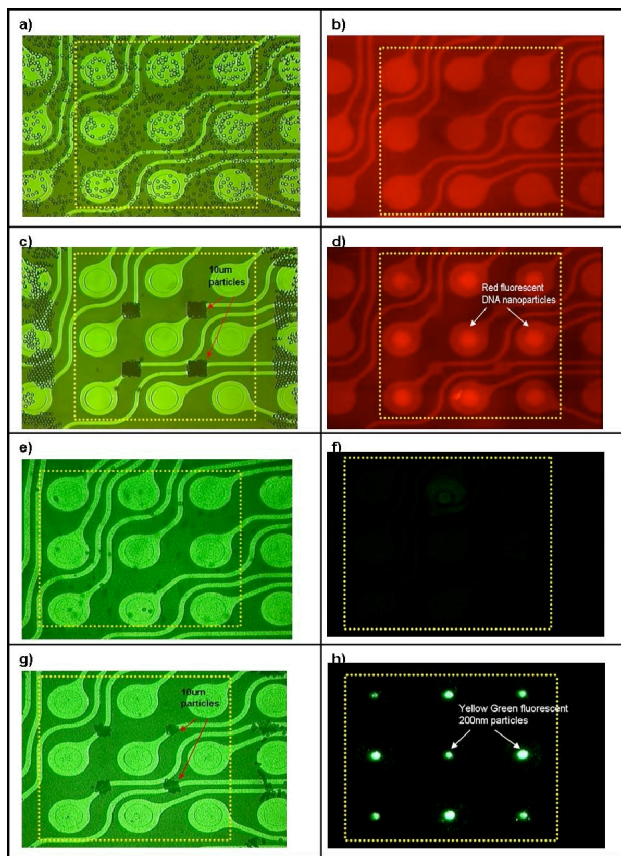


Figure 2.2. DEP separation at low conductivity for 60nm DNA derivatized nanoparticles and 10µm particles in MilliQ water ($5.5 \mu\text{S/m}$). a) Image under white light before the AC electric field is applied shows random distribution of the 10µm particles across the microarray. b) Initial conditions under red fluorescence detection shows red fluorescent haze across the microarray from the 60nm DNA derivatized nanoparticles. c) Image after the AC DEP field was applied for 30 seconds showing the 10µm particles have now concentrated in orderly arrangements into the negative DEP low field regions (note that particles outside the AC activated microelectrode area indicated by the yellow dotted square have not been as affected by the DEP field). d) Fluorescent image after one-minute application of the AC field showing the 60nm DNA derivatized nanoparticles concentrated onto the positive DEP high field regions over the microelectrodes. e) Initial image of DEP separation experiment using the 200nm nanoparticles with 10µm particles in 0.01x TBE (1.81 mS/m) showing a random distribution of the 10µm particles before DEP is applied. f) Fluorescence image showing green fluorescence from the 200nm nanoparticles. g) Image after AC field is applied for 20 minutes showing the 10µm particles concentrated into the low field regions. h) Fluorescent image after 20 minutes showing the 200nm nanoparticles highly concentrated into the positive DEP high field regions.

2.3 Results

2.3.1 Low conductivity DEP experiments

Before starting the low conductance DEP experiments, the array was flushed with buffer to thoroughly wet the hydrogel layer, prevent bubbles [30], and to ensure that the array has uniform conductivity. The initial set of experiments involved DEP separations in low conductivity buffers to confirm proper functioning of the system. These first experiments involved separating 60nm DNA derivatized nanoparticles from 10 μ m particles in MilliQ water (5.5 μ S/m). The experiments were performed at 10 kHz AC at 10 volts peak to peak (pk-pk). The initial conditions under white light and before the AC electric field is applied, show a random distribution of the 10 μ m particles over the microelectrode area encompassed by the yellow rectangle (Figure 2.2a). The initial conditions under red fluorescence detection show a red fluorescent haze across the microarray as would be expected from the 60nm DNA derivatized nanoparticles (Figure 2.2b). After the AC DEP field was applied for 30 seconds, most of the 10 μ m particles have concentrated in very orderly arrangements into the negative DEP low field regions (Figure 2.2c). After 1 minute application of the AC field, the 60nm DNA derivatized nanoparticles have concentrated onto the positive DEP high field regions over the microelectrodes (Figure 2.2d). The high fluorescent intensity on the microelectrodes together with the decrease of fluorescent intensity in the surrounding areas indicates that major portion of the nanoparticles have concentrated into the high field regions. This DEP separation

experiment was now repeated using the 200nm nanoparticles mixed with 10 μm particles in 0.01x TBE (1.81 mS/m). In order to obtain good fluorescence intensity measurements over time, all experiments were run for 20 minutes or longer and video recorded. DEP was also now carried out at 3 kHz AC at 10 volts pk-pk. Individual image frames were then isolated at specific time points. Since the experiments are recorded for 20 minutes in fluorescence view, all white light images of the 10 μm particles are taken before the AC field is applied and 20 minutes after DEP is started. However, the actual time taken for the 10 μm particles to concentrate into the low field regions was generally shorter than 20 minutes. Again, the initial white light view shows a random distribution of the 10 μm particles before the field is applied (Figure 2.2e), and the green fluorescence view shows no accumulation of the 200nm nanoparticles in the high field regions (Figure 2.2f). After 20 minutes, the 10 μm particles are concentrated into the low field regions (Figure 2.2g), and the 200nm nanoparticles are highly concentrated into the positive DEP high field regions (Figure 2.2h). These low conductivity DEP results are generally consistent with other low conductivity DEP nanoparticle separations cited in the literature [31-34].

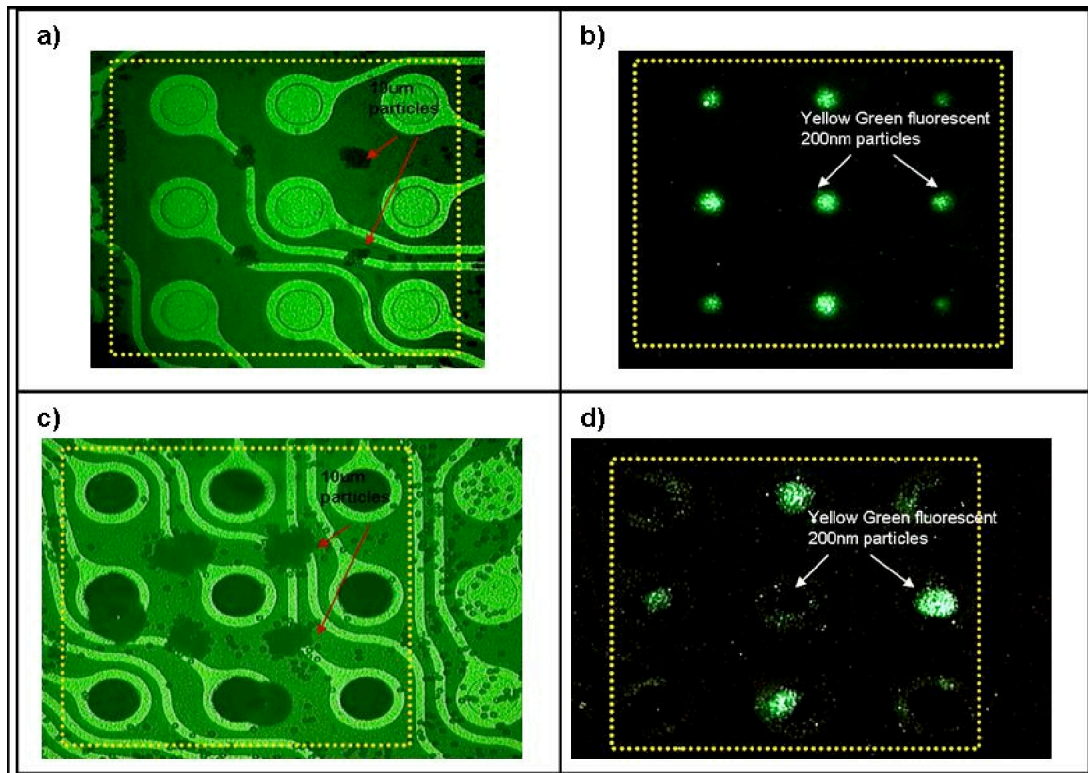


Figure 2.3. DEP separation of 200nm nanoparticles and 10 micron particles in high conductance buffers 1x TBE (~ 109 mS/m) and 1x PBS (1.68 S/m). a) Shows the concentration of the 10µm particles into the negative DEP low field regions after the AC field was applied for 20 minutes in 1x TBE buffer (109 mS/m). b) Green fluorescent image showing the concentration of the 200nm nanoparticles in the positive DEP high field regions on top of the microelectrodes. c) Shows the results of DEP experiments carried out in 1x PBS (1.68 S/m) after 20 minutes with the 10µm particles concentrated into the low field regions. d) Green fluorescence image after 20 minutes showing concentration of the 200 nm nanoparticles in the positive DEP high field region over the microelectrodes.

2.3.2 High conductivity experiments

The next set of DEP experiments involved separations of 60nm DNA derivatized nanoparticles, 200nm nanoparticles and 10 μ m particles in buffer solutions with conductivities greater than 100 mS/m. In general, these experiments were performed in the same manner as the low conductivity experiments. For the initial conditions before the DEP field was applied, all 60nm DNA derivatized nanoparticle images looked exactly like Figures 2.2a and 2.2b, and all the 200nm nanoparticle images looked like Figures 2e and 2f. After the AC field was applied for 20 minutes, the separation between 200nm nanoparticles and 10 μ m particles in 1x TBE (0.109 S/m) under white light conditions showed the 10 μ m particles concentrated in the low field regions (Figure 2.3a). Under green fluorescence, the 200nm nanoparticles were concentrated in the positive DEP high field regions on top of the microelectrodes (Figure 2.3b), very similar to what was shown previously in Figure 2.2h. For DEP experiments carried out in 1x PBS (1.68 S/m), after 20 minutes the 10 μ m particles are concentrated into the low field regions (Figure 2.3c), as was previously seen in (Figures 2.2g and 2.3a), However, the microelectrodes now show some darkening and two of the microelectrodes show bubbling. The green fluorescence 20 minute image for the high conductance 1x PBS buffer experiment was taken after removal of some small bubbles and at an increased gain of 3.75 times. (Figure 2.3d) The image clearly shows that 200 nm nanoparticles have concentrated into the positive DEP high field regions of four microelectrodes. (It should be noted that this increased gain image was not used

in the fluorescence intensity calculations in Figure 2.6b). The fact that the 200nm nanoparticles have predominantly concentrated on these four microelectrodes is consistent with the fact that they produce slightly higher fields (see black electrodes in Figure 2.1c). The high conductance experiments in 1x PBS buffer that were carried out using 60nm DNA derivatized nanoparticles also yielded similar results, i.e., in that the 60nm nanoparticles were still observed to concentrate in the positive DEP high field regions over three of the microelectrodes.

Further analysis of the fluorescence images was performed in MATLAB to produce three-dimensional peaks, which better demonstrate the concentration of the fluorescent nanoparticles over the high field regions. For the 1x TBE experiments with 60nm DNA derivatized nanoparticles, the 3D fluorescent data showed a significant increase from time points 0 minutes (Figure 2.4a), 2 minutes (Figure 2.4b), 8 minutes (Figure 2.4c) and 16 minutes (Figure 2.4d). Similarly, the 3D fluorescent data for the 200nm nanoparticles in 1x PBS also shows a significant increase from time points 0 minutes (Figure 2.4e), 8 minutes (Figure 2.4f), 16 minutes (Figure 2.4g), and after 20 minutes (Figure 2.4h). For the 60nm DNA derivatized nanoparticles in 1x PBS, there is still significant concentration as is seen in as seen in the fluorescent image (Figure 2.5a) The 3D fluorescent image data also shows a similar fluorescence increase over 0 minutes (Figure 2.5b), 8 minutes (Figure 2.5c) and 20 minutes (Figure 2.5d). Due to the inactivation of one of the microelectrodes (3rd row, 2nd column) shown in Figure

2.5a, the electric field pattern is slightly altered. Nevertheless, nanoparticles are still concentrated onto the high field regions of the active electrodes.

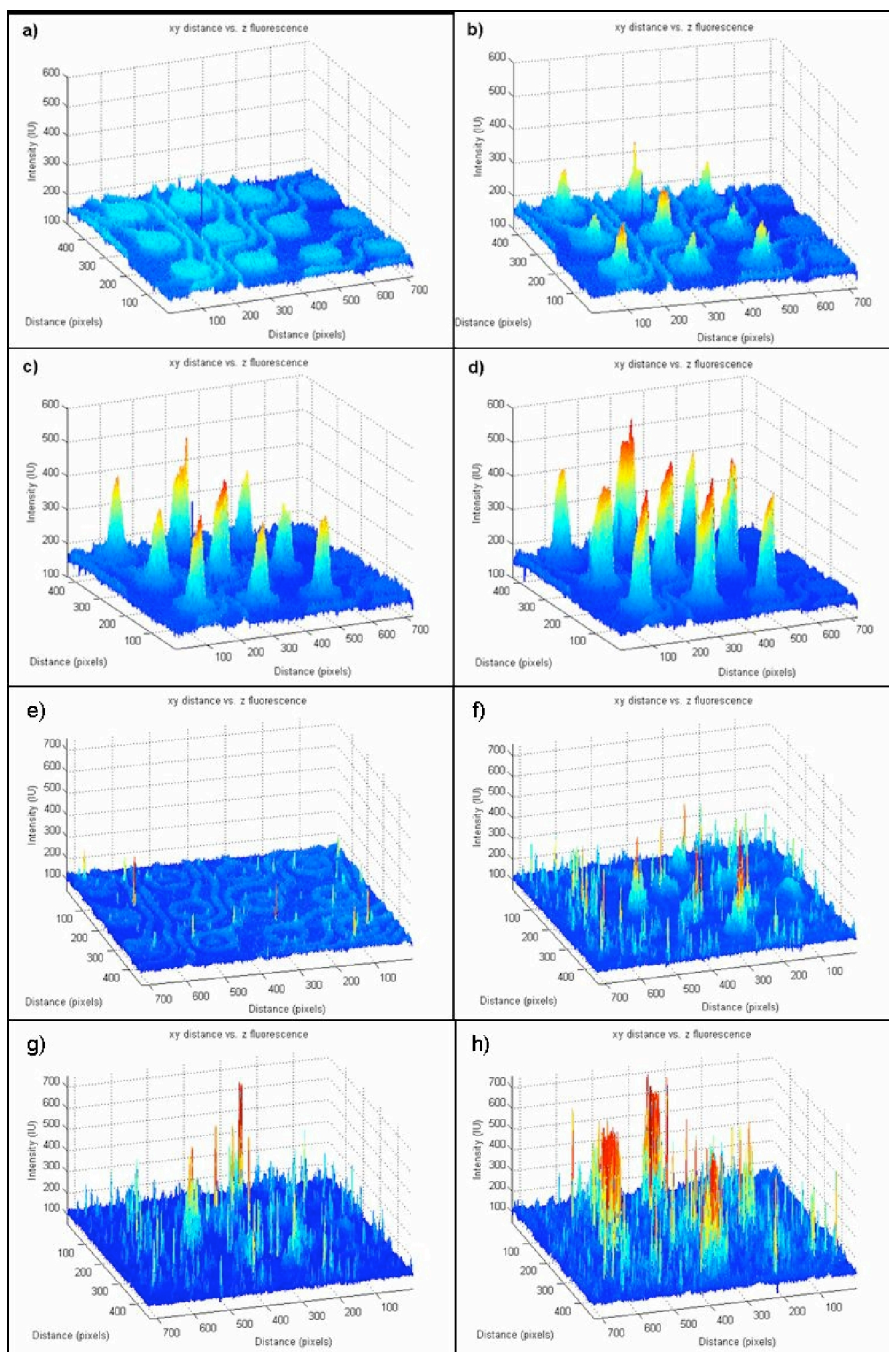


Figure 2.4. Three dimensional fluorescence peak images, showing increasing fluorescent signal on microelectrodes for 60nm DNA derivatized nanoparticles in 1x TBE buffer (109 mS/m) at time points after start of experiment: a) 0 minutes. b) 2 minutes. c) 8 minutes. d) 16 minutes. 3D fluorescence peak data of 200nm nanoparticles in 1x PBS buffer (1.68 S/m) at time points after start of experiment: e) 0 minutes. f) 4 minutes. g) 8 minutes. h) 20 minutes.

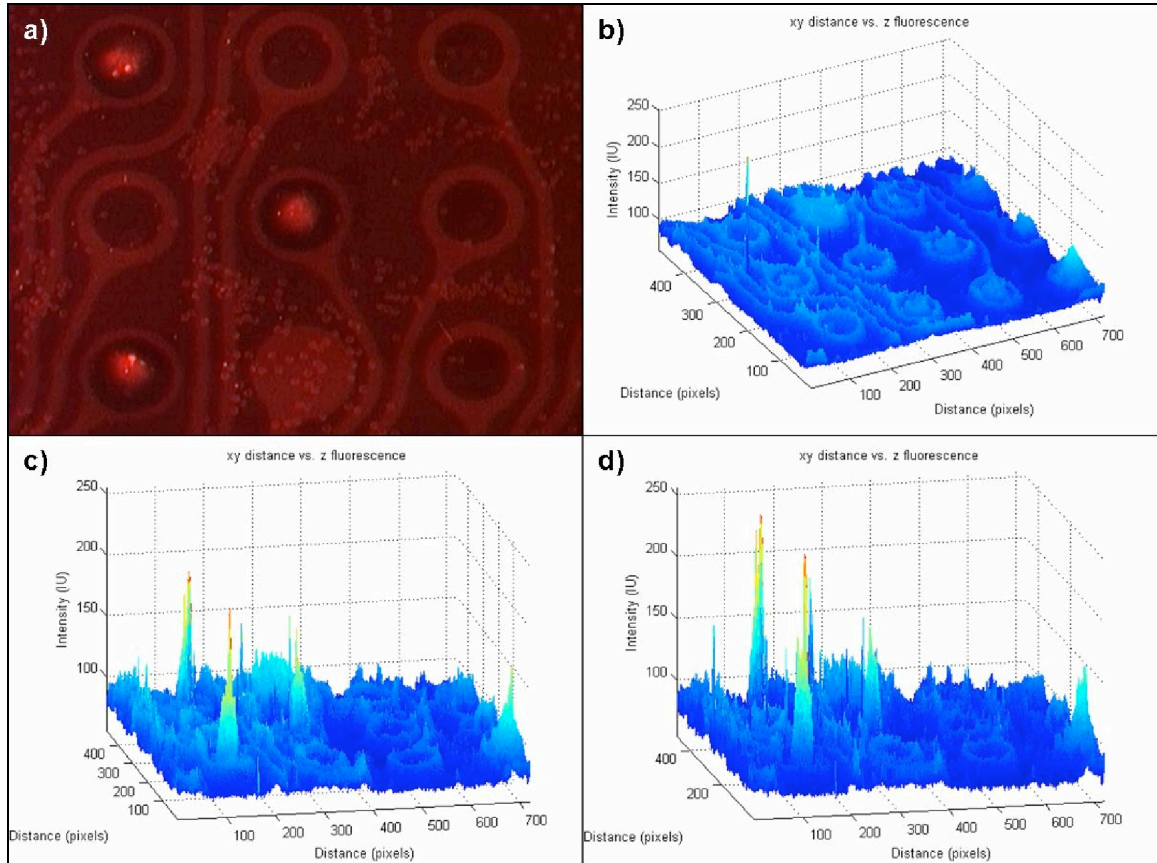


Figure 2.5. Red fluorescence image and 3D fluorescence peak images for 60nm derivatized nanoparticles in 1x PBS (1.68 S/m), showing increasing fluorescent signal on microelectrodes a) Red fluorescence image at 20 minutes after start of AC field, showing concentration of red fluorescence nanoparticles on microelectrodes. b) 3D fluorescence peak images at the time points after start of experiment: a) 0 minutes. b) 8 minutes. c) 20 minutes.

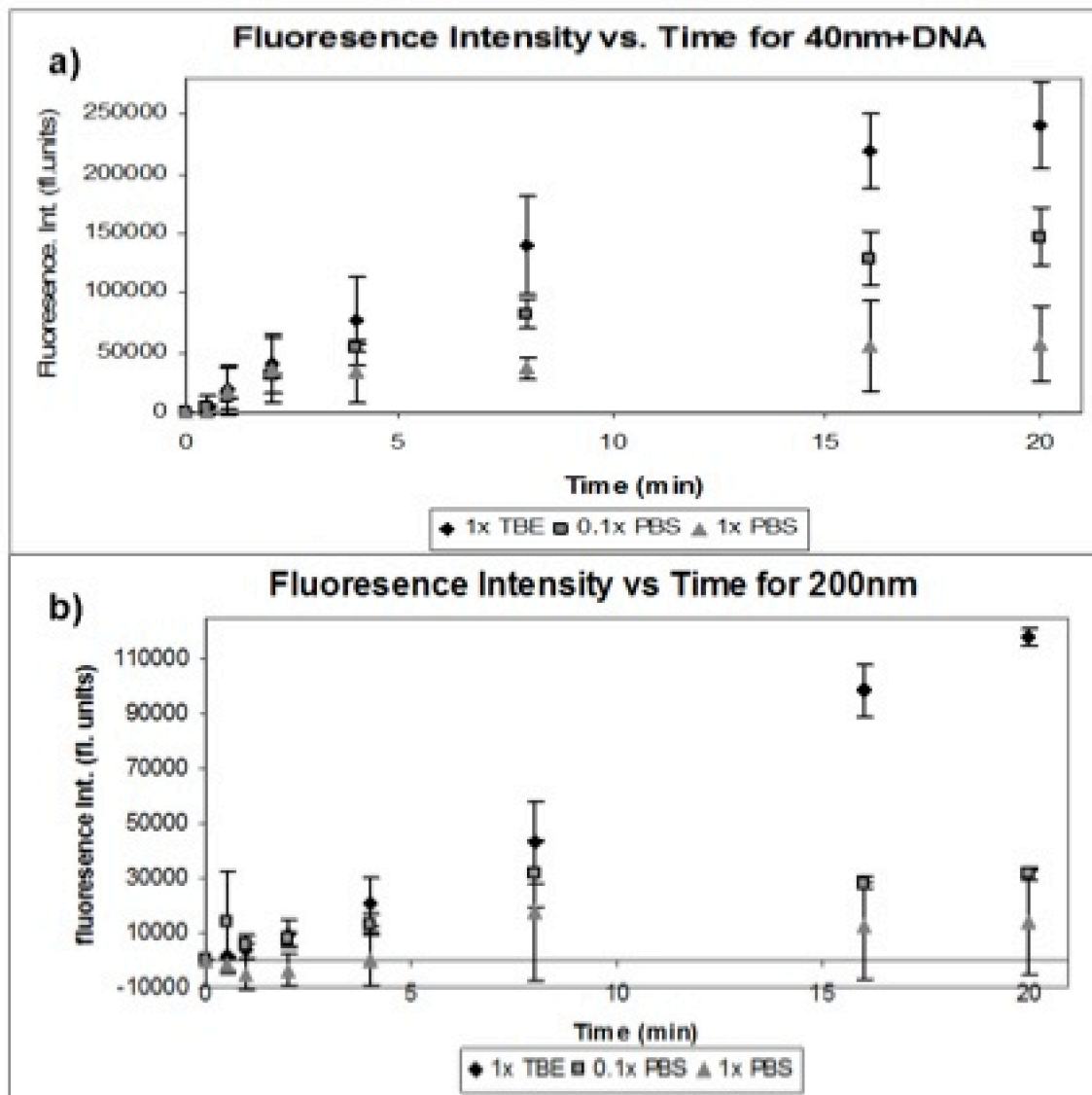


Figure 2.6. Fluorescence intensity Graphs. a) Graph of fluorescence intensity on microelectrodes versus time for 1x TBE (109 mS/m), 0.1x PBS (177 mS/m) and 1x PBS (1.68 S/m) for 60nm DNA derivatized nanoparticles. b) Graph of fluorescence intensity on microelectrode versus time for 1x TBE (109 mS/m), 0.1x PBS (177 mS/m) and 1x PBS (1.68 S/m) for 200nm nanoparticles.

The overall fluorescence data was compiled using MATLAB for experiments in buffers of 1x TBE, 0.1x PBS (0.177 S/m) and 1x PBS at the time points of 0, 0.5, 1, 2, 4, 8, 16, and 20 minutes. The results for the 60nm DNA derivatized nanoparticles are shown Figure 2.6a, and the results for the 200nm nanoparticles are shown in Figure 2.6b. The data for each particular experiment had the initial background (time 0) for each microelectrode subtracted from all other data points and then averaged with other experiments at that conductivity to create the standard deviation bars. (The fact that the error bars for 1x PBS in Figure 2.6b drop below zero, is most likely due the darkening of the electrodes which causes a decrease in the relative fluorescent intensity level. Figure 2.3d clearly shows that fluorescent nanoparticles have accumulated on the electrodes at these conditions). The overall data indicates an increase in concentration of the fluorescent nanoparticles over time. The data also shows a decrease in overall concentration of the fluorescent nanoparticles as the conductivity of the buffers increases. Nevertheless, fluorescent nanoparticle concentration in the high field regions is still observed for the high conductance 1xPBS buffers. Lastly, Figure 2.7 shows the theoretical curves and the ranges for the experimental results for the real part of the Clausius-Mossotti factor ($\text{Re}(K(\omega))$) versus conductivity for the 60nm DNA derivatized nanoparticles and the 200nm nanoparticles. The graph indicates that the theoretical $\text{Re}(K(\omega))$ values should be negative for the conductivities used in the experiments, and therefore the nanoparticles should have accumulated in the low field regions. However, our

experimental results clearly show the accumulation of nanoparticles continues in the high field region, as shown in Figure 2.7.

2.4 Discussion

AC electrokinetic techniques and dielectrophoresis (DEP) in particular offer an attractive mechanism for the separation of cells, biomarkers and nanoparticles, however the technique is generally limited to low conductance solutions. Thus, the results of the high conductivity buffer (1x PBS) experiments demonstrating that both the 60nm DNA derivatized nanoparticles and 200nm nanoparticles could be separated from 10 micron polystyrene spheres was unexpected (Figure 2.3 & Figure 2.5). The initial reasons for carrying out this work were to determine the cross over frequencies (positive to negative DEP) for the 60nm to 200nm nanoparticles in the 10 to 100 mS/m range (0.1-1x TBE), and to investigate the DEP separation process in the 1000Hz to 10,000Hz frequency ranges. The nanoparticles used in the experiments served as models for more clinically relevant entities which included high molecular weight DNA (DNA nanoparticulates) and drug delivery nanoparticles in the 60nm to 200nm range, while the 10 micron polystyrene spheres were used as a model for cells. Initial experiments, even at the intermediate conductance range (~100 mS/m) appeared somewhat inconsistent with DEP theory in terms of the relative speed of the separation process for both the 60nm and 200nm nanoparticles in 1x TBE (~109 mS/m). More specifically, the 60nm and 200nm nanoparticles continued to be rapidly concentrated in the “positive” or high field DEP regions above the

microelectrodes, while the 10 micron particles continued to concentrate into the “negative” or low field DEP regions between the microelectrodes (Figure 2.3a-b). Even more unexpectedly, while the separation process carried out at high conductivity (1x PBS) was somewhat slower, the accumulation of both the 60nm and 200 nm nanoparticles continued in the high field regions, while 10 micron particles concentrated into the low field regions. (Figure 2.3c-d & Figure 2.5a). Since 1x PBS (149 mM) has a conductivity of ~ 1.68 S/m, these results clearly deviate from conventional DEP (Figure 2.7). In order to be more certain about the results, the fluorescent images of the array were converted to three dimensional fluorescent intensity images using MATLAB (Figure 2.4). For the high conductivity buffers (1x PBS), both the 60nm DNA derivatized nanoparticles and the 200nm nanoparticles show 3D fluorescent peaks in the positive high field regions over three of the microelectrode structures (Figure 2.4e-h & Figure 2.5b-d). A key observation at high conductance was the production of bubbles and an overall darkening of the microelectrodes (Figure 2.3c). The presence of bubbles on some of the microelectrodes also explains why there is limited concentration of nanoparticles on those locations. Competition from electrochemistry may also be the reason why the accumulation rate of nanoparticles is slower at the higher conductance conditions.

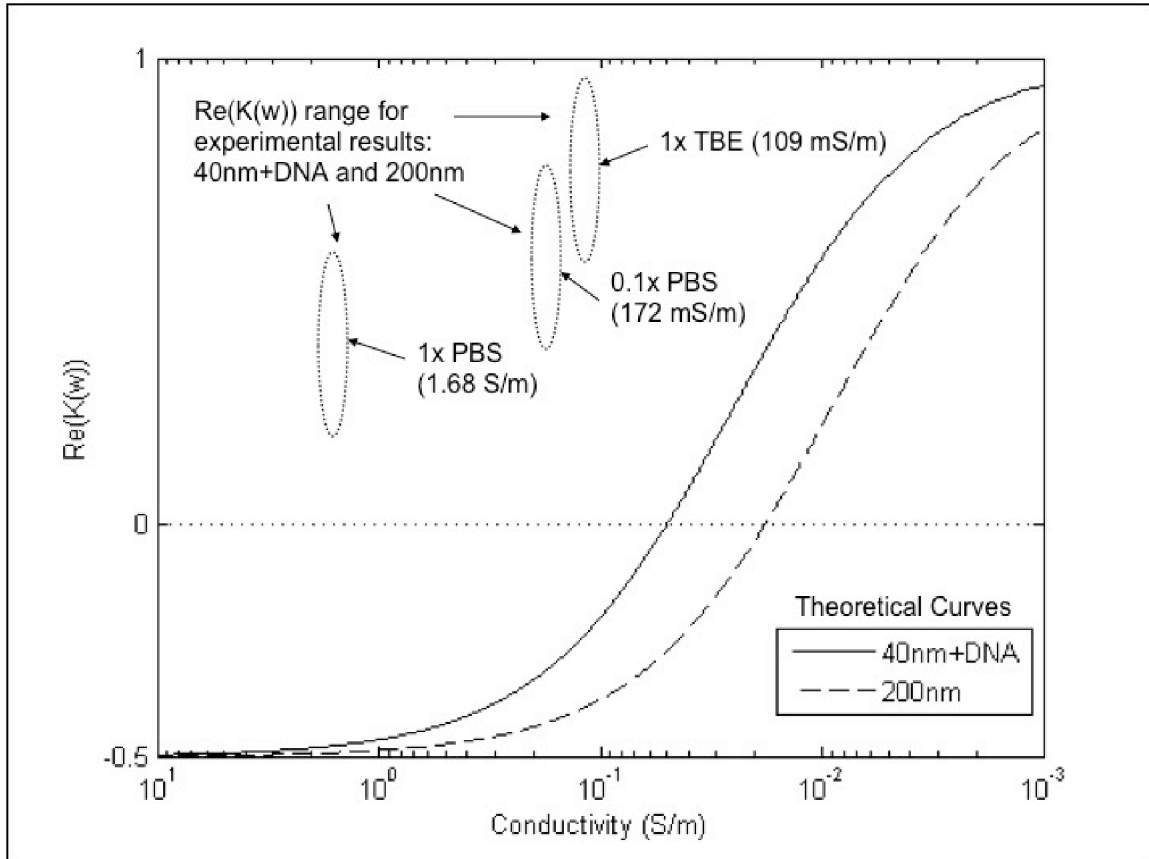


Figure 2.7. Graph of real part of Clausius-Mossotti factor ($\text{Re}(K(w))$) versus conductance for 60nm DNA derivatized nanoparticles and 200nm polystyrene nanoparticles. The dashed line represents 200nm nanoparticles and the solid line represents 60nm DNA nanoparticles (roughly the size of 40nm nanoparticles and 51mer DNA), according to current DEP theory [19]. The dashed ovals indicate the experimental data ranges reported in this paper for 60nm DNA nanoparticles and for 200nm nanoparticles. Since the actual values for $\text{Re}(K(w))$ could not be calculated, ranges for the values for each conductivity are given. The results in Figure 2.6 indicate that the speed of accumulation decreases with increasing conductivity and therefore the dashed ovals are lowered on the y-axis accordingly.

While the experimental evidence clearly shows that nanoparticles continue to be concentrated into the positive high field regions at high conductance conditions ($> 1\text{S/m}$) (Figure 2.6a-b), an exact explanation of the electrokinetic mechanism is not possible at this time. Nevertheless, the particular arrangement of circular microelectrodes over-coated with a thin porous hydrogel may have something to do with the phenomena. The thin hydrogel layer provides some level of protection from electrochemical effects including H_2 and O_2 bubbles, and extremes of pH which occur on the microelectrode surface when using high conductance buffers and lower AC frequencies in the 3 kHz–10 kHz range. Such adverse (electrochemical) effects may have prevented the observation of nanoparticle accumulation on bare electrode surfaces used in more conventional DEP devices. Another possibility is that the circular microelectrodes and the particular AC field geometry used in these experiments are responsible for the results. These electrode arrangements and geometries are somewhat different than those used by other DEP researchers, which include *parallel plates*, *castellated* and *polynomial electrodes* [17, 33, 34]. The arrangements used in this study may lead to stronger AC field effects than would be produced using the more conventional DEP devices. Finally, there is also a possibility that AC electroosmotic fluid movement influences nanoparticle isolation and concentration [17]. Fluid convection would be expected to occur on electrode surfaces under low frequency and high conductance conditions, and it could induce movement of nanoparticles which helps transport them into the high field regions. Future work on this project will now be directed at better understanding

of the electrokinetic mechanism, and on developing higher performance devices with improved separation speed. The advent of such devices which allow the direct, rapid and highly sensitive analysis of small amounts of blood for rare cells (cancer), high molecular weight DNA markers and drug delivery nanoparticles would represent a major advance in diagnostics.

Chapter 2, in full, is a reprint of the material as it appears in *Electrophoresis*: Krishnan R, Sullivan BD, Mifflin RL, Esener SC, Heller MJ. Alternating current electrokinetic separation and detection of DNA nanoparticles in high-conductance solutions. *Electrophoresis* 2008, 29(9): 1765-1774. The dissertation author was the primary investigator and author of this paper.

Chapter 3: AN AC ELECTROKINETIC METHOD FOR ENHANCED DETECTION OF DNA NANOPARTICLES

Reprinted from: Journal of Biophotonics (2009)

3.1 Introduction

The separation and detection of low numbers of bacteria and virus; drug delivery nanoparticles, high molecular weight (hmw) DNA biomarkers, antibodies and other entities from blood and other complex biological samples remains a significant challenge [1-6]. For many research and clinical applications, sample preparation is used to enrich a specific analyte before detection is carried out. Such processes involve a variety of physical, electronic and biological methods and techniques that include centrifugation, gel filtration, affinity binding, magnetic beads and electrophoresis [7, 8]. Many of these techniques are relatively time consuming, costly and often lead to significant loss of the analyte. AC electrokinetic techniques, like dielectrophoresis (DEP) have been attractive because they allow cells [9-11], hmw-DNA biomarkers [12-15] and proteins [16] to be rapidly isolated and concentrated into specific microscopic locations. Dielectrophoresis (DEP) is an induced motion of particles produced by the dielectric differences between the particles and media in an AC electric field [17, 18]. Unfortunately, conventional forms of DEP have limited research and diagnostic applications, because they require relatively low ionic strength conditions (conductance $<10\text{-}100\text{mS/m}$) [19]. Thus, biological samples such as blood or plasma that have ionic strengths in the $100\text{-}150\text{ mM}$ ($\sim 1\text{S/m}$) [20] range

must be significantly diluted. In cases where a sample (one ml blood) has to be diluted 10 to 100 fold, now means that a very large sample volume must be processed which is often unacceptable. By way of more specific examples, the isolation of low concentrations of DNA, RNA and protein biomarkers from blood will be important for future clinical diagnostics, including monitoring cancer chemotherapy [21], residual disease [22] and early cancer detection [23, 24, 25]. Sample processing that requires centrifugation, filtration and washing procedures can cause the release of DNA molecules from normal cells that are damaged, as well as shear hmw-DNA into smaller fragments. Sample processing is also highly inefficient and > 65% of the DNA can be lost [26]. Recently, we have demonstrated that the DEP separation of nanoparticles from micron size particles could be achieved under high conductance conditions [27]. We now show that both nanoparticles and high molecular weight (hmw) DNA can be concentrated and detected in high conductance buffers (> 100 mS/m).

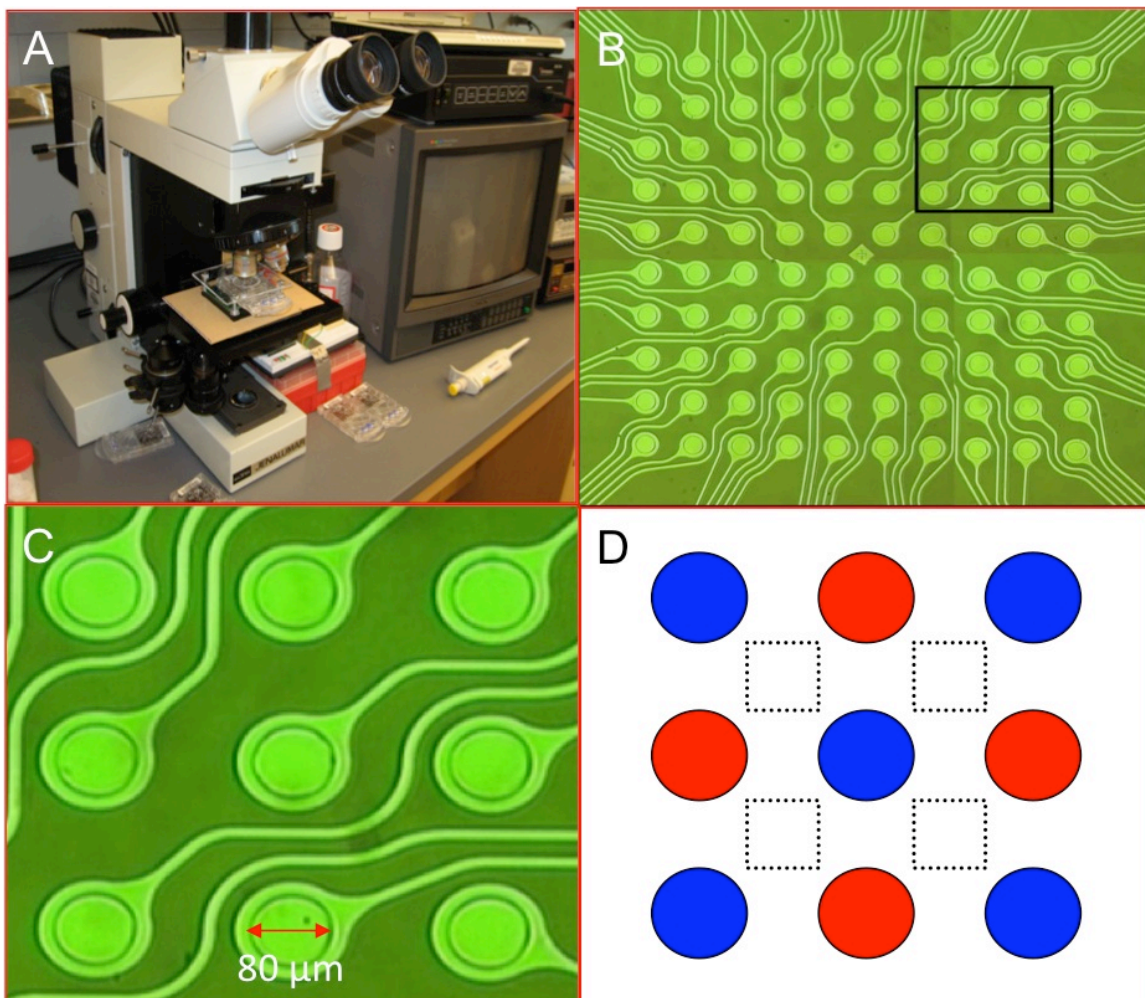


Figure 3.1. A) The epifluorescent microscope and DEP microelectrode array device on the microscope stage. B) The DEP microelectrode array device with 100 platinum microelectrodes (80 μm diameter). C) A 10x magnified view of the 3x3 matrix of nine microelectrodes used to carry out DEP separations. D) DEP field where red and blue colors indicate the relative AC polarity biased on each microelectrode in a checkerboard geometry setup. The dotted squares between the microelectrodes indicate the negative DEP low field areas, the positive DEP high field areas are on the microelectrodes.

3.2 Materials and Methods

3.2.1 Buffers and Conductivity Measurements

The conductivity measurements for the buffers were done in the same manner as reported previously [27]. Concentrated 5x Tris Borate EDTA (TBE) buffer solution was obtained from USB Corporation (Cleveland, Ohio, USA), and was diluted using deionized Milli-Q Ultrapure water (55 nS/cm) to the following concentrations: 0.01x TBE, 0.1x TBE and 1x TBE. Dulbecco's Phosphate Buffer Saline (1x PBS) solution was obtained from Invitrogen (Carlsbad, CA, USA) and was diluted using Milli-Q water to 0.1x PBS. Conductivity measurements were made with an Accumet Research AR-50 Conductivity meter (Fisher Scientific). The following buffer conductivities were measured: 0.01x TBE – 18.1 μ S/cm; 0.1x TBE – 125 μ S/cm; 1x TBE – 1.09 mS/cm; 0.1x PBS – 1.77 mS/cm; and 1x PBS – 16.8 mS/cm.

3.2.2 Particles, Cells, Nanoparticles and DNA Derivatization

Fluorescent polystyrene nanoparticles (FluoSpheres) with NeutrAvidin coated surfaces were purchased from Invitrogen (San Diego, CA, USA). The nanoparticle diameters were 0.04 μ m (40nm) and 0.2 μ m (200nm). The 40nm nanoparticles were red fluorescent (ex:585/em:605) and the 200nm nanoparticles were yellow-green fluorescent (ex:505/em:515). Larger 10.14 μ m carboxylated polystyrene particles were obtained from Bangs Labs (Fishers, IN, USA). Human Jurkat cells were obtained from ATCC. Biotinylated DNA oligonucleotides were obtained from Trilink Bio Technologies (San Diego, CA,

USA). The 51mer – [5]'-Biotin- TCA GGG CCT CAC CAC CTA CTT CAT CCA CGT TCA CTC AGG GCC TCA CCA CCT [3]' and 23mer - [5]'-Biotin- GTA CGG CTG TCA TCA CTT AGA CC [3]' DNA oligonucleotides and derivatization of the 40nm NeutrAvidin nanoparticles were described in reference [27]. For the 40nm DNA derivatized nanoparticle and 200nm nanoparticle experiments, 0.5 μ L of the stock solution was added to 299 μ L of the appropriate buffer. Finally, 1 μ L of either the 10.14 μ m particle stock solution or 1 μ L Jurkat cells at (10^6 cells/ml) was added to the samples, the samples were then slowly mixed for about 10 seconds.

3.2.3 High Molecular Weight (hmw) DNA

The 40 kilobase single stranded hmw DNA was prepared in the following manner. A single stranded DNA referred to as pp-strepapt-p53c248 was circularized by Rolling Circle Amplification (RCA) using DNA referred to as tp53c248. The high molecular weight (hmw) DNA is believed to form a cluster or ball-like structure due to internal self-hybridization, and was designed to serve as a model for clinically relevant circulating hmw DNA. The hmw DNA was stained using 1:100 Quant-iT™ OliGreen® ssDNA Reagent (Invitrogen, USA). The fluorescence excitation and emission maxima for the dye are 500nm and 525nm. For the DEP experiments, 12 μ L of the 50 μ L stock solution of RCA hmw-DNA (2nM) was added to 24 μ L of OliGreen (1:100 dilution) mixed and then allowed to sit for 10 minutes. About 300 μ L buffer was then added to this solution and mixed. About 150 μ L was added to the array (final volume ~ 20 μ L).

3.2.4 DEP microelectrode array device

The microelectrode arrays were obtained from Nanogen (San Diego, CA, USA, NanoChip® 100 Cartridges). Figure 3.1A shows an image of the general setup used in the experiments. The cartridge is attached to a custom made switching system that allows individual voltage control for each microelectrode. An epifluorescent microscope is used to visualize the array. Figure 3.1B shows a close up of the 100 microelectrode array used in the experiments. The circular microelectrodes are 80 μ m in diameter and made of platinum. The microarray is over-coated with 10 μ m polyacrylamide hydrogel layer. The microarrays are enclosed in a microfluidic cartridge, which forms a 20 μ L sample chamber. Electrical connections to each microelectrode are pinned out to the bottom of the cartridge. Only a 3x3 subset of nine microelectrodes was used to carry out DEP (see Figure 3.1C). Alternating current (AC) electric fields were applied to the nine microelectrodes in a checkerboard addressing pattern. The corresponding computer model for the asymmetric electric field distribution has been discussed previously [28]. This model indicates that the positive DEP field maxima (high field regions) exist at (on) the microelectrodes and the negative DEP field minima (low field regions) exist in the areas between the electrodes (see Figure 3.1D). Before each experiment, the microarray is flushed 10 times with 200 μ L of buffer. The cartridge is allowed to sit for 5 minutes, then washed 2 times with 200 μ L of buffer. A total of 150 μ L of the sample is then slowly injected into the cartridge, a final volume of about 20 μ L remains in the cartridge.

3.2.5 Experimental Setup and Measurements

The microelectrodes were set to the proper AC frequency and voltages using an Agilent 33120A Arbitrary Function Generator (Santa Clara, CA, USA). AC frequencies ranged from 3000Hz to 10,000Hz, at 10 volts peak to peak (pk-pk). The wave form used for all experiments was sinusoidal. The experiments were visualized using a 10x PL Fluotar objective in a JenaLumar epifluorescent microscope (Zeiss, Jena, Germany) employing the appropriate excitation and emission filters (green fluorescence Ex 505nm, Em 515nm; red fluorescence Ex 585nm, Em 605nm). Both back lighted and the fluorescent images were captured using an Optronics 24-bit RGB CCD camera (Goleta, CA, USA). The image data was processed using a Canopus ADVC-55 video capture card (San Jose, CA, USA) connected to a laptop computer using Windows Movie Maker. The final fluorescence data was analyzed by inputting individual fluorescent image frames of the video into MATLAB (Mathworks, Natick, MA, USA). The 3D representations in Figures 3.4ab and 3.6bdfh were obtained through MATLAB modeling. The average scatter plot graphs of radius vs. intensity in Figure 3.4 and Figure 3.5def were also created using MATLAB analysis of individual electrodes using polar coordinates from center with pixel distance from center being the measure of distance, then summing up all the fluorescent intensities of each pixel and then dividing by the number of pixels to obtain mean pixel intensity for that distance.

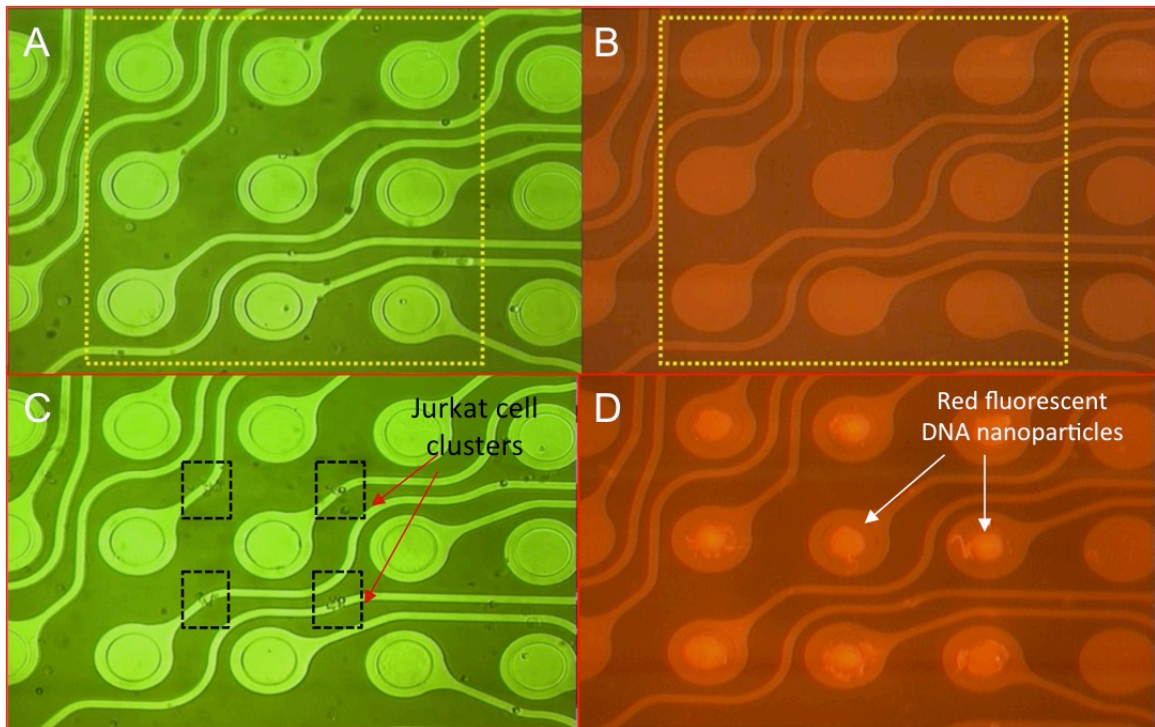


Figure 3.2. Shows the DEP separation of 40nm red fluorescent nanoparticles from Human Jurkat (T Lymphocyte) cells. Figure 3.2A and 3.2B show the microelectrode array in bright field and red fluorescence, before the DEP field is applied. Figure 3.2C and 3.2D show the concentration of the Jurkat cells into the low field regions and concentration of the 40nm red fluorescent nanoparticles into the high field regions after the DEP field is applied for 5 minutes.

3.3 Results and Discussion

3.3.1 Low Conductivity and Cell Experiments

In previous work, the separation of 40nm DNA derivatized red fluorescent nanoparticles from 10 μ m microspheres was demonstrated in high conductivity buffers (>100 mS/m) [27]. In those experiments the 40nm DNA derivatized red fluorescent microspheres were used as an analog for high molecular weight (hmw) DNA nanoparticulates found in blood, and the 10 μ m microspheres were used as an analog for cells. The following experiment now demonstrates the DEP separation of 40nm red fluorescent nanoparticles from Human Jurkat (T Lymphocyte) cells. In this experiment, 1 μ l of $\sim 10^6$ Jurkat cells/mL in media was added to 199 mL of 1x TBE containing 1.4×10^{12} particles/mL of the 40nm red fluorescent nanoparticles. Figures 3.2A and 3.2B show the microelectrode array in bright field and red fluorescence, before the DEP field is applied. A random distribution of the cells and nanoparticles is seen with no specific concentration at any given point. Nine microelectrodes are then activated in the checkboard fashion (Figure 3.1D) for 5 minutes at 10kHz, 10Vpk-pk. After 5 minutes, the Jurkat cells form clusters in the low field region (Figure 3.2C see black dashed boxes) and the 40nm red fluorescent nanoparticles have concentrated onto the high field regions of the microelectrodes (Figure 3.2D). Further experiments in low conductivity buffer were performed to demonstrated the basic capability of DEP to rapidly separate both 40nm DNA derivatized red fluorescent nanoparticles at 1.42×10^{12} nanoparticles/mL and 200nm yellow-green fluorescent nanoparticles at 1.13×10^{10} nanoparticles/mL in 0.01x TBE (1.81

mS/m) from $10\mu\text{m}$ microspheres at 1×10^5 microspheres/mL. In these experiments nine microelectrodes are activated in a checkboard fashion for 20 minutes at 10kHz, 10Vpk-pk. Figures 3.3A and 3.3C show the microelectrode array in green light and red fluorescence before the DEP field is applied. A random distribution of the $10\mu\text{m}$ microspheres and 40nm DNA derivatized red fluorescent nanoparticles is seen with no specific concentration. After 20 minutes of DEP, the $10\mu\text{m}$ microspheres form clusters in the low field region (Figure 3.3B) and the 40nm DNA derivatized red fluorescent nanoparticles are concentrated into the high field regions (Figure 3.3D). In most cases, the nanoparticles are actually separated and concentrated in less than 5 minutes. For the separation of $10\mu\text{m}$ microspheres and 200nm yellow-green fluorescent nanoparticles, Figures 3.3E and 3.3G show the microelectrode array in green light and green fluorescence, before the DEP field is applied. A random distribution of the $10\mu\text{m}$ microspheres and 200nm yellow-green fluorescent nanoparticles is seen with no specific concentration. After 20 minutes of DEP the $10\mu\text{m}$ microspheres form clusters in the low field region (Figure 3.3F) and the 200nm yellow-green fluorescent nanoparticles are found highly concentrated into the high field regions of the nine activated microelectrodes (Figure 3.3H). It should be noted that in all images after DEP is carried out no fluorescent nanoparticles have concentrated onto the microelectrodes, which have not been activated (the three electrodes on the far right side of the images).

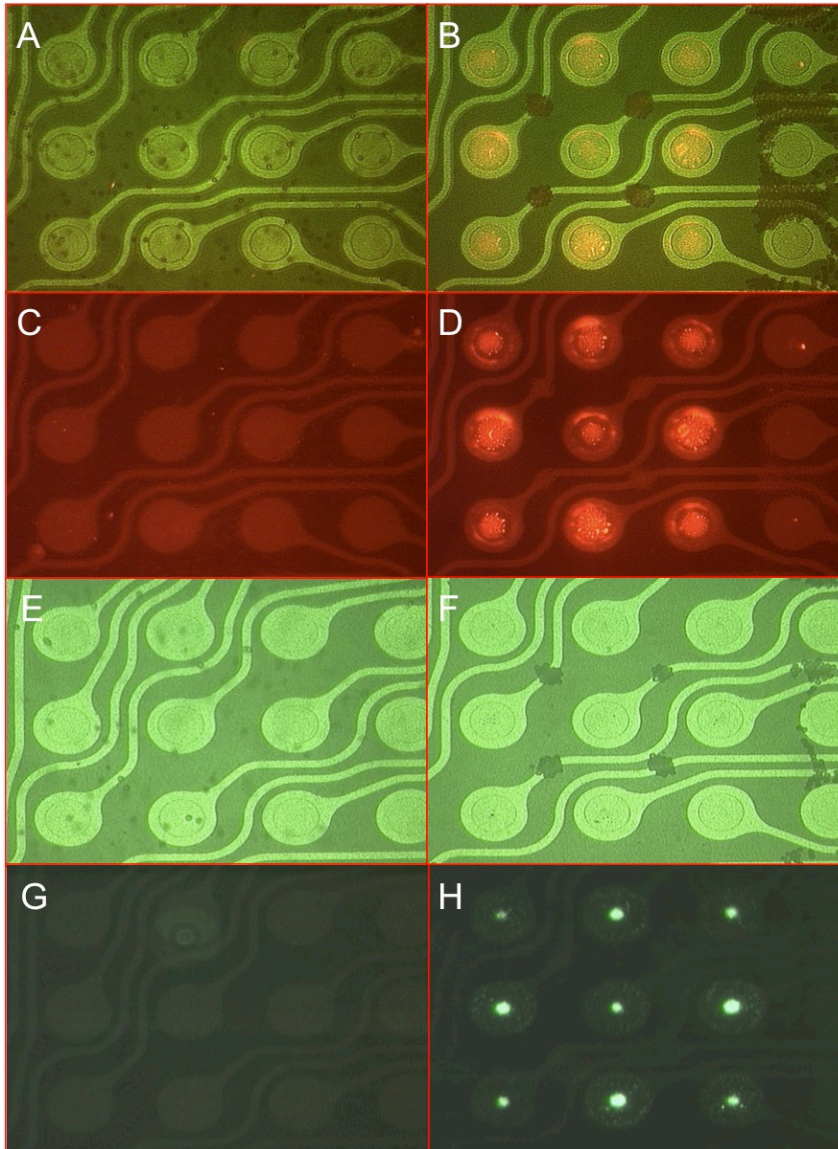


Figure 3.3. Shows the DEP separation of both 40nm DNA derivatized red fluorescent nanoparticles and 200nm yellow-green fluorescent nanoparticles from 10 μ m microspheres in 0.01x TBE (1.81 mS/m). Figures 3.3A and 3.3C show the microelectrode array in bright field and red fluorescence before the DEP field is applied. After 20 minutes of DEP, the 10 μ m microspheres form clusters in the low field region (Figure 3.3B) and the 40nm DNA derivatized red fluorescent nanoparticles are concentrated into the high field regions (Figure 3.3D). Figures 3.3E and 3.3G show the microelectrode array in green light and green fluorescence, before the DEP field is applied. After 20 minutes of DEP the 10 μ m microspheres form clusters in the low field region (Figure 3.2F) and the 200nm yellow-green fluorescent nanoparticles are concentrated into the high field regions of the nine activated microelectrodes (Figure 3.2H).

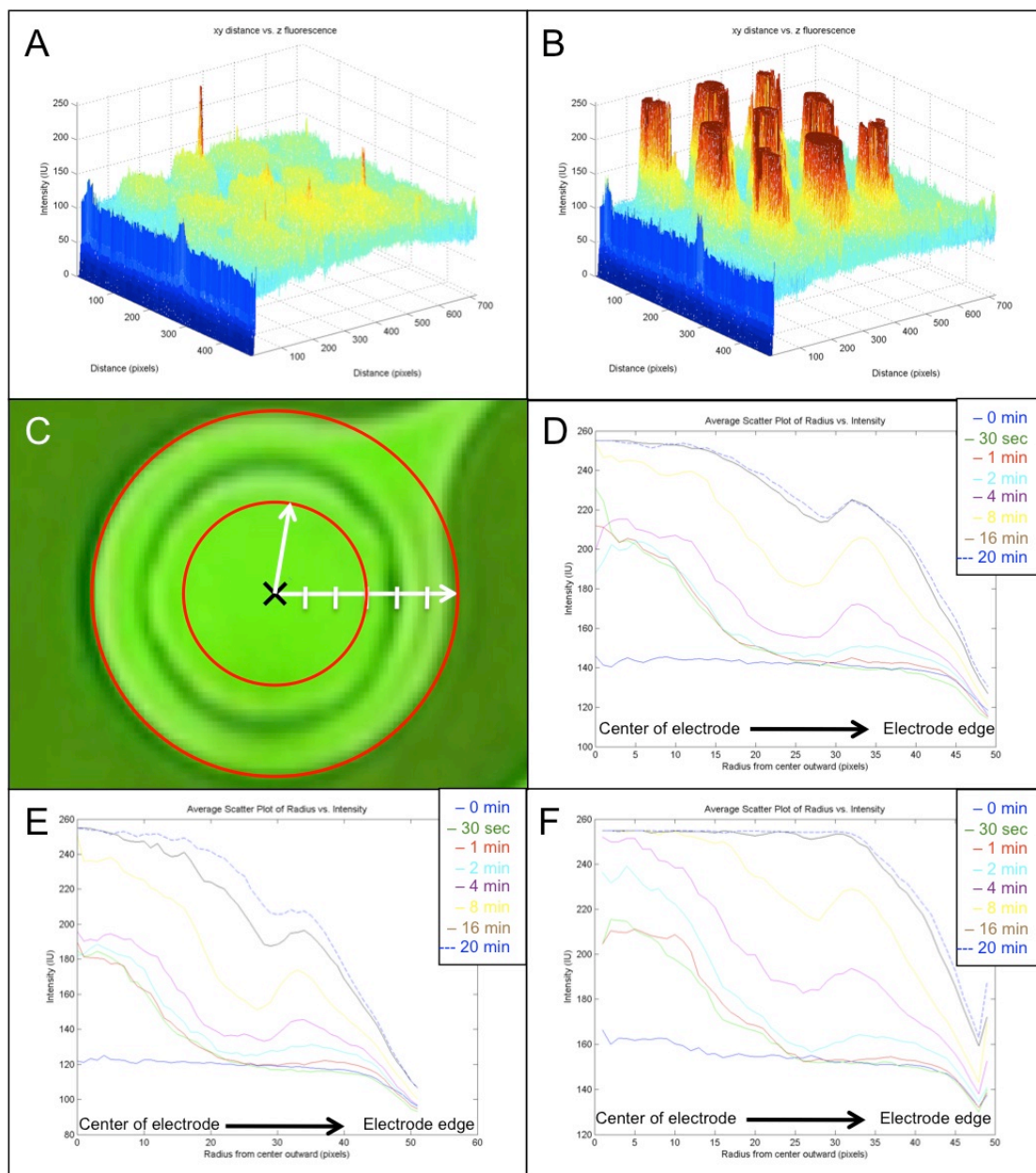


Figure 3.4. Figure 3.4A and 3.4B are the 3D representations from Figure 3.3C and 3.3D at 0 and 20 min time points, with x and y being the microelectrode dimension (actually 80mm in diameter) and the z dimension representing the relative fluorescence intensity on the surface (in arbitrary units). Figure 3.4C shows the second method of fluorescence analysis using polar coordinates to measure fluorescence through intensity vs. pixel distance from center of the microelectrode. Figure 3.4D-3.4F all show examples of concentration of the 40nm DNA derivatized nanoparticles in 0.01xTBE onto the individual microelectrodes over the 20 minute time period.

3.3.2 Fluorescence Analysis and High Conductivity Experiments

In order to analyze the concentration of fluorescence nanoparticles over time for the DEP separation of 40nm red fluorescent nanoparticles and 10mm microspheres, the whole DEP experiment was recorded on video. Images at specific time points were taken from the videos and inputted into MATLAB for further analysis. Fluorescent images corresponding to the following time points: 0 min, 30 sec, 1 min, 2 min, 4 min, 8 min, 16 min and 20 min were used for data analysis. These images were inputted into MATLAB to generate 3D mesh representations of the red fluorescence intensity data in order to better see nanoparticle concentration over time. Figure 3.4A and 3.4B are the 3-Dimensional representations from Figure 3.3C and 3.3D (0 and 20 min time points) with x and y being the microelectrode dimension (80mm in diameter) and the z dimension representing the relative fluorescence intensity on the surface (in arbitrary units). The data clearly shows the increase in red fluorescence from time 0 and 20 minutes. Figure 3.4C illustrates the second method of fluorescence detection and analysis that was used. Images were inputted into MATLAB, and polar coordinates were used for pixel distance with the microelectrode center representing pixel distance 0. At each additional pixel distance, all the fluorescent intensities were summed up and divided by the total number of pixels in polar coordinates to get the average (mean) fluorescent intensity per pixel distance from the center of the microelectrode. This was done because the nanoparticles tend to gather more toward the center of the microelectrode, and it was important to distinguish between which sections of the microelectrode have nanoparticles

gathering on them. Figure 3.4D-3.4F all show examples of individual microelectrodes over the 20 minute period for 40nm DNA derivatized nanoparticles in 0.01xTBE. The time points described earlier were used to ascertain the increase of fluorescence and its location as a function of the distance from the center of the electrode. Using the fluorescence analysis shown in Figures 3.4C-3.4F, an interesting effect of nanoparticle concentration was discovered when comparing different conductivities. Figure 3.5A and 3.5C show 40nm DNA and 200nm nanoparticles concentration in 1x TBE buffer (109 mS/m) respectively. The data is similar to that in Figure 3.4D-3.4F. However, when the same experiment was carried out in 1x PBS (1.68 S/m) which is roughly 15x the conductivity, the areas of nanoparticle concentration differ. As seen in Figure 3.5B which represents 40nm DNA nanoparticles and Figure 3.5D which represents 200nm nanoparticles in 1x PBS, the areas of nanoparticle concentration are skewed further towards the edges of the microelectrodes rather than the center over the 20 minute time points. In fact there is a decrease in fluorescence intensity at the center of the microelectrode, which is a result of the darkening of the electrode due to electrolysis effects shown previously [27].

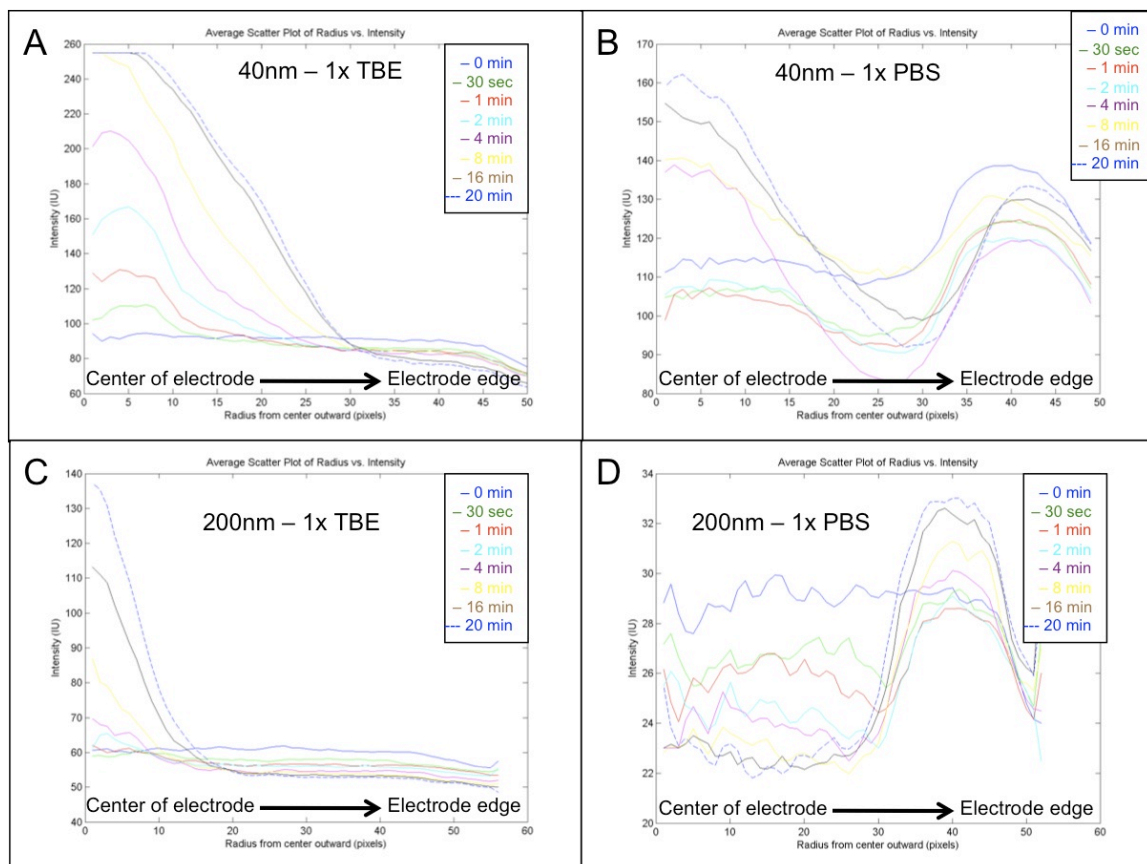


Figure 3.5. Figure 3.5A and 3.5C show the concentration of 40nm DNA derivatized nanoparticles and 200nm nanoparticles on to the microelectrodes in 1x TBE buffer (109 mS/m) vs. area of concentration on the electrode. Figure 3.5B and 3.5D shows the same for 40nm DNA derivatized nanoparticles and 200nm nanoparticles onto the microelectrodes in 1x PBS (1.68 S/m).

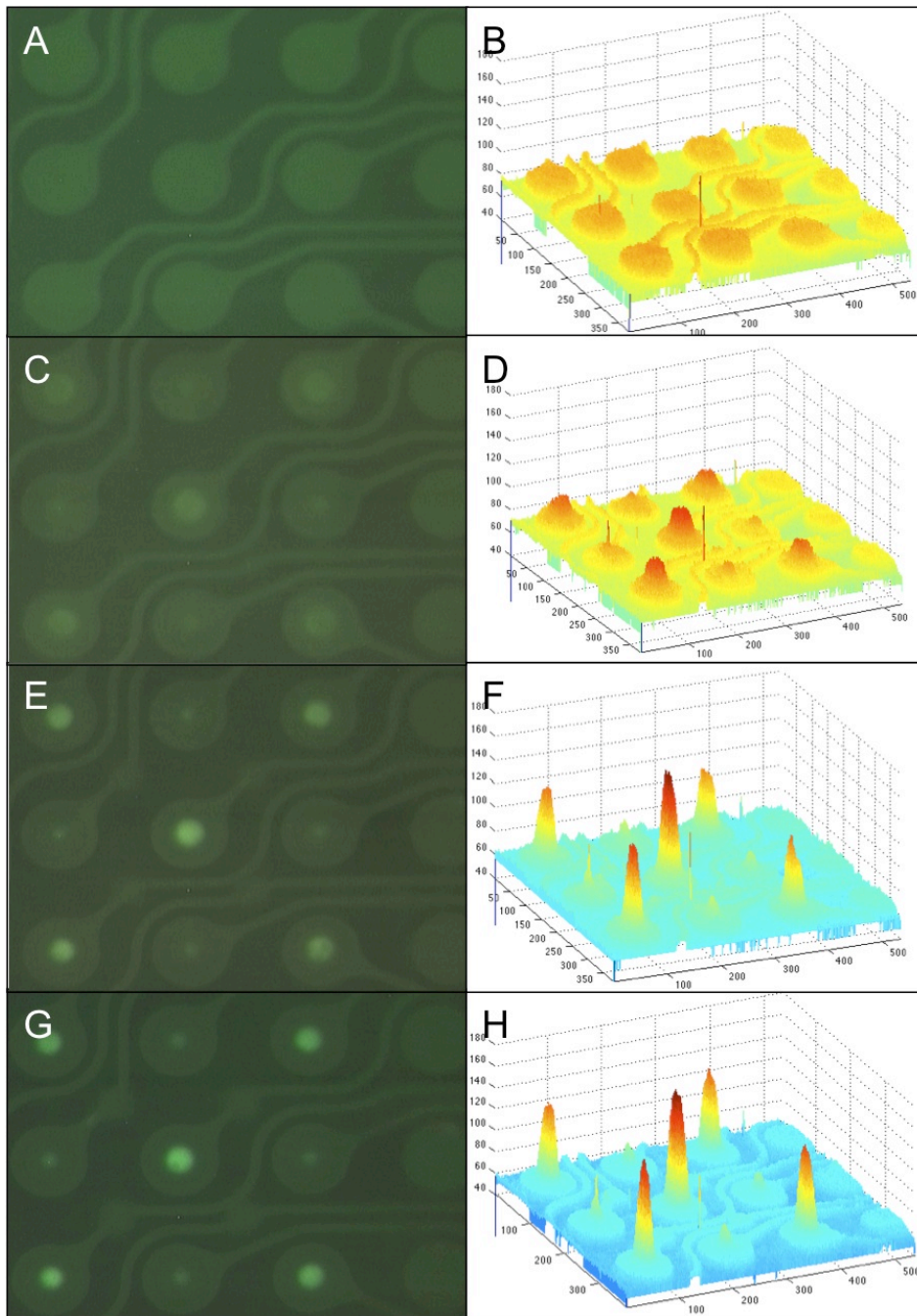


Figure 3.6. Shows the DEP separation of hmw-DNA and 10 μ m microspheres in 1x TBE (109mS/m). Figure 3.6A, 3.6C, 3.6E and 3.6G show green fluorescent images of the OliGreen fluorescent stained hmw-DNA concentrating into the high field regions at time points: 0 min, 1 min, 3 min and 5 min. Figure 3.6B, 3.6D, 3.6F, 3.6H show the 3D representation of the increasing fluorescence intensity.

The final experiments being reported demonstrate the separation OliGreen fluorescent stained high molecular weight (hmw) DNA clusters (40 kb) and 10 μ m microspheres. These DEP experiments were carried out using a mixture of the OliGreen hmw-DNA at 150ng/mL with 10 μ m microspheres at 1x10⁵ microspheres/mL in 1x TBE (109mS/m). Video recording of the DEP experiment was taken for 5 minutes, and showed the concentration of the hmw-DNA into the high field regions, and accumulation of the 10 μ m microspheres in the low field regions (not shown). Figure 3.6A, 3.6C, 3.6E and 3.6G show green fluorescent views of the OliGreen fluorescent stained hmw-DNA concentrating into the high field regions at time points: 0 min, 1 min, 3 min and 5 min. Figure 3.6B, 3.6D, 3.6F, 3.6H show the 3D representation of the increasing fluorescence intensity. It can clearly be seen from the Figure 3.6 images that hmw-DNA concentrates onto the microelectrodes during the 5 minutes of DEP.

3.4 Conclusions

AC dielectrophoresis (DEP) offers a particularly attractive mechanism for concentrating nanoparticles into microscopic areas for subsequent detection by epifluorescent microscopy. However, until more recently the DEP technique has been limited to low conductance solutions. The results of this study and sets of experiments now clearly show that DEP can be used under relatively high conductance conditions to: (1) separate and concentrate nanoparticles from human Jurkat and other cells, and (2) to separate and concentrate hmw-DNA from micron size particles. The study also shows that the DEP process allows

relatively dilute nanoscale entities such as hmw-DNA and nanoparticles to be highly concentrated into defined microscopic regions in relatively short period of time. Overall, this work helps set the stage for a new generation of sample to answer diagnostic systems; i.e., a process where a complex sample is run through the device, and the specific analytes are rapidly concentrated onto microscopic locations and subsequently detected. Such devices will allow highly complex clinical and other biological samples such as blood, plasma and serum to be rapidly and directly analyzed for rare cells, DNA biomarkers and drug delivery nanoparticles.

Chapter 3, in full, is a reprint of the material as it appears in Journal of Biophotonics: Krishnan R, Heller MJ. An AC electrokinetic method for enhanced detection of DNA nanoparticles. J. Biophoton. 2009, 2(4): 253-261. The dissertation author was the primary investigator and author of this paper.

Chapter 4: INTERACTION OF NANOPARTICLES AT THE DEP MICROELECTRODE INTERFACE UNDER HIGH CONDUCTANCE CONDITIONS

Reprinted from: Electrochemistry Communications (2009)

4.1. Introduction

Dielectrophoresis (DEP) has long offered an attractive mechanism for the high-resolution separation of cells [1-2], viruses [3], DNA [4, 5], proteins [6] and non-biological nanoparticles [7]. However, until recently DEP separations had to be carried out in low conductance (ionic strength) solutions, which greatly limited practical applications for biological research or clinical diagnostics [8-13]. Now, the DEP separation of nanoparticles and DNA has been demonstrated under high conductance conditions using hydrogel over-coated microarray devices. Unfortunately, microelectrode darkening and bubbling are also observed [14, 15]. While electrochemical effects have been non-consequential for low conductance DEP applications, their effects under high conductance conditions and at lower AC frequencies [<10 kHz] are more pronounced. Thus, in order to create new viable DEP devices for biological and clinical applications, it is critically important to better understand the complex interactions and electrochemical effects that occur at the microelectrode interfaces under high conductance conditions.

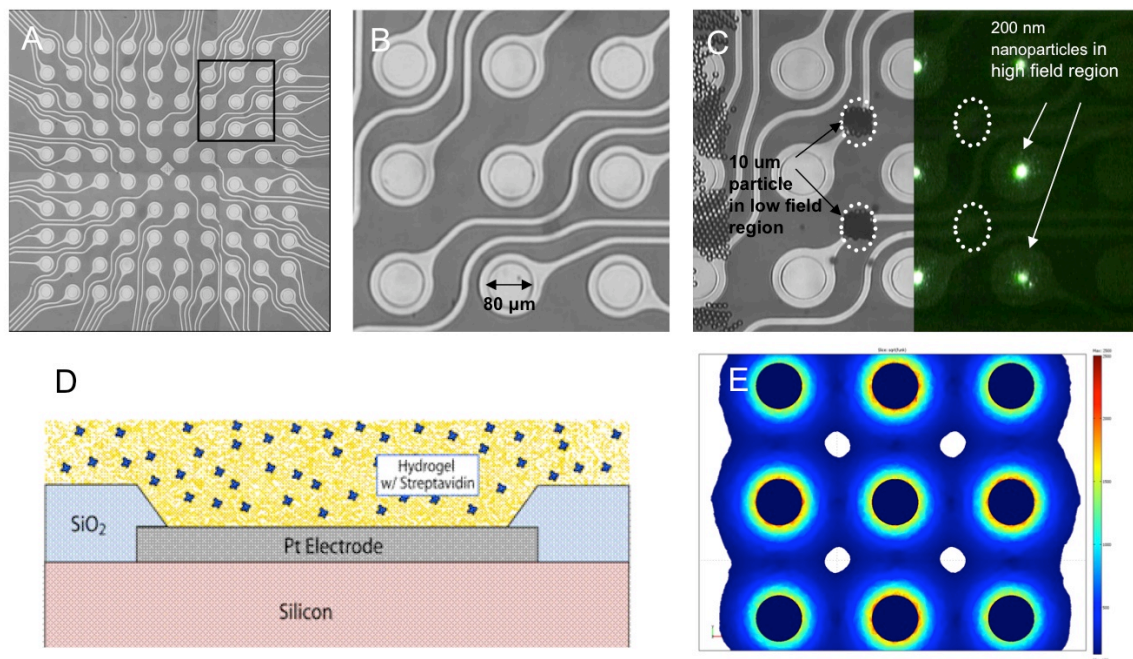


Figure 4.1. DEP experimental setup pictures. (A) Microarray with 100 platinum microelectrodes with hydrogel layer. (B) 3x3 subset of microelectrodes. (C) Composite image of half bright field/half green fluorescence showing the separation of 10μm particles into the low field regions and the fluorescent 200nm nanoparticles in the high field regions (D) Cross-sectional view of the microarray. (E) Electric field model for the microarray without the hydrogel layer, positive DEP field on edge of microelectrodes and negative DEP field between the electrodes (white circles).

4.2. Experimental Section

DEP experiments were carried out using both hydrogel over-coated platinum microelectrodes and un-coated platinum microelectrodes. Figure 4.1A shows the 100 microelectrode array device (Nanogen, San Diego, CA, USA). The circular platinum microelectrodes are 80 μ m in diameter and over-coated with a 10 μ m thick porous polyacrylamide hydrogel. Experiments involving no hydrogel layer were performed on pre-cartridge fabricated microarrays (FCOS). Only a 3x3 subset of nine microelectrodes was used for the experiments (see Figure 4.1B). Alternating current (AC) electric fields were applied to the nine microelectrodes in a checkerboard-addressing pattern [9]. Figure 4.1C shows a composite image of the separation of 10 μ m microspheres from 200nm yellow-green fluorescent (505/515) nanoparticles in 0.01x TBE on a hydrogel microarray. As demonstrated previously [14, 15], the 200nm nanoparticles concentrate in the DEP field maxima (high field regions) on the center of the microelectrode, and the 10 μ m microspheres concentrate in the DEP field minima (low field regions) between the microelectrodes. Figure 4.1D shows a cross-sectional view of the microarray. To predict nanoparticle concentration on the FCOS array, COMSOL Multiphysics Modeling (COMSOL Inc., Los Angeles, CA) was used to model the electric field. Figure 4.1E shows the electric field at the surface, with the field intensity strongest at the edge of the microelectrodes and weakest between the microelectrodes. TBE is Tris Borate EDTA buffer pH 8.3

and PBS is phosphate buffered saline (sodium chloride) pH 7.4. For more detailed information on materials and methods see references [14, 15].

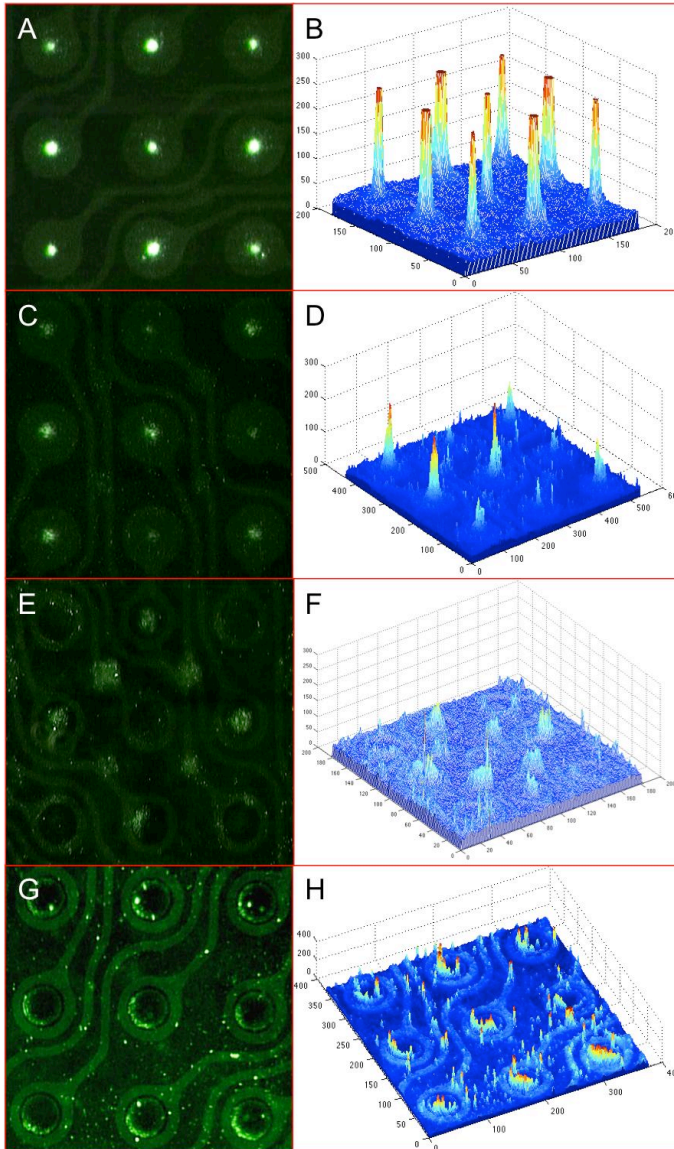


Figure 4.2. DEP separation of 200nm green fluorescent nanoparticles under different conductance conditions, with hydrogels (A-F) and without hydrogels (G-H). (A) Separation of nanoparticles into the high field regions in low conductance 0.01x TBE buffer, four minutes at 3000 Hz and 10 volts pk-pk. (B) 3D relative fluorescence intensity images (MATLAB). (C) Separation of nanoparticles into the high field regions in intermediate conductance 1x TBE buffer, four minutes at 3000 Hz and 10 volts pk-pk. (D) 3D relative fluorescence intensity images. (E) Separation of nanoparticles into the high field regions in a high conductance 1x PBS buffer, four minutes at 3000 Hz and 10 volts pk-pk. (F) 3D relative fluorescence intensity images. (G) Separation of nanoparticles into high field regions in 1x PBS without hydrogel, field applied for four minutes at 5000 Hz and 10 volts pk-pk. (H) 3D relative fluorescence intensity images.

4.3. Results and Discussion

4.3.1. High Conductivity Experiments

Initial experiments involved the separation of 200nm fluorescent nanoparticles from 10 μ m microspheres under different conductance (ionic strength) conditions on microelectrodes with hydrogels (Figure 4.2A-F), and without a hydrogel layers (Figure 4.2G-H). The DEP results for all buffers 0.01x TBE (1.81 mS/m), 1x TBE (109 mS/m), 1x PBS (1.68 S/m) show the separation of the 200nm nanoparticles into the high field regions over the microelectrodes, and the concentration of 10 μ m microspheres into the low field regions between the microelectrodes. The concentration of the nanoparticles is highest for 0.01x TBE, decreases as the buffer ionic strength increases (see Figure 4.2B, 4.2D, 4.2F, and 4.2H) and occurs more at the center of microelectrodes with hydrogels and at the perimeter for un-coated microelectrodes (Figure 4.2A, 4.2C, 4.2E, 4.2G). Significant microelectrode darkening occurred in 1x PBS for both the hydrogel over-coated microelectrodes (Figure 4.2E) and the un-coated microelectrodes (Figure 4.2G), and increased micro-bubbling occurred in 1x PBS for both the hydrogel over-coated and the un-coated microelectrodes after four minutes.

DEP was carried out in high conductivity 1x PBS buffer using un-coated microelectrodes with no nanoparticles present. The microarray was washed, dried and imaged by a Scanning Electron Microscope (SEM). Figure 4.3 shows

the light microscope images of an un-activated control microelectrode (Figure 4.3A), and an activated microelectrode (Figure 4.3B) after 10 minutes of DEP at 3000Hz, 10 volts pk-pk in 1x PBS. Figure 4.3C and Figure 4.3D shows the SEM images of an un-activated microelectrode and an activated microelectrode which is partially degraded. Figures 4.3E and Figure 4.3F are higher magnification SEM images showing further degradation of the microelectrode (Figure 4.3F). Experiments were now carried out in high conductance 1x PBS buffer with 200nm nanoparticles present. Figure 4.4A shows SEM images of the un-activated control microelectrode after two minutes of DEP at 3000Hz, 10 volts pk-pk in 1x PBS. Figure 4.4B shows a higher magnification SEM image of the edge of a control microelectrode with some nanoparticles between the edge and the dielectric material. Figure 4.4C shows the SEM image of a microelectrode activated for 2 minutes, with a large number of nanoparticles concentrated at the edge. A close-up image (Figure 4.4D) shows clusters of nanoparticles and some degradation of the microelectrode. Figure 4.4E and Figure 4.4F show images of an activated microelectrode after 5 minutes of DEP with more nanoparticle clustering and a severely degraded microelectrode. Figure 4.4G is a higher magnification SEM image of the edge of the microelectrode showing clustering of the nanoparticles. Figure 4.4H is a higher magnification image of the degraded microelectrode showing fused nanoparticles clusters.

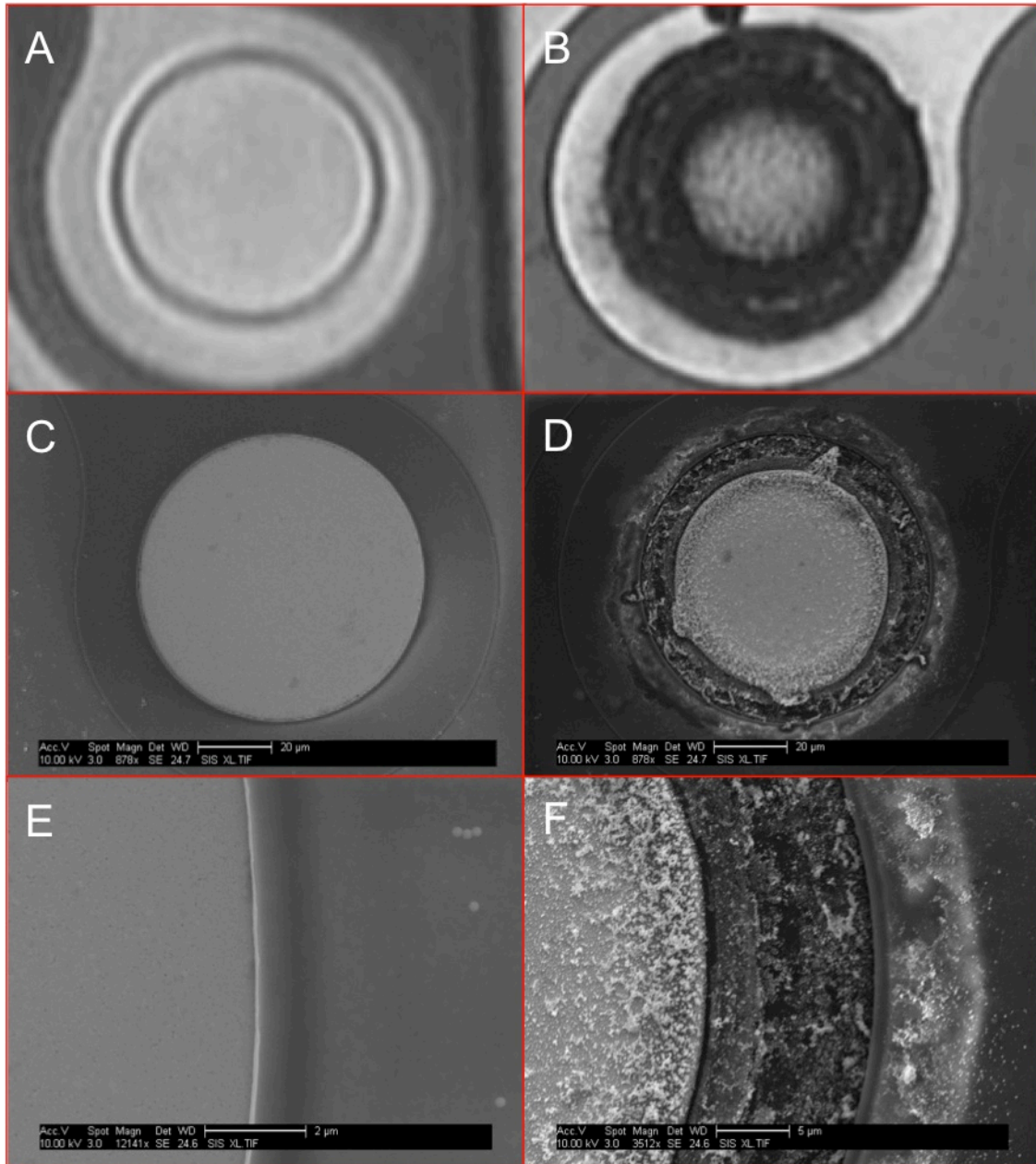


Figure 4.3. Microscope and SEM images of an un-coated control (un-activated) microelectrode and an un-coated (activated) microelectrode in high conductivity 1x PBS buffer without nanoparticles. (A) Light microscope image of the un-activated control microelectrode. (B) Light microscope image of the activated microelectrode after 10 minutes DEP at 3000Hz, 10 volts pk-pk. (C) SEM image of the un-activated control microelectrode. (D) SEM image of the activated microelectrode. (E) Higher magnification SEM image of the edge of the un-activated control microelectrode (F) Higher magnification SEM image of the edge of the activated microelectrode.

4.3.2. Electrochemical effects at microelectrode surface

In earlier DEP work a significant increase in the level of micro-bubbling and darkening of the platinum microelectrodes was observed in higher conductance buffers [14, 15]. These adverse effects were suspected to be due to increased electrochemical activity. The results of the present study now clearly show the exact nature of the microelectrode/nanoparticle/electrolyte interactions under high ionic strength conditions. Initial experiments at different ionic strength conditions with a hydrogel layer (Figure 4.2A-F), and without a hydrogel layer (Figure 4.2G-H) show: (1) the concentration of 200nm nanoparticles is highest for 0.01x TBE, and decreases as the buffer ionic strength is increased; (2) the concentration of nanoparticles occurs more at the center of microelectrodes with hydrogels, and at the outside perimeter for the un-coated microelectrodes; and (3) darkening/bubbling of the microelectrodes occurs at the highest buffer conductance (1x PBS). The un-coated microelectrodes allowed use of SEM to better analyze the electrochemical effects and to verify nanoparticle concentration. In the first experiments, DEP was carried out in high conductivity 1x PBS buffer on un-coated microelectrodes with no nanoparticles present. Figure 4.3B, 4.3D and 4.3F show that significant damage and degradation occurs on the activated platinum microelectrode after 10 minutes. Subsequent DEP experiments carried out with the nanoparticles present show after 2 minutes that a large number of nanoparticles have concentrated and adhered to the microelectrode edge (Figure 4.4C). The close-up image (Figure 4.4D) shows the

concentrated nanoparticle clusters and some degradation at the microelectrode edge. Figure 4.4E and 4.4F show, after 5 minutes of DEP, more pronounced concentration and clustering of the nanoparticles and a more severely degraded microelectrode. Such microelectrode degradation can only be produced by very aggressive electrochemical effects. Figure 4.4G is a higher magnification SEM image of the microelectrode edge showing clustering of nanoparticles, and Figure 4.4H shows nanoparticle clusters interspersed with what appears to be fused or melted nanoparticles. These fused or melted nanoparticle clusters most certainly have resulted from the aggressive electrochemical activity (heat, H^+ and OH^-) and the longer DEP times.

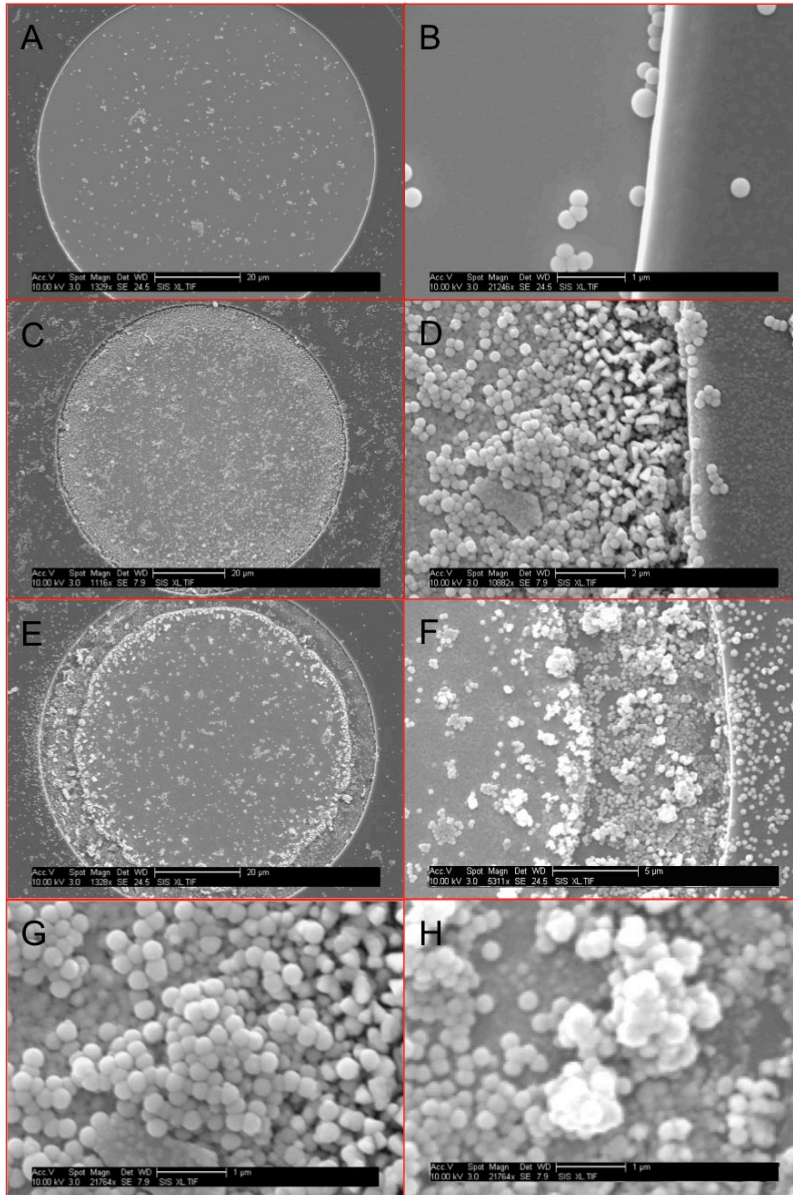


Figure 4.4. SEM images of control and DEP activated microelectrodes with 200nm nanoparticles in high conductivity 1x PBS buffer. (A) Control microelectrode with no activation with nanoparticles. (B) Higher magnification image of edge of control microelectrode. (C) Image of microelectrode activated at 5000 Hz for 2 minutes with nanoparticles. (D) Higher magnification image of the edge of the activated microelectrode. (E) Image of a microelectrode activated at 5000 Hz for 5 minutes with nanoparticles. (F) Higher magnification image of the edge of the activated microelectrodes. (G) Close-up image of the edge of the microelectrode from Figure 4.4D. (H) Close-up image of the gap left by the disintegrated microelectrode in Figure 4.4F.

4.4. Conclusions

The results of this study clearly support the earlier hypothesis [14, 15] that DEP at high conductance conditions (>200 mS/m) greatly increases electrochemical activity causing micro-bubbling and microelectrode darkening. This study also shows that significant degradation of the platinum microelectrodes is occurring under these conditions and as the DEP activation time increases. In spite of DEP being an AC electrokinetic process, these results can be directly attributed to DC electrolysis reactions, which would produce O_2 , H_2 , H^+ , OH^- , heat and bubbles. The presence of high levels of sodium (Na^+), potassium (K^+) and chloride (Cl^-) ions probably also contributes to the corrosive conditions. While the hydrogel coating *ameliorates* some of the adverse effects of the electrolysis products, which are produced on the surface of the platinum microelectrodes, darkening of the underlying microelectrodes and some bubbling is still observed. The hydrogel layer does reduce the direct effects of the electrolysis products on nanoparticles, as compared to the un-coated microelectrodes where the nanoparticles are literally fused into the degraded microelectrode structure (see Figure 4.4H). The over-coating also reduces the *active* bubbling, probably by allowing better gas diffusion and less bubble nucleation. These results immediately make it clear as to why classical DEP, which utilizes less robust sputtered gold electrodes, required low conductance conditions [7, 10-13]. While the hydrogel over-coated microelectrodes do allow separation of nanoparticles at high conductance conditions, they are far from optimal. Thus, the further identification and understanding of these limitations

now opens the door for designing more robust DEP devices for detecting nanoparticles and disease related biomarkers directly in blood and other biological samples.

Chapter 4, in full, is a reprint of the material as it appears in *Electrochemistry Communications*: Krishnan R, Dehlinger DA, Gemmen GJ, Mifflin RL, Esener SC, Heller MJ. Interaction of nanoparticles at the DEP microelectrode interface under high conductance conditions. *Electrochem. Comm.* 2009, 11(8): 1661-1666. The dissertation author was the primary investigator and author of this paper.

Chapter 5: ISOLATION AND DETECTION OF DNA NANOPARTICULATES DIRECTLY FROM BLOOD

5.1 Introduction

Two major challenges for new clinical diagnostics are the detection of early disease biomarkers and the ability to carry out such diagnostics in point-of-care (POC) settings.[1-3] Cell free circulating DNA nanoparticulates represent an important class of biomarkers for early cancer detection and screening [4], residual disease detection [5] and chemotherapy monitoring.[6] Cell free circulating DNA nanoparticulates are a heterogeneous mix of high molecular weight (hmw) DNA clusters and macromolecules that are a *potential generic and specific* early disease biomarker released by many hematological cancers and solid tumors.[7-8] DNA nanoparticulates are produced during the necrotic death of cancer cells, and are not normally present in blood. [9-10] Low level amounts of low molecular weight (lmw) DNA are present in normal blood samples. [7] For early stage disease diagnostics, it will be necessary to detect the DNA nanoparticulate biomarkers at concentrations of less than 100ng/mL of blood. [4-7] Presently, these biomarkers cannot be *directly* isolated or detected in whole blood and samples must be processed to either plasma or serum, from which the DNA is extracted. Unfortunately, the overall process for isolating DNA biomarkers is complex, expensive and time consuming. [4-12] Adding even more challenge is the fact that an initially large blood sample (1-20ml) may be needed for these assays because of the low level of biomarker present in early stage disease.

Thus, the sample preparation (from whole blood) is more often the weak link in diagnostics than the intrinsic sensitivity of the downstream detection technology (PCR, bionanosensors, etc.). The sample preparation process for blood involves centrifugation, filtration, washing, extractions and a number of other steps, before the DNA can be analyzed and genotyped by PCR or DNA sequencing [4-12] (to determine cancer type). The extended amount of time between blood drawing, cell separation, DNA extraction and the final DNA analysis also leads to significant loss of sensitivity and selectivity, degradation of the hmw-DNA and the introduction of extraneous DNA from normal cells damaged in the process.[8-9]

The difficulty and expense for carrying out the isolation of DNA nanoparticulates from blood has prevented these important biomarkers from being widely used for cancer diagnostics, and completely precludes it from any rapid and cost-effective point of care (POC) or early screening applications. Additionally, with the enormous amount of activity now being directed at new drug delivery nanoparticle therapeutics, it will also be important to develop rapid, sensitive and inexpensive blood monitoring techniques for this nanomedicine application.[2, 13-15]

Thus, there is a critical need for novel robust technology and devices, which will allow a variety of important nanoscale entities to be manipulated, isolated and rapidly detected directly from whole blood and other biological samples. Dielectrophoresis (DEP) is an intrinsically powerful technique for separating human cells, bacteria, virus, nanoparticles and biomolecules [16-19].

DEP is the induced motion of particles produced by the dielectric differences between the particles and media in an asymmetric alternating current (AC) electric field.[20] For spherical particles, the DEP force equation is given by:

$$F_{DEP} = 2\pi\epsilon_m r^3 \text{Re}[K(\omega)] \nabla E_{RMS}^2 \quad (1), \text{ where}$$

$$\text{Re}[K(\omega)] = \text{Re}\left(\frac{\epsilon_p^* - \epsilon_m^*}{\epsilon_p^* + 2\epsilon_m^*}\right) \quad (2)$$

where ϵ_p^* and ϵ_m^* are the complex dielectric permittivities of the particle and medium respectively, defined by $\epsilon^* = \epsilon - j\sigma/\omega$, where $j^2 = -1$, ϵ is the dielectric constant and σ is the conductivity. If a particle has a positive $\text{Re}[K(\omega)]$, it will migrate to the high field regions, and if it has a negative $\text{Re}[K(\omega)]$, it will migrate to the low field regions. Unfortunately, the use of DEP for any practical application has been greatly limited by the need to carry out the process under low conductance (ionic strength) conditions [21-22]. This means that blood or any other high ionic strength biological sample (plasma, serum, urine) or buffer has to be significantly diluted before DEP can be carried out. [23] Recently, we have developed a high conductance (HC) DEP method that allows both hmw-DNA nanoparticulates and polystyrene nanoparticles to be manipulated, isolated and detected under high ionic strength conditions [24-26]. We now show in this study that hmw-DNA can be isolated and detected directly from whole blood and buffy coat blood samples. HC-DEP sets the stage for new “seamless” sample to answer diagnostic systems, which will allow a variety of important nanoscopic disease biomarkers and nanoparticles to be rapidly isolated and analyzed from clinically relevant amounts of complex un-diluted biological samples.

5.2 Experimental

5.2.1 DEP Microelectrode Array and Nanoparticle Separation Process

All high conductance dielectrophoresis (HC-DEP) experiments were carried out using a microelectrode array device with 100 circular platinum microelectrodes 80 μ m in diameter (Figure 5.1a). The microarray is over-coated with a 10 μ m thick porous polyacrylamide hydrogel layer and enclosed in a microfluidic cartridge which forms a 20 μ L sample chamber. Only a 3x3 subset of microelectrodes was used for the DEP experiments (Figure 5.1b) however, all 100 microelectrodes could be used if desired. AC electric fields were applied to the nine microelectrodes in a checkerboard-addressing pattern where each microelectrode has the opposite bias of its nearest neighbor. The computer model [24-26] for the asymmetric electric field distribution produced by this pattern shows the DEP positive (high field) regions are on the microelectrodes, and the DEP negative (low field) regions are between the microelectrodes (Figure 5.1c). For AC frequencies in the 5000Hz to 10,000Hz range, nanoparticles, cellular nanoparticulates (hmv-DNA, mitochondria, antibody complexes, etc.), virus and other nanoscale entities from about 10nm to 500nm will concentrate in the DEP high-field regions over the microelectrodes, while micron-size particles and cells will concentrate in the low-field regions between the microelectrodes [24-26]. While HC-DEP at 5000 to 10,000 Hz frequencies provides a general nanoscopic window into blood, it should be kept in mind that at higher AC frequencies (>10,000Hz) DEP has the intrinsic ability for higher

resolution separation of different nanoparticles based on their AC cross-over frequency and dielectric properties [27-30]. The general scheme for the HC-DEP separation for hmw-DNA nanoparticulates and nanoparticles from whole blood (red and white cells) is shown in Figures 5.1d-f. When the DEP field is applied, the DNA nanoparticulates (green dots) concentrate into the high-field regions (represented as domes) where they are held firmly on the microelectrodes, and blood cells move into the low-field regions between the microelectrodes where they are held less firmly (Figure 5.1e). A simple fluidic wash easily removes the blood cells while the DNA nanoparticulates remain in the high-field regions (Figure 5.1f). The DNA nanoparticulates, which are highly concentrated in specific microscopic areas, can now be easily detected and analyzed in-situ. In the case of hmw-DNA, specific DNA fluorescent dyes can be used for detection, and the DNA can be further analyzed by PCR or other genotyping techniques.

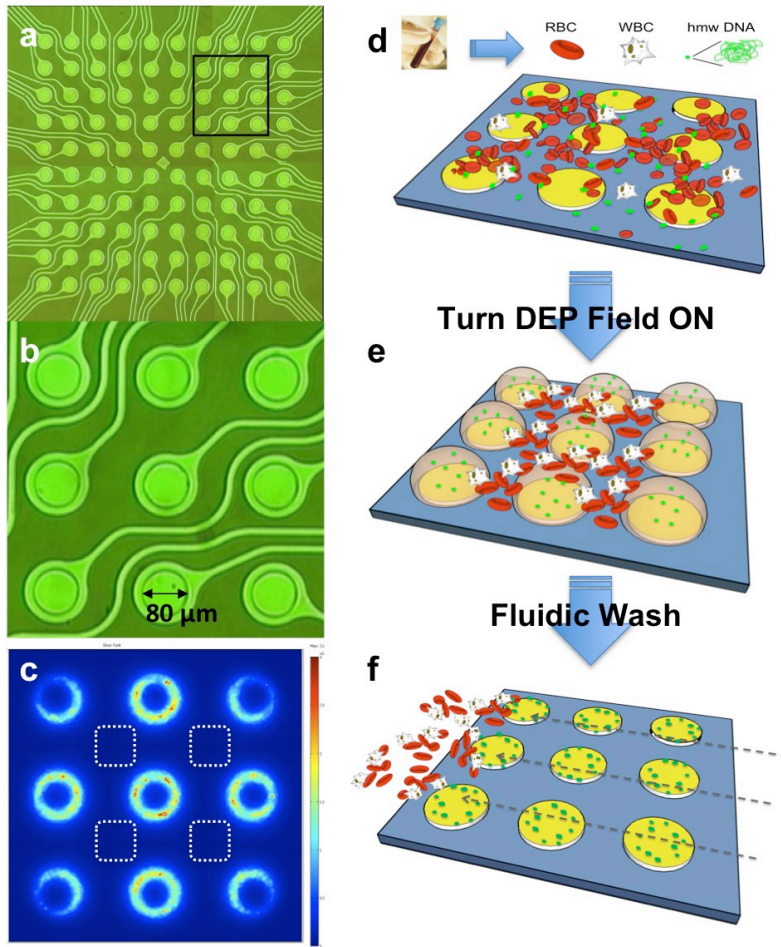


Figure 5.1. Microarray device and flow diagram for the separation of green fluorescent hmw-DNA nanoparticulates from blood. (a) Shows the electronic microarray device with 100 circular platinum microelectrodes 80 μ m in diameter, over-coated with a 10 μ m thick porous polyacrylamide hydrogel layer. Only a 3x3 subset of nine microelectrodes was used to carry out the DEP experiments in this study (b). Alternating current (AC) electric fields were applied to the nine microelectrodes in a checkerboard addressing pattern. In this addressing pattern each microelectrode has the opposite bias of its nearest neighbor. The electric field model for this geometry indicates that the positive DEP field maxima or high-field regions exist on or around the microelectrodes and the negative DEP field minima or low-field regions exist in the areas between the electrodes (white dotted square) (c). (d) Shows the diagram of the microarray with red and white blood cells and green fluorescent hmw-DNA nanoparticulates before the DEP field is applied. (e) Shows the microarray after the DEP field is applied, with the green fluorescent hmw-DNA nanoparticulates moving to the high-field regions above the microelectrodes and the red and white blood cells moving to the low-field regions between the microelectrodes. (f) Shows fluidic wash removing the blood cells, while the hmw-DNA nanoparticulates remain in the high-field regions.

5.2.2 Buffers, Blood Samples, Microparticles and Conductivity

Measurements

Concentrated 5x Tris Borate EDTA (TBE) buffer solution was obtained from USB Corporation (Cleveland, Ohio, USA), and diluted to 1x. Dulbecco's Phosphate Buffer Saline (1x PBS) solution was obtained from Invitrogen (Carlsbad, CA, USA) and diluted to 0.5x. Human Buffy Coat Blood was obtained from San Diego Blood Bank (San Diego, CA). Buffy Coat Blood contains ~1/10 the number of red blood cells as whole blood. Whole blood samples were obtained from adult female Sprague Dawley rats using proper protocols. 10.14 μ m carboxylated polystyrene particles were obtained from Bangs Labs (Fishers, IN) and 1 μ L of the stock solution was added to 300 μ L of either 1x TBE or 0.5x PBS along with the high molecular weight (hmw) DNA. Conductivity measurements were made with an Accumet Research AR-50 Conductivity meter using 2 cell (range: 10-2000 μ S) and 4 cell (range: 1-200 mS) electrodes. Buffer conductivities were: 1x TBE: 1.09 mS/cm; 0.5x PBS: 7.6 mS/cm; Whole Rat Blood: 7.7mS/cm; Buffy Coat Blood: 8.6 mS/cm.

5.2.3 High Molecular Weight (hmw) and Low Molecular Weight (lmw)

DNA

The procedure for preparing the 40-45 kb high molecular weight single-stranded (hmw-ss) DNA was described previously. [25] The hmw-ss-DNA forms a clusters or ball-like structures due to internal self-hybridization, and is a model for cell free circulating hmw-DNA. Samples of the hmw-ss-DNA were stained

using 1:100 Quant-iT™ OliGreen® (Invitrogen). The stained DNA (ex 500, em 525nm) was visualized using a fluorescent microscope. For the hmw-ss-DNA experiments (Figure 5.2), 12 μ L of the 50 μ L stock solution of RCA hmw-DNA (2nM or 260ng/mL) was added to 24 μ L of OliGreen (1:100 dilution). About 300 μ L of undiluted whole rat blood was then added to this solution. About 150 μ L was run through the microarray for the DEP experiments (final sample volume 20 μ L). Very high molecular weight (hmw) double-stranded (ds) DNA was obtained from Sigma (St. Louis, MO, *Micrococcus Luteus lysodeikticus*, Type XI, Highly Polymerized). It was diluted in 2.5mL of 1x TBE to create 2 μ g/ μ L of hmw-ds DNA. For the experiment 20 μ L of hmw-ds DNA was added to 2 μ L of 100x SYBR Green (Invitrogen), and 178 μ L of Human Buffy Coat Blood. The mixture was allowed to sit for 5 minutes, after which it was inserted into the microarray, where the DEP field was applied (Figure 5.3). For the DEP experiments involving hmw-DNA post-staining, about 20 μ L of the 50 μ L stock solution of RCA hmw DNA (2nM) and 1 μ L of the 10 μ m microspheres were added to 180 μ L of 0.5x PBS. The sample was then put into the microarray and the DEP field (10,000 Hz, 20 volts pk-pk) was applied for 10 minutes. The microarray was washed with 0.5x PBS and then 200 μ L of a mixture of 1:100 OliGreen to 0.5x PBS (200 μ L to 400 μ L) was pumped in the microarray at a rate of 40 μ L/min for 5 minutes. After the dye was added, the solution incubated for 5 minutes. To characterize the approximate size of the hmw-ss-DNA sample, a 10 μ L aliquot was stained with 1x GelRed (Biotium, Hayward, CA) and placed on a 0.7% Agarose Gel with 1x TAE buffer. The hmw-ss-DNA was run against a 10kb DNA ladder, and visualized with

a transilluminator. The hmw-DNA did not enter the gel, indicating it was >10 kb. The low molecular weight (lmw) DNA oligonucleotide sequence was obtained from Trilink Bio Technologies (San Diego, CA). The single-stranded (ss) 23mer DNA oligonucleotide with a Cy3 fluorescent dye (ex550/em570) had the sequence 5'-Cy3- ATT CCA TTC GAT TCC ATT CGA TC-3'. For the lmw-DNA experiments the sample was diluted from a 23 μ M stock solution to 150nM by adding 2 μ L of the stock DNA to 300 μ L of either 1x TBE or 0.5x PBS along with 1 μ L of the 10.14 μ m microspheres.

5.2.4 Experimental Setup and Measurements

The microarrays were controlled using a custom made switching system that allows individual control over the voltage applied to each microelectrode. The microelectrodes were set to proper AC frequency and voltages using an Agilent 33120A Arbitrary Function Generator. AC frequencies ranged from 1000Hz to 10,000Hz, at 20 volts peak to peak (pk-pk). The waveform used was sinusoidal. The experiments were visualized using a JenaLumar epifluorescent microscope (OliGreen-DNA, and SYBR Green-DNA: Ex 505nm, Em 520nm; red fluorescence nanoparticles Ex 585nm, Em 605nm; orange/red fluorescence for Cy3 Ex:560, Em:Long Pass 570). Both green light and fluorescent images were captured using an Optronics 24-bit RGB CCD camera. The image data was processed using a Canopus ADVC-55 video capture card connected to a laptop computer with Adobe Premiere Pro and Windows Movie Maker. The final

fluorescence intensity data images were created by inputting fluorescent image frames of the video into MATLAB.

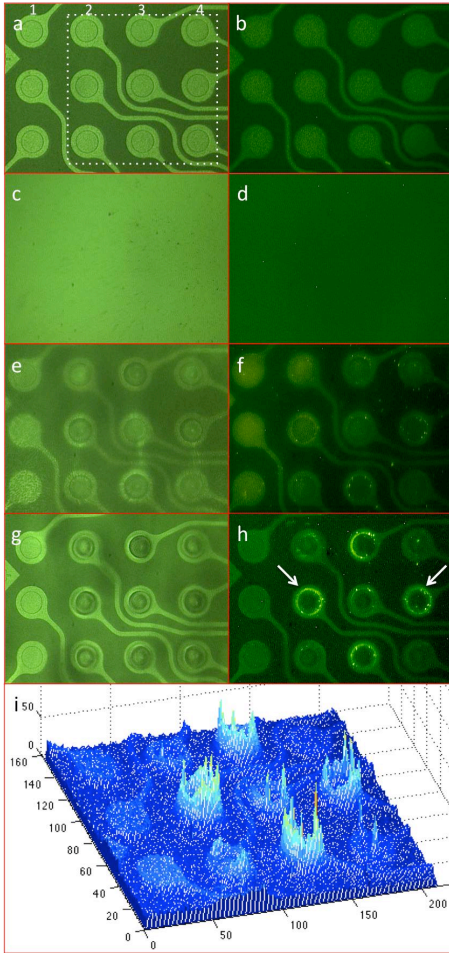


Figure 5.2. Separation and detection of fluorescent high molecular weight (hmw) single-stranded (ss) DNA in whole blood. (a, b) show the microarray in green light and green fluorescence before the whole blood sample was added. (c, d) Show the microarray in green light and green fluorescence after 20 μ L of whole blood containing 260ng/mL of fluorescent OliGreen stained hmw-ss-DNA was added, but before applying the DEP field. (e, f) Show the microarray after the DEP field was applied at 10,000 Hz and 20 volts pk-pk for 14 minutes to the nine microelectrodes, and then washed one time with 0.5x PBS with the DEP field left on. The green light image shows the microelectrodes with some cells still present, and the green fluorescent image shows fluorescence from the OliGreen stained hmw-ss-DNA concentrated around the microelectrodes. (g, h) Show the microarray after it was washed three more times with 0.5x PBS, the green light image shows no cells are present, and the green fluorescent image shows fluorescence from the hmw-ss-DNA concentrated around the nine microelectrodes. (i) 3D fluorescent intensity image showing the relative levels of fluorescence on all nine of the microelectrodes (produced using MATLAB).

5.3 Results

5.3.1 Separation of High Molecular Weight (hmw) Single-Stranded (ss) DNA in Whole Blood

HC-DEP experiments were carried out on the microelectrode array device demonstrating the separation of OliGreen fluorescent stained hmw-ss-DNA from undiluted whole blood (7.7 mS/cm). Figures 5.2a and 5.2b show the microarray in green light and green fluorescence before the sample was added. About 20 μ L of whole blood containing ~260ng/mL of hmw-DNA (~40-45kb DNA clusters stained with OliGreen fluorescent dye) was now added. Figures 2c and 2d show the microarray in green light and green fluorescence, the microelectrodes are no longer visible because of the very high cell density. The DEP field was then applied at 10,000 Hz and at 10 volts pk-pk for 14 minutes to nine microelectrodes. The microarray was washed one time with 0.5x PBS, while the DEP field was left on. The green light image shows some cells still present (Figure 5.2e), and the green fluorescent image now shows fluorescence from the hmw-DNA concentrated around the nine microelectrodes, which were activated (Figure 5.2f). Figures 5.2g and 5.2h show the microarray after washing three more times with 0.5x PBS. Figure 5.2g shows no cells are present, and the green fluorescent image (Figure 5.2h) clearly shows intense fluorescence from the hmw-DNA concentrated around the nine microelectrodes, which were activated. The three un-activated microelectrodes on the left side of the microarray show no fluorescence. The fluorescence signal appears higher for the middle microelectrodes (columns 2 and 4) and the upper and lower microelectrodes of

column 3, due to a somewhat greater electric field gradient at these high-field microlocations as shown in Figure 5.1c. Finally, Figure 5.2i is a 3D fluorescent intensity image showing the relative fluorescence levels for hmw-DNA on the nine activated microelectrodes versus the three un-activated microelectrodes. The overall time from sample application to detection was less than 30 minutes.

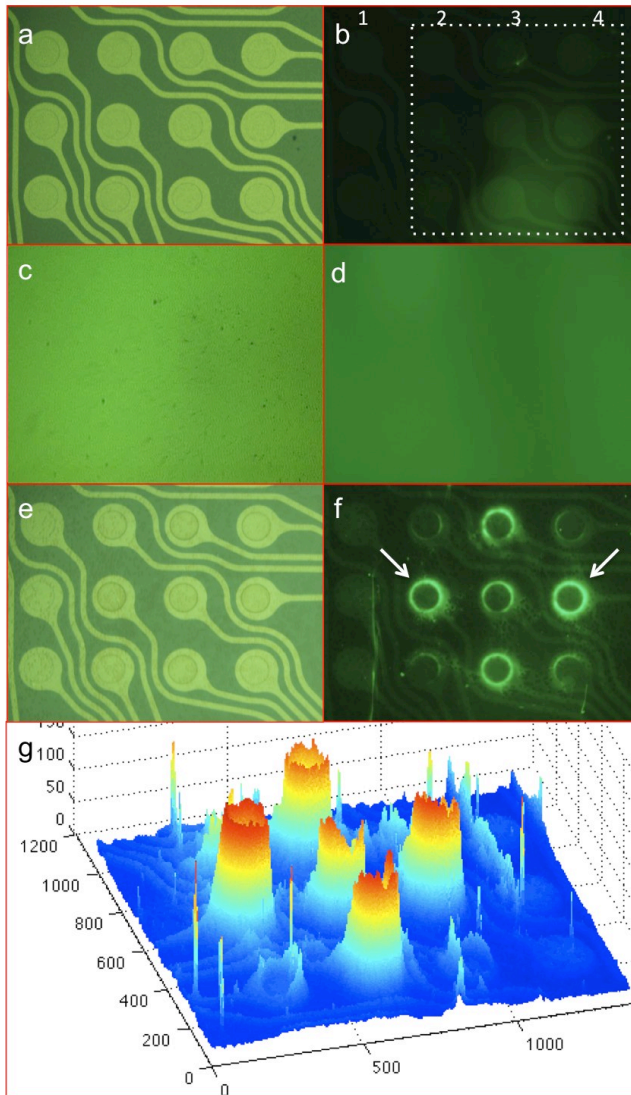


Figure 5.3. Separation and detection of fluorescent high molecular weight (hmw) double-stranded (ds) DNA in buffy coat blood. **(a, b)** Shows the microarray in green light and green fluorescence before the buffy coat blood sample was added. **(c, d)** Shows the microarray in green light and green fluorescence after 20 μ L of buffy coat blood containing \sim 200ng/ μ l of SYBR-Green stained hmw-ds-DNA was added, but before the DEP field was applied. **(e, f)** Show the microarray in green light and green fluorescence after the DEP field was then applied at 10,000 Hz and 10 volts pk-pk for 14 minutes, and the microarray was washed 3 with 0.5x PBS. Intense fluorescence from the SYBR-Green stained DNA can be seen concentrated around the microelectrodes. **(g)** is a 3D image showing the relative fluorescence intensity levels for SYBR-Green stained DNA on the nine activated microelectrodes versus the three un-activated microelectrodes (the image is the reverse of the 3f image).

5.3.2 Separation of High Molecular Weight (hmw) Double-Stranded (ds) DNA in Buffy Coat Blood

HC-DEP experiments were now carried out demonstrating the separation of SYBR Green stained high molecular weight (>40kb) ds-DNA from human buffy coat blood (8.6 mS/cm). Buffy coat blood has only 5-10% of the blood cells remaining, but actually has a higher conductivity than whole blood. Figures 5.3a and 5.3b show the microarray in green light and green fluorescence before the sample was added. About 20 μ L of buffy coat blood containing 200ng/ μ L of SYBR-Green stained hmw-ds DNA was now added to the microarray. Figures 5.3c and 5.3d show the microarray in green light and green fluorescence. Again, the microelectrodes are no longer visible because of the high cell density. The DEP field was then applied at 10,000 Hz and 10 volts pk-pk for about 15 minutes to nine microelectrodes. The microarray was washed one time with 0.5x PBS, while the DEP field was left on. The green light image shows some cells still present (Figure 5.3e), and the green fluorescent image (Figure 5.3f) now shows very intense fluorescence from the hmw-ds-DNA concentrated around the microelectrodes. Finally, Figure 5.3g is a 3D fluorescent intensity image showing the relative fluorescence levels for hmw-ds-DNA on the nine activated microelectrodes versus the three un-activated microelectrodes. The overall time from sample application to detection was less than 30 minutes.

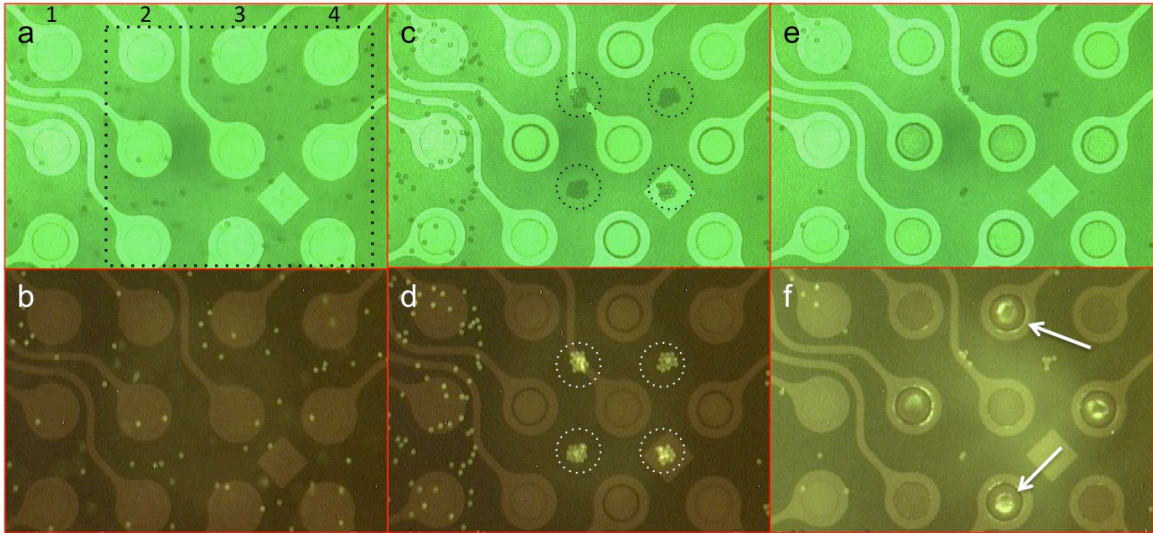


Figure 5.4. Post staining of high molecular weight (hmw) single-stranded (ss) DNA after DEP. (a, b) Show the microarray in green light and green fluorescence after a 20ul sample containing both 10µm microparticles and 800 ng/mL of hmw-ss-DNA “un-stained” in 0.5x PBS was added, but before the DEP field has been applied. A random distribution of the 10µm microparticles is seen over the microarray and the microparticles have some intrinsic green fluorescence. (c, d) Show the microarray after the DEP field was applied at 10,000 Hz and at 20 volts pk-pk for 10 minutes. Both the green light image and the fluorescent image show that the 10µm microparticles have now concentrated into the DEP low-field regions between the microelectrodes, while no fluorescence is seen in the high-field regions on or around the microelectrodes. (e, f) Show the microarray after a solution containing OliGreen fluorescent dye was flushed over the microarray at a rate of 40µL per minute for 5 minutes. The green light image shows most of the 10µm microparticles have been removed by the fluidic wash, while the green fluorescent image now shows fluorescence in the DEP high-field regions, indicating that the previously un-stained hmw-ss-DNA had been concentrated during the initial DEP process.

5.3.3 Post-Staining and Low Molecular Weight (lmw) DNA Experiments

The final two experiments were carried out to demonstrate: (1) that HC-DEP can be used to first concentrate un-labeled hmw-DNA into the high-field regions, and then post-staining can be carried out with a fluorescent dye for subsequent detection; and (2) that the same AC frequency and voltage used for isolating hmw-DNA into the high-field regions does not cause the low molecular weight (lmw) DNA (<100 bases) to concentrated. These experiments were carried out in high conductance 0.5x PBS buffer (7.6 mS/cm). For the OliGreen post-staining hmw DNA experiments, Figures 5.4a and 5.4b show the microarray in green light and green fluorescence after a 20 μ L sample containing both 10 μ m microspheres and 800 ng/mL of un-stained hmw-ss-DNA in 0.5x PBS was added. Both images show a random distribution of the microspheres over the microarray. The DEP field was then applied at 10,000 Hz and at 10 volts pk-pk for 10 minutes to nine microelectrodes. The green light image shows the microspheres have now concentrated into the DEP low-field regions (Figure 5.4c). The green fluorescent image (Figure 5.4d) shows some fluorescence from microspheres concentrated into the low-field regions, however no green fluorescent signal is observed in the DEP high-field regions around the microelectrodes. With the DEP field still activated, a solution containing OliGreen fluorescent dye was now flushed over the microarray (40 μ L/min for 5 minutes).

Figure 5.4e shows most of the microspheres have been removed by the wash, and Figure 5.4f now shows a green fluorescent signal in the DEP high-field regions. This clearly indicates that the previously un-stained hmw-ss-DNA had been captured during the initial DEP process. Finally, for the low molecular weight (lmw) DNA experiments, Figures 5.5a and 5.5b show the microarray in green light and red fluorescence before the sample was added. Figures 5.5c and 5.5d show the microarray in green light and red fluorescence after a 20 μ L sample containing both 10 μ m microspheres and 345ng/mL of fluorescent (Cy3 labeled-23mer) lmw-DNA in 0.5x PBS was added. Figures 5.5e and 5.5f show the microarray after the DEP field has been applied for 10 minutes. Figure 5.5e shows that the 10 μ m microspheres have been concentrated into the DEP low field regions, while Figure 5.5f shows no detectable fluorescent signal in the DEP high field regions indicating that the fluorescent lmw-DNA did not concentrate.

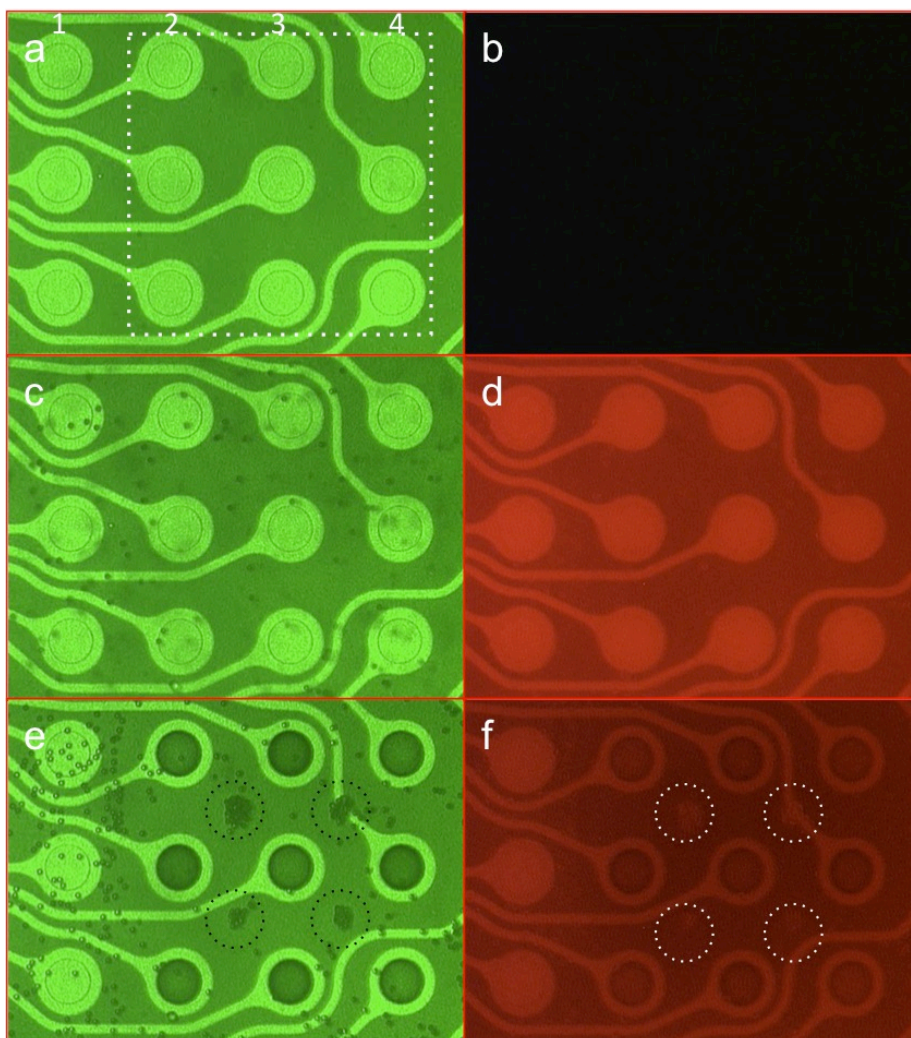


Figure 5.5. DEP of fluorescent low molecular weight (lmw) DNA. (a, b) Show the microarray in green light and red fluorescence before the sample was added. (c, d) Show the microarray in green light and red fluorescence after a 20 μ L sample containing both 10 μ m microparticles and 345ng/mL of lmw DNA in 0.5x PBS was added, but before the DEP field has been applied. (e, f) Show the microarray in green light and red fluorescence after the DEP field was applied at 10,000 Hz and at 20 volts pk-pk for 10 minutes. The green light image shows that the 10 μ m microparticles have been concentrated into the DEP low-field regions between the microelectrodes, while the fluorescent image shows no fluorescent signal concentrated in the DEP high-field regions on/or around the microelectrodes indicating that the fluorescent lmw-DNA did not concentrate.

5.4 Discussion and Conclusions

Having previously demonstrated that the DEP separation of hmw-DNA and nanoparticles from human cells and microspheres could be achieved in high conductance buffer solutions [24-26], we have now been able to show that hmw-DNA can also be isolated and detected directly from undiluted whole blood and buffy coat blood. Blood not only represents one of the most complex biological samples, but is also one of the most important for clinical diagnostics. In these studies, the hmw-ss-DNA and hmw-ds-DNA clusters served as a model for cell free circulating hmw-DNA biomarkers, which are important for early cancer screening and diagnostics. The initial experiment clearly showed the ability of HC-DEP to separate hmw-ss-DNA clusters from whole blood in about 15 minutes. The overall process time for isolation and detection of hmw DNA from the blood samples, including washing steps, was less than thirty minutes. With a fully automated fluidic system, the process time would take less than twenty minutes, and with a more robust, higher voltage DEP device (>20 volts) the total time for separation and detection could be less than 10 minutes. This DEP based method allowed for the isolation of hmw-ss-DNA at concentrations well within the range for clinically relevant DNA biomarkers at 260 ng/mL. The second HC-DEP experiment demonstrated the detection of hmw-ds-DNA from buffy coat blood within 15 minutes. Again, while buffy coat blood has only 5-10% of the blood cells remaining, its conductance is higher than whole blood. The reason is that the cells in blood add resistance to the flow of ions in the fluid. Since resistance is

the inverse of conductance, the more cells that are in blood, the greater the resistance and the lower the conductance. [31-32] Buffy coat blood (~8 mS/cm) more closely approaches the conductance of plasma (~10 mS/cm). Thus, this experiment shows hmw-DNA can be isolated from even high conductance biological samples.

The final two HC-DEP experiments were important because they verified: (1) that un-labeled hmw-DNA could first be concentrated into high field regions, and then post-stained for subsequent detection; and (2) that the same AC frequency (10,000 Hz) used for isolating hmw-DNA does not cause lmw-DNA (<100 bases) to concentrate. The ability to post-label a specific biomarker or analyte will prove to be a significant advantage for future diagnostic applications. The lmw-DNA results demonstrated that HC-DEP in the 10kHz range has a selectivity window that allows red and white blood cells and 10 μ m particles to be concentrated into low field regions, hmw DNA and nanoparticles to be concentrated into the high field regions, while low molecular weight molecules (lmw DNA) are not affected by the process. Additionally, an experiment was run in which we attempted to concentrated Texas-red labeled Streptavidin, roughly the same size and molecular weight as albumin in blood, and were unable to do so under the same conditions (un-published results). Since we are not seeing accumulation of streptavidin onto the high-field regions, we believe that the DEP field in these frequency ranges does not affect small protein molecules, such as albumin.

Some DEP device performance limitations were observed in these experiments, which included the formation of bubbles on some of the microelectrodes and darkening of the microelectrodes. As was discussed in previous work [24-26], heat and DC electrochemistry leads to this bubble formation and the darkening of the microelectrodes. Work is now in progress on developing more robust high performance DEP devices. Overall, this work sets the stage for a new generation of “seamless” sample to answer diagnostic systems; i.e., where a complex sample (blood, plasma, urine, etc.) is run through the HC-DEP device, and rare cells, bacteria, virus, drug delivery nanoparticles and various disease biomarkers are rapidly concentrated onto known microscopic locations for subsequent detection. The HC-DEP method is unique in that cells or biomarkers can be labeled either before or after the separation process. Additionally, molecular biological detection techniques including PCR and immunochemistry are compatible with the HC-DEP process, and can be easily carried out in-situ i.e., in the same sample chamber used to achieve separation. The ability to have a seamless sample to answer system for early disease screening also means that these important molecular diagnostics could be carried more cost effectively and in point-of-care settings.

Chapter 5, in full, is currently being prepared for submission for publication of the material: Krishnan R, Marciniak JY, Sonnenberg AV, Carson DA, Esener SC, Heller MJ. Isolation and detection of DNA nanoparticulates directly from blood. The dissertation author was the primary investigator and author of this paper.

Chapter 6: SEPARATION OF NANOPARTICLES DIRECTLY FROM BLOOD FOR NANOMEDICINE APPLICATIONS

6.1 Introduction

While the potential applications of nanotechnology in medicine are rapidly growing, a number of issues still need to be resolved before nanomedicine translates from the lab to the bedside. [1] Two important challenges will be the monitoring of drug delivery nanoparticles and the detection of cell free circulating (cfc) DNA nanoparticulate biomarkers. [2,3] Presently, considerable research efforts are being carried out on the development of new drug delivery nanoparticle therapeutics. [4,5] For both research and clinical applications it will be important to develop rapid, sensitive and inexpensive monitoring techniques for determining levels of drug delivery nanoparticles directly in patient blood. [2,6-8]. In another related area, the ability to detect cfc-DNA, cfc-RNA and other cell free circulating nanoparticulate biomarkers directly in blood would represent a major advance for early cancer screening [9], residual disease detection [10] and chemotherapy monitoring.[11]

Unfortunately, present methods for isolating nanoparticles and nanoparticulate biomarkers in the 10nm to 500nm range from blood are complex, expensive and time consuming [6-11]. Adding even more challenge is that relatively large blood samples (1-10ml) are needed when assaying for very low

levels of nanoparticles or biomarkers. Thus, sample preparation is more often the weak link in monitoring and diagnostic assays than is the intrinsic sensitivity of the downstream detection technology. The sample preparation process for blood often involves centrifugation, filtration, washing, extractions and a number of other steps before the analyte(s) can be identified [6-11]. The extended amount of time between blood drawing, cell separation, analyte extraction and the final analysis also leads to significant loss of sensitivity and selectivity, and to the degradation of the analytes [9-11]. Thus, there is a critical need for a novel robust technology, which will allow a variety of nanoscale entities to be manipulated, isolated and rapidly detected **directly** from whole blood and other biological samples. Meeting this challenge will be required before therapeutic monitoring can be carried out in cost-effective point of care (POC) settings.

Dielectrophoresis (DEP) is an intrinsically powerful technique for separating cells and nanoparticles [12-17]. DEP is the induced motion of particles produced by the dielectric differences between the particles and media in an asymmetric alternating current (AC) electric field [18]. For spherical particles, the DEP force equation is given by:

$$F_{DEP} = 2\pi\epsilon_m r^3 \text{Re}[K(\omega)] \nabla E_{RMS}^2 \quad (1), \text{ where}$$

$$\text{Re}[K(\omega)] = \text{Re}\left(\frac{\epsilon_p^* - \epsilon_m^*}{\epsilon_p^* + 2\epsilon_m^*}\right) \quad (2)$$

where ϵ_p^* and ϵ_m^* are the complex dielectric permittivities of the particle and medium respectively, defined by $\epsilon^* = \epsilon - j\sigma/\omega$, where $j^2 = -1$, ϵ is the dielectric

constant and σ is the conductivity. If a particle has a positive $\text{Re}[K(\omega)]$, it will migrate to the high field regions, and if it has a negative $\text{Re}[K(\omega)]$, it will migrate to the low field regions. Unfortunately, the use of DEP for practical applications has been limited by the need to carry out the process under low conductance (ionic strength) conditions. [19-20] Thus, blood or any other high ionic strength sample has to be significantly diluted before DEP separations can be carried out. [20] Recently, we have developed a high conductance (HC) DEP method that allows both nanoparticles and hmw-DNA nanoparticulates to be manipulated, isolated and detected under high ionic strength conditions [21-23]. We now show in this study that fluorescent nanoparticles can be isolated and detected directly from whole blood samples in clinically relevant ranges. HC-DEP sets the stage for new “seamless” sample to answer systems, which will allow a variety of drug delivery nanoparticles and other nanoscale biomarkers to be rapidly isolated and analyzed from clinically relevant amounts of complex un-diluted biological samples.

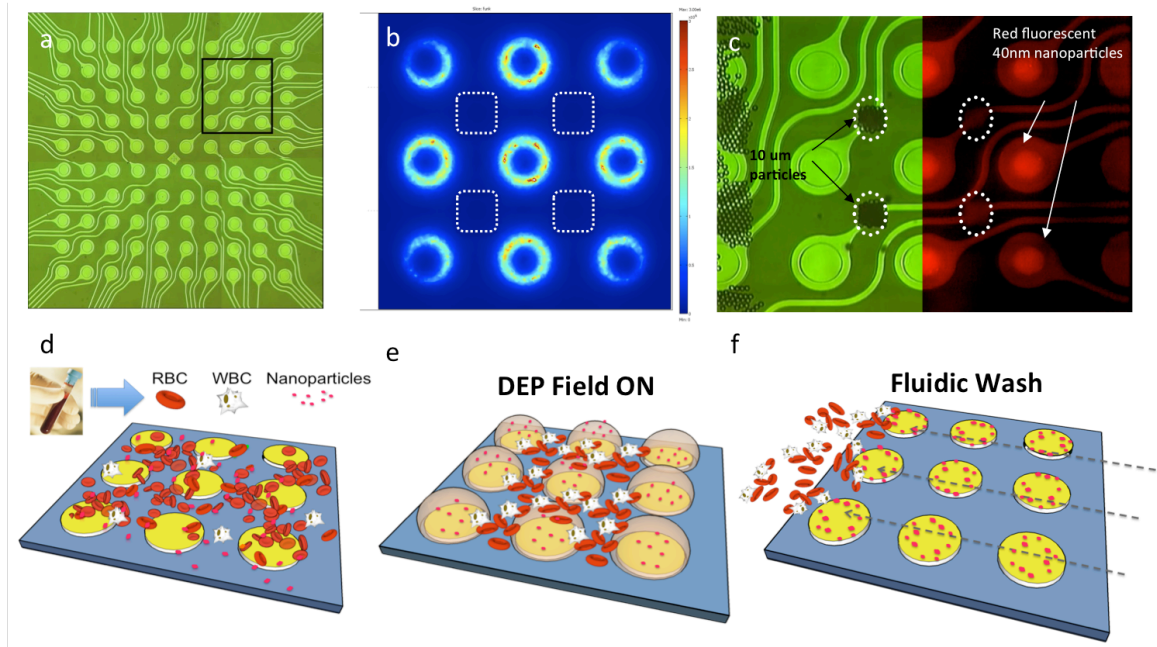


Figure 6.1. Microarray device and flow diagram for the separation of nanoparticles from blood. **(a)** Shows the electronic microarray device with 100 circular platinum microelectrodes $80\mu\text{m}$ in diameter, over-coated with a $10\mu\text{m}$ thick porous polyacrylamide hydrogel layer. Only a 3×3 subset of nine microelectrodes was used to carry out the DEP experiments in this study. **(b)** Alternating current (AC) electric fields were applied to the nine microelectrodes in a checkerboard addressing pattern. The electric field model for this geometry indicates that the positive DEP field maxima or high-field regions exist on or around the microelectrodes and the negative DEP field minima or low-field regions exist in the areas between the electrodes (white dotted square). **(c)** Shows a composite half bright field/half red fluorescence image for a prior DEP separation where $10\mu\text{m}$ particles are isolated into the low-field regions and red fluorescent 40nm nanoparticles are concentrated into the high-field regions **(d)** Shows the diagram of the microarray with red and white blood cells and red fluorescent nanoparticles before the DEP field is applied. **(e)** Shows the microarray after the DEP field is applied, with red fluorescent nanoparticles moving to the high-field regions above the microelectrodes and the larger red and white blood cells moving to the low-field regions between the microelectrodes. **(f)** Shows fluidic wash removing the blood cells, while the nanoparticles remain in the high-field regions.

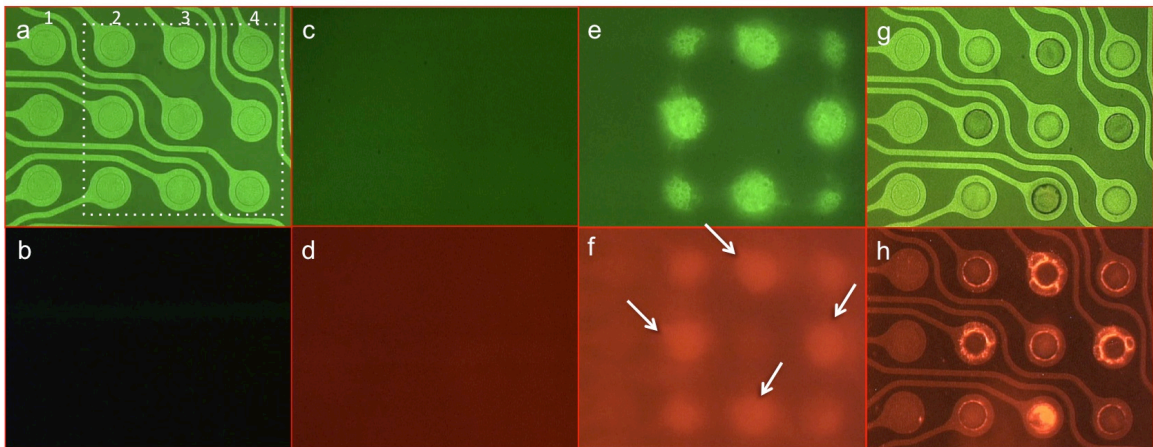


Figure 6.2. Separation and detection of 40nm red fluorescent nanoparticles in buffy coat blood. (a, b) Show the microarray in bright field and red fluorescence before the buffy coat blood sample was applied to the microarray. (c, d) Show the microarray in bright field and red fluorescence after 20 μ L of buffy coat blood containing about 300ng/ul of 40nm red fluorescent nanoparticles were added to the microarray, but no DEP field has been applied. (e, f) Show the microarray after the DEP field has been applied for 12 minutes at 10,000 Hz and at 20 volts pk-pk to a set of nine microelectrodes (columns 2, 3, and 4), while the three electrodes in the column 1 remained un-activated. The blood cells begin to move away from the microelectrodes while the red fluorescent nanoparticles begin to concentrate on the microelectrodes. (g, h) Show the microarray after it was washed with 0.5x PBS buffer to remove the buffy coat blood cells, the red fluorescent image now shows the fluorescent nanoparticles concentrated on the microelectrodes.

6.2 Materials and Methods

6.2.1 DEP Device

In these studies, all HC-DEP experiments were carried out using an electronic microarray device with 100 circular platinum microelectrodes 80 μ m in diameter (Figure 6.1a). The microarray is over-coated with a 10 μ m thick porous polyacrylamide hydrogel layer and enclosed in a microfluidic cartridge, which forms a 20 μ L sample chamber. While only a 3x3 subset of microelectrodes was used for the DEP experiments, all 100 microelectrodes can be used if desired. AC electric fields were applied to the nine microelectrodes in a checkerboard-addressing pattern where each microelectrode has the opposite bias of its nearest neighbor. Figure 6.1b shows the asymmetric electric field distribution, which produces DEP positive (high-field) regions on the microelectrodes and the DEP negative (low-field) regions between the microelectrodes [21-23]. At AC frequencies in the 5000Hz to 10,000Hz range, nanoparticles, hmw-DNA and other cellular nanoparticulates from about 10nm to 500nm in size will concentrate in the DEP high-field regions over the microelectrodes, while micron-size particles and cells will concentrate in the low-field regions. Figure 6.1c shows a composite half bright field/half fluorescence image for a prior DEP separation of 10 μ m polystyrene particles and 40nm red fluorescent nanoparticles carried out in 1x TBE buffer. The 10 μ m particles are isolated into the low-field regions, and 40nm red fluorescent nanoparticles are concentrated into the high-field regions. Detailed procedures for high conductance (HC) DEP separations were described earlier [21-23]. The general scheme for the HC-DEP separation of nanoparticles

from whole blood (red and white cells) is shown in Figures 6.1d-f. When the DEP field is applied, the nanoparticles (red dots) concentrate into the high-field regions where they are held firmly on the microelectrodes, and blood cells move into the low-field regions between the microelectrodes where they are held less firmly (Figure 6.1e). A simple fluidic wash easily removes the blood cells while the nanoparticles remain in the high-field regions (Figure 6.1f). The highly concentrated fluorescent nanoparticles can now be easily detected.

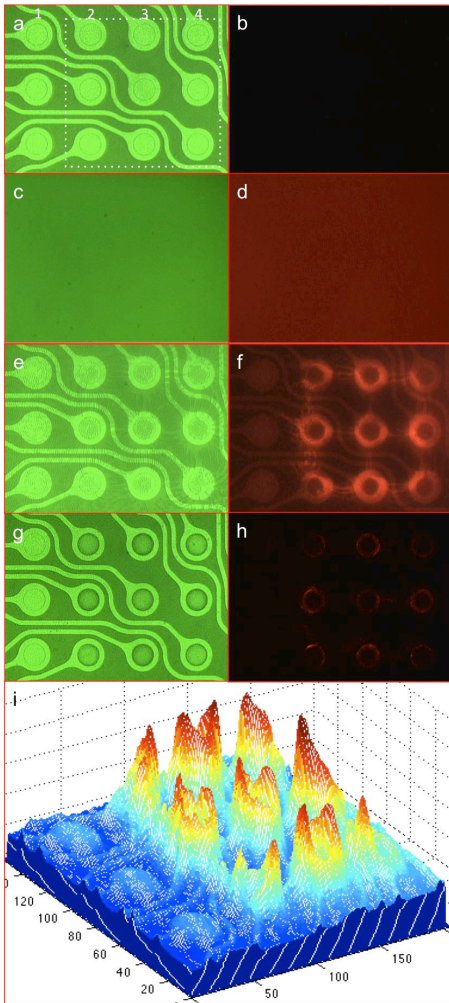


Figure 6.3. Separation and detection of 40nm red fluorescent nanoparticles in whole blood. (a, b) Show the microarray in bright field and red fluorescence before the whole blood sample was added. (c, d) Show the microarray in bright field and red fluorescence after 20 μ L of whole blood containing 300ng/ μ L of 40nm red fluorescent nanoparticles were added, but no DEP field has been applied. (e, f) Show the microarray after the DEP field was applied at 10,000 Hz and 20 volts pk-pk for 11 minutes to a set of nine microelectrodes (columns 2, 3, and 4), and the blood was removed. The bright field image shows the underlying microelectrodes with some blood cells scattered across the surface, and the red fluorescent image shows the fluorescent nanoparticles concentrated over the microelectrode structures (columns 2, 3, and 4). (g, h) Show the microarray after being washed five times with 0.5x PBS, the final bright field image shows no cells remaining on the microarray, and the fluorescent image shows red fluorescence from nanoparticles still remaining on the microelectrodes. (i) Is the 3D fluorescent intensity image after the first 0.5x PBS buffer wash showing the relative levels of fluorescence on all nine microelectrodes (produced using MATLAB).

6.2.2 Buffy Coat Blood and Whole Blood

For the HC-DEP experiments, concentrated 5x Tris Borate EDTA (TBE) buffer solution was obtained from USB Corporation (Cleveland, Ohio, USA) and diluted to 1x concentration and Dulbecco's Phosphate Buffer Saline (1x PBS) solution was obtained from Invitrogen (Carlsbad, CA, USA) and diluted to 0.5x concentration. Human Buffy Coat Blood was obtained from San Diego Blood Bank (San Diego, CA). Buffy Coat Blood contains ~1/10 the number of red blood cells as whole blood. Whole blood samples were obtained from adult female Sprague Dawley rats using proper protocols. Conductivity measurements were made with an Accumet Research AR-50 Conductivity meter using 2 cell (range: 10-2000 μ S) and 4 cell (range: 1-200 mS) electrodes. Buffer conductivities were: 1x TBE: 1.09 mS/cm; 0.5x PBS: 7.6 mS/cm; Buffy Coat Blood: 8.6 mS/cm, Whole Rat Blood: 5.2 mS/cm (nanoparticle experiments). Fluorescent polystyrene nanoparticles (FluoSpheres) with NeutrAvidin were purchased from Invitrogen (Carlsbad, CA). The nanoparticles were 0.04 μ m (40nm) in diameter and red fluorescent (ex585/em605). For human buffy coat blood experiments and rat blood experiments, 10 μ L of the 40nm red fluorescent nanoparticles were added from the stock solution to 300 μ L of either buffy coat blood or whole rat blood. For comparison purposes, the number of nanoparticles in an Abraxane dosage²⁴ was calculated by using the recommended dosage of 260mg/m² combined with an average estimated Body Surface Area of 1.92m² leading to a value of approximately 0.5g of Abraxane per dosage. Since the mean diameter of an Abraxane nanoparticle is 130nm, and estimating a density of ~1g/mL, the

number of circulating nanoparticles was calculated to be approximately 7.5×10^{10} nanoparticles per ml of blood (assuming 6 liters of blood). The red fluorescent nanoparticles were thus serially diluted to the following amounts: 9.5×10^9 , 9.5×10^{10} and 9.5×10^{11} per mL in Human Buffy Coat Blood. The microarrays were controlled using a custom made switching system that allows individual control over the voltage applied to each microelectrode. The microelectrodes were set to proper AC frequency and voltages using an Agilent 33120A Arbitrary Function Generator. AC frequencies ranged from 1000Hz to 10,000Hz, at 20 volts peak to peak (pk-pk). The DEP field was generally applied for about 10-20 minutes. The DEP separations were visualized using a JenaLumar epifluorescent microscope (red fluorescence nanoparticles Ex 585nm, Em 605nm). Both bright field and red fluorescent images were captured using an Optronics 24-bit RGB CCD camera. The image data was processed using a Canopus ADVC-55 video capture card connected to a laptop computer with Adobe Premiere Pro and Windows Movie Maker. The final fluorescence intensity data images were created by inputting fluorescent image frames of the video into MATLAB.

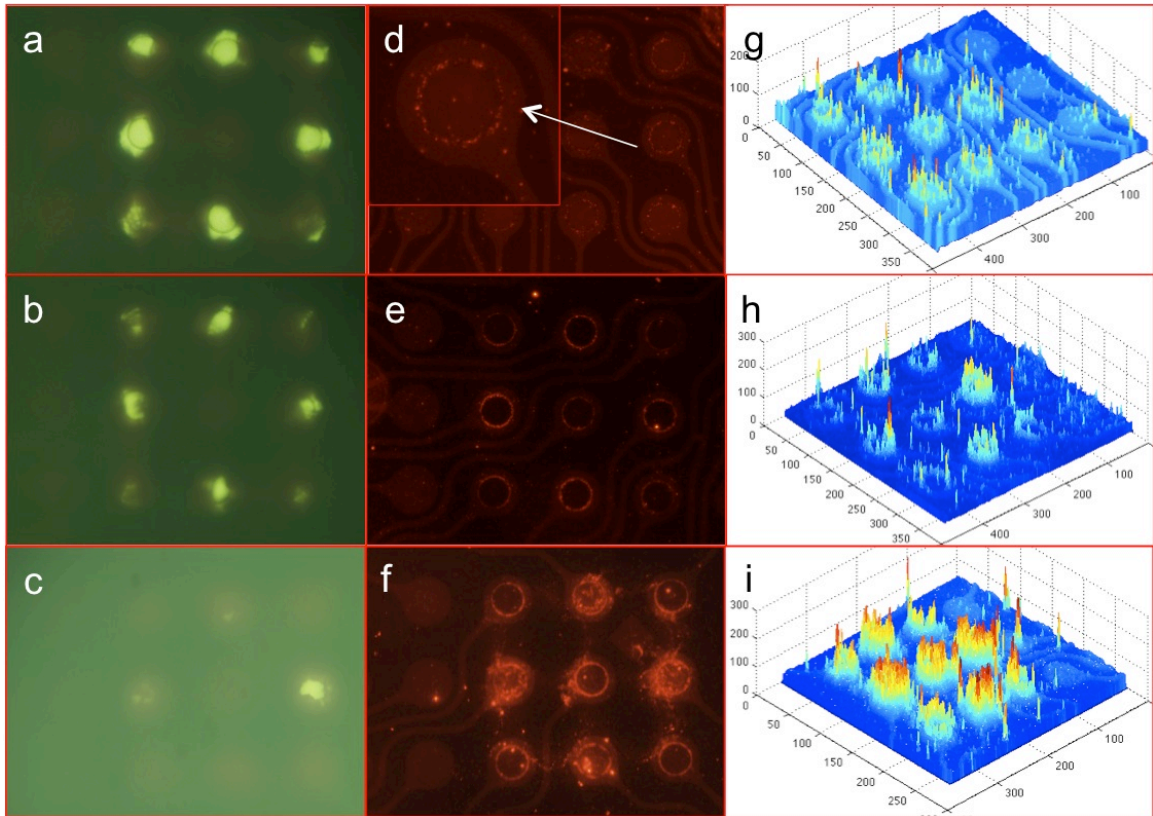


Figure 6.4. Detection levels of nanoparticles in buffy coat blood. HC-DEP was carried out at 10,000 Hz and 10 volts pk-pk for 20 minutes on samples of red fluorescent 40nm nanoparticles at 9.5×10^9 , 9.5×10^{10} and 9.5×10^{11} particles/mL made up in buffy coat blood Figure 4a, 4b and 4c show the bright field image for the three different nanoparticle concentrations at 9.5×10^9 , 9.5×10^{10} and 9.5×10^{11} particles/mL respectively, with blood cells seen moving away from the activated microelectrodes. Figures 4d, 4e and 4f show the red fluorescent images of the three different concentrations of nanoparticles after the microarray was washed with 0.5x PBS. Figure 4d, with an enlargement of one of the microelectrodes, shows nanoparticles detectable at the lowest concentration (9.5×10^9 particles/mL). Figure 4g, 4h and 4i are the 3D images showing the relative fluorescence intensity levels on the activated microelectrodes versus the un-activated microelectrodes.

6.3 Results and Discussion

The initial HC-DEP experiment demonstrates the separation and detection of 40nm red fluorescent nanoparticles in human buffy coat blood (0.86 S/m). Buffy coat blood was used in this experiment because it allows the complete DEP separation process to be observed. The DEP experiment was carried out at 10,000 Hz and 10 volts pk-pk. Figures 6.2a and 6.2b show the microarray in bright field and red fluorescence before the buffy coat blood sample was applied. Twelve microelectrodes are seen in the bright field image (Figure 6.2a), and the red fluorescence image is dark (Figure 6.2b). *All images show twelve microelectrodes, with the three control microelectrodes in column 1 not activated, and nine microelectrodes in columns 2, 3, and 4, which are activated.* Figures 6.2c and 6.2d show images of the microarray in bright field and red fluorescence after 20 μ L of buffy coat blood containing 300ng/ μ L of 40nm red fluorescent nanoparticles was added. The microelectrodes are not visible in the bright field image because of the high cell density (Figure 6.2c), but a red fluorescent background is now seen in the fluorescent image (Figure 6.2d). Figures 6.2e and 6.2f show the microarray after the DEP field has been applied for 12 minutes to the nine microelectrodes. The bright field image shows the microelectrodes becoming more visible as the blood cells move into the low-field regions (Figure 6.2e), and the fluorescent image shows the red fluorescent nanoparticles concentrating in the high-field regions around the microelectrodes (Figure 6.2f). Finally, Figures 6.2g and 6.2h show the microarray after washing with 0.5x PBS buffer to remove the blood cells. The bright field image shows the microarray is

clear of cells (Figure 6.2g), while the red fluorescent image shows intense fluorescence from the concentrated nanoparticles (Figure 6.2h). The overall time from sample application to detection was less than 30 minutes.

The second HC-DEP experiment demonstrates the separation and detection of 40nm red fluorescent nanoparticles in undiluted whole rat blood (0.52 S/m). This experiment was carried out at 10,000Hz and 10 volts pk-pk. Figures 6.3a and 6.3b show the microarray before the whole blood sample was added. Figure 6.3c and 6.3d show images of the microarray after 20 μ L of whole blood containing 300ng/ μ L of 40nm red fluorescent nanoparticles was added. The DEP field was then applied for 11 minutes. Because of the very high cell density of whole blood, the movement of cells into the low-field regions and concentration of fluorescent nanoparticles into the high-field regions was not observable (while blood cells are present). After one fluidic wash with 0.5X PBS, the bright field image shows the microelectrodes with only a few cells present (Figure 6.3e), and the red fluorescent image shows intense fluorescence from the nanoparticles concentrated around the microelectrodes (Figure 6.3f). The microarray was then washed five times with 0.5x PBS, and the final images show no cells present (Figure 6.3g), and significant red fluorescence remaining on the microelectrodes (Figure 6.3h). Figure 6.3i is a 3D fluorescent intensity image (after the first wash) showing the relative levels of fluorescence on the activated microelectrodes versus the un-activated microelectrodes. The overall time from sample application to detection was less than 30 minutes.

HC-DEP experiments were now carried out in-order to determine if nanoparticles could be detected in blood at the basic dosage range used for present drug delivery nanoparticles. By way of example, the dosage for Abraxane drug delivery nanoparticles is approximately 7.5×10^{10} particles/mL blood [24]. Red fluorescent 40nm nanoparticles at 9.5×10^9 , 9.5×10^{10} and 9.5×10^{11} particles/mL were made up in buffy coat blood, and HC-DEP was carried out at 10,000 Hz and 10 volts pk-pk for 20 minutes. Figure 6.4a, 6.4b and 6.4c show the bright field image for the three different concentrations of nanoparticles, where the blood cells can be seen moving away from the activated microelectrodes into the low-field regions. Figures 6.4d, 6.4e and 6.4f now show the red fluorescent images of the three different concentrations of nanoparticles after the microarray was washed with 0.5x PBS. Figure 6.4d shows the nanoparticles at the lowest concentration (9.5×10^9 particles/mL), with the enlargement of the microelectrode clearly showing fluorescence from the concentrated nanoparticles. Figure 6.4g, 6.4h and 6.4i are the 3D fluorescent intensity images showing the relative levels of fluorescence on the activated microelectrodes versus the un-activated microelectrodes. These results demonstrate the intrinsic ability of HC-DEP to detect nanoparticles in blood at dosage levels now used for drug delivery nanoparticles.

Further experiments were carried out to determine the detection levels for the red fluorescent 40nm nanoparticles in 1x TBE using dilution series of

nanoparticles, which ranged from 2.8×10^8 to 2.8×10^{10} particles/mL. HC-DEP was carried out at 10,000 Hz and 10 volts pk-pk for 15 minutes. The results are presented in Figure 6.5a (graph) and show that the nanoparticles can be detected down to the 2.8×10^8 particles/mL level. Because only a $1 \mu\text{L}$ volume of solution is actually being affected by the DEP field (on nine microelectrodes), the true number of nanoparticles being detected on each microelectrode is $<3 \times 10^5$ particles per microelectrode. A final experiment was now carried out to verify by Scanning Electron Microscopy (SEM) that the 40nm nanoparticles are truly being deposited into the high-field regions on the microelectrodes. For these experiments a microelectrode array without a hydrogel layer was used. Figure 6.5d shows a red fluorescent image of one the microelectrodes before the DEP field is applied. Figure 6.5e shows an image of the microelectrode after the DEP field was applied at 10,000Hz and 10 volts pk-pk for 4 minutes. Red fluorescence can be clearly seen concentrated around and on the microelectrode. Finally, figure 6.5f shows the SEM image of the same microelectrode with clusters of the 40nm nanoparticles clearly visible. In previous work, we had shown similar SEM results for HC-DEP using 200nm nanoparticles [23].

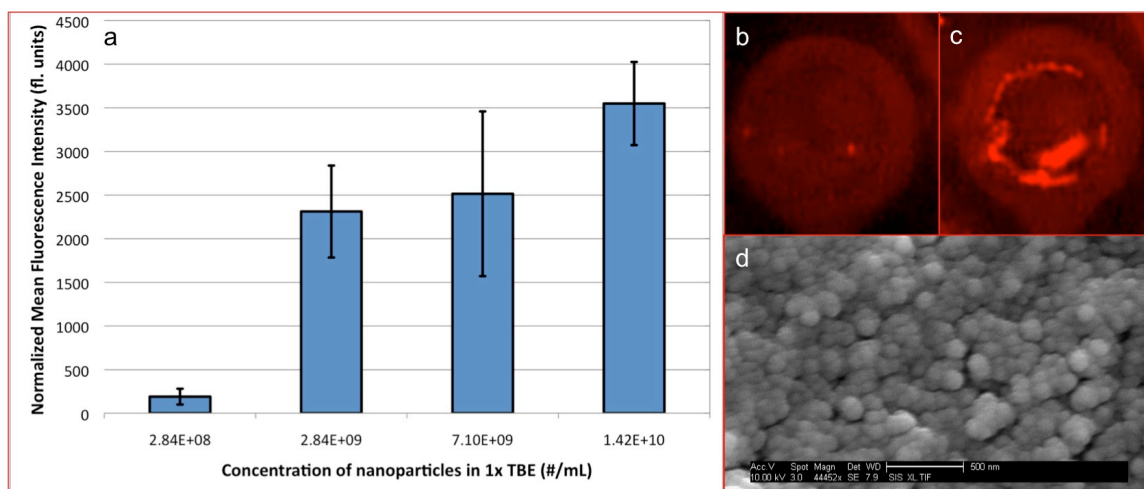


Figure 6.5. Detection levels for the red fluorescent 40nm nanoparticles in 1x TBE buffer. Figure 5a graph shows results for a dilution series of nanoparticles, which ranged from 2.8×10^8 to 2.8×10^{10} particles/mL. HC-DEP was carried out at 10,000 Hz and 10 volts pk-pk for 20 minutes. Nanoparticles could be detected down to the 2.8×10^8 particles/mL level. Figure 5b-d shows fluorescent images (5b,c) and an SEM image (5d) image of 40nm nanoparticles in 1x PBS buffer deposited in the DEP high-field region and on the microelectrode. Figure 5d shows a red fluorescent image of microelectrode before the DEP field is applied, and Figure 5c shows an image of the microelectrode after the DEP field was applied at 10,000Hz and 10 volts pk-pk for 4 minutes. Figure 5d is the SEM image of the microelectrode with clusters of the 40nm nanoparticles clearly visible.

6.4 Conclusions

The ability to rapidly detect and monitor the concentration of drug delivery nanoparticles will be important for future nanomedicine applications. We have now been able to demonstrate the rapid isolation and detection of 40nm nanoparticles from whole blood and buffy coat blood at clinically relevant levels, $\sim 9 \times 10^9$ particles/mL. Further studies in buffer show that even lower detection limits can easily be achieved, 2.8×10^8 particles/mL. The fact that the isolation of nanoparticles can be carried out directly in whole blood, with no sample processing, means that HC-DEP holds considerable promise for being a viable and cost effective method for point of care applications. At the AC frequencies being used (5000-10,000kHz), HC-DEP provides a powerful nanoscopic tool that will allow a variety of important nanoscale entities in the 10nm to 500nm range to be manipulated and isolated relative to larger cells (red and white blood cells) and numerous smaller proteins and metabolic biomolecules. In addition to having high conductance (0.5-0.9 S/m) [25-26], whole blood is also one of the most complex of biological samples. Other important nanoscale entities that could be isolated using HC-DEP include: nanoparticle imaging agents, virus, prions, chylomicrons, large antibody and immunoglobulin complexes, and other cellular nanoparticulate biomarkers (nuclei, mitochondria, ribosomes, lysosomes and various storage vacuoles). It should also be kept in mind that at higher AC frequencies ($>10,000$ Hz) DEP has the intrinsic ability for the higher resolution separation of different nanoparticles based on their AC cross-over frequency and dielectric properties [27-30]. A final advantage for HC-DEP is the fact that the

entities being isolated do not have to be labeled. The ability to post-label a specific biomarker or analyte will prove to be a significant advantage for future drug monitoring and diagnostic applications. Thus, numerous molecular biological detection techniques including PCR, immunochemistry, specific fluorescent dyes and in-situ hybridization can be easily carried out in the same sample chamber. Overall the results of this study have shown that HC-DEP has enormous potential for a number of new “seamless” sample to answer nanomedicine applications.

Chapter 6, in full, is currently being prepared for submission for publication of the material: Krishnan R, Marciniak JY, Sonnenberg AV, Carson DA, Esener SC, Heller MJ. Separation of nanoparticles directly from blood for Nanomedicine Applications. The dissertation author was the primary investigator and author of this paper.

Chapter 7: OVERALL CONCLUSIONS AND FUTURE WORK

During the dissertation research effort, a novel DEP technique for separation of nanoparticles and hmw-DNA (~5nm to 500nm in diameter) from microspheres & cells under high conductance conditions was identified. Further separation of 40nm and 200nm nanoparticles from undiluted whole blood, buffy coat blood and plasma was also tested and proven to work. Once this was accomplished, Separation of spiked ss- and ds-hmw-DNA from undiluted whole blood, buffy coat blood and plasma was also proven using the DEP technique. After this, 50+ CLL whole blood samples were tested versus normal samples and high levels of SYBR green stained DNA were detected. At the same time, lower levels of SYBR green stained DNA were detected during tests in CLL, pancreatic and ovarian cancer patient plasma and serum samples. The technique was also used to isolate hmw-DNA and post-staining it with fluorescent dye. However, the technique was shown not to affect lmw DNA (<100bp). Finally, the technique was shown to separate out mitochondria, large antibody complexes (PE-IgG-IgG-F-IgG), bacteriophage and Cancer cells using pH imbalance.

Future study on this technique will involve further testing for cfc-DNA /RNA from CLL, pancreatic and ovarian cancer patient whole blood samples. It will also be important to ID and verify nature of cfc-DNA/RNA and other cellular nanoparticulates nanoparticulates (nuclei, mitochondria, endoplasmic reticulum, lysosomes, vesicles, etc.) isolated from CLL and other blood samples.

REFERENCES

References are broken up by Chapter.

Chapter 1:

- [1] Tong Y-K, Lo YMD. *Clinica Chimica Acta* 2006, 363:187-196
- [2] Bao WH, Dalferes ER, Srinivasan SR, Webber LS, Berenson GS. *Preventive Medicine* 1993, 22(6): 825-837
- [3] Szenajch J, Jasiński B, Synowiec A, Kulik J, Chomicka M, Struzyna J et al. *Clin. Chem.* 2003, 49: 1450-1457
- [4] Wang, B, Huang H, Chen Y, Bristow R, Kassaei K, Cheng C, Roden R, Sokoll L, Chan D, Shih I. *Cancer Research* 2003, 63: 3966-3968.
- [5] Schwarzenbach H, Muller V, Stahmann N, Pantel K. *Annals of NY Academy of Sciences* 2004, 1022: 25-32.
- [6] Wong I, Lo YM, Johnson P. *Annals of NY Academy of Sciences* 2001, 945: 36-50.
- [7] Su Y, Wang M, Brenner D, Ng A, Melkonyan H, Umansky S, Syngal S, Block T. *Jrnl of Molecular Diagnostics* 2004, 6(2): 101-107.
- [8] Herrera L, Raja S, Gooding W, El-Hefnawy T, Kelly L, Luketich J, Godfrey T. *Clinical Chemistry* 2005, 51(1): 113-118.
- [9] Gingeras T, Higuchi R, Kricka L, Lo YM, Wittwer C. *Clinical Chemistry* 2005, 51(3): 661-671.
- [10] Gilbey AM, Burnett D, Coleman RE, Holen I. *Jrnl Clinical Pathology* 2004, 57: 903-911.
- [11] Chang H, Lee S, Goodman S, Singer G, Cho S, Sokoll L, Montz F, Roden R, Zhang Z, Chan D, Kurman R, Shih I. *Jrnl of the Natl Cancer Institute* 2002, 94(22): 1697-1703.
- [12] Holdenrieder S, Stieber P, Chan L, Geiger S, Kremer A, Nagel D, Lo YM. *Clinical Chemistry* 2005, 51(8): 1544-1546.

- [13] Jahr S, Hentze H, Englisch S, Hardt D, Fackelmayer F, Hesch R, Knippers R. *Cancer Research* 2001, 61: 1659-1665.
- [14] Huang P, Robertson LE, Wright S, Plunkett W. *Clinical Cancer Research* 1995, 1: 1005-1013.
- [15] Higuchi Y. *Biochemical Pharmacology* 2003, 66: 1527-1535.
- [16] Higuchi Y, Matsukawa S. *Free radical biology & medicine* 1997, 23: 90-99.
- [17] Hannun, Y. *Jrnl of Amer. Soc. of Hematology* 1997, 89(6) 1845-1853.
- [18] Chan KC, Zhang J, Chan A, Lei K, Leung S, Chan L, Chow K, Lo YM. *Cancer Research* 2003, 63: 2028-2032.
- [19] Wong T, Kwong D, Sham J, Wei W, Kwong Y, Yuen A. *Clinical Cancer Research* 2004, 10: 2401-2406.
- [20] Cheng J et al. *Nature Biotechnology* 1998, 16: 541-546
- [21] Cheng J et al. *Analytical Chemistry* 1998, 70(11): 2321-2326
- [22] Huang Y, Ewalt KL, Tirado M, Haigis R, Forster A, Ackley D, Heller MJ, O'Connell JP, Krihak M. *Analytical Chemistry* 2001, (73):1549-59.
- [23] Huang Y, Joo S, Duhon M, Heller MJ, Wallace B, Xu X. *Analytical Chemistry* 2002, 74: 3362-71.
- [24] Krishnan R, Sullivan BD, Mifflin RL, Esener SC, Heller MJ. *Electrophoresis* 2008, 29(9): 1765-1774.
- [25] Krishnan R, Heller MJ. *J. Biophoton.* 2009, 2(4): 253-261.
- [26] Krishnan R, Dehlinger DA, Gemmen GJ, Mifflin RL, Esener SC, Heller MJ. *Electrochem. Comm.* 2009, 11(8): 1661-1666.
- [27] Holzel R, Calander N, Chiragwandi Z, Willander M, Bier FF. *Phys. Rev. Lett.* 2005, 95: 128102.
- [28] Kadaksham AT, Singh P, Aubry N. *Electrophoresis* 2004, 25: 3625-3632.
- [29] Hirsch et al. *Blood* 1950, 5(11): 1017-1035.

- [30] Washizu M, Kurosawa O, Arai I, Suzuki S, Shimamoto N. *Industry Applications, IEEE Transactions on* 1995, 31: 447-456
- [31] Asbury CL, Van Den Engh G. *Biophys J.* 1998, 74: 1024-1030.
- [32] Asbury CL, Diercks AH, Van Den Engh G. *Electrophoresis* 2002, 23: 2658-2666
- [33] Ramos A, Morgan H, Green NG, Castellanos A. *J. Phys. D: Appl. Phys.* 1998, 31: 2338–2353
- [34] Rustin GJ, Nelstrop AE, McClean P. et al. *J. Clin. Oncol.* 1996, 14(5): 1545–51
- [35] Kelly WK, Scher HI, Mazumdar M, Vlamis V, Schwartz M, and Fossa SD. *J. Clin. Oncol.* 1993, 11(4): 607–15.
- [36] Baselga J, Tripathy D, Mendelsohn J. et al. *J. Clin. Oncol.* 1996, 14: 737-44.
- [37] Sozzi G, Conte D, Mariani L, Vullo SL, Roz L, Lombardo C, Pierotti MA, Tavecchio L. *Cancer Res.* 2001, 61: 4675-4678
- [38] Board RE, Knight L, Greystoke A, Blackhall, FH, Hughes A, Dive C, Ranson M. *Biomarker Insights* 2007, 2:307-319
- [39] Diehl F, Li M, Dressman D. et al. *Proc. Natl. Acad. Sci. U.S.A* 2005, 102(45):16368–73.
- [40] Maebo A. *Nihon Kyobu Shikkan Gakkai Zasshi* 1990, 28(8):1085–91.
- [41] Wu TL, Zhang D, Chia J, Tsao K, Sun C, Wu J. *Clin Chim Acta.* 2002, 321(1-2): 77-87.
- [42] Gormally E, Caboux E, Vineis P, Hainaut P. *Mutation Research/Reviews in Mutation Research* 2007, 635: 105-117.
- [43] Jen J, Wu L, Sidransky D. *Ann. N.Y. Acad. Sci.* 2000, 906: 8–12.
- [44] Stroun M, Anker P, Lyautey J, et al. *Eur J Cancer Clin Oncol* 1987, 23:707–712

Chapter 2:

- [1] Kraeft S-K, Sutherland R, Gravelin L, Hu G-H et al. *Clin. Cancer Res.* 2000, 6: 434-442.
- [2] Guiver M, Borrow R, Marsh J, Gray SJ et al. *FEMS Immunol. Med. Mic.* 2000, 28: 173–179.
- [3] Kramvis A, Bukofzer S, Kew MC. *J Clin Microbiol.* 1996, 34: 2731–2733.
- [4] Lacroix J, Becker HD, Woerner SM, Rittgen W. et al. *Int. J. Cancer* 2001, 92: 1-8.
- [5] Tong Y-K, Lo YMD. *Clinica Chimica Acta.* 2006, 363: 187-196.
- [6] Mu L, Feng SS, *J. Control. Release* 2003, 86: 33-48.
- [7] Liu RH, Yang J, Lenigk R, Bonanno J, Grodzinski, P. *Anal. Chem.* 2004, 76: 1824 – 1831.
- [8] Heller MJ, in: Heller MJ, Guttman A. (Eds.), *Integrated Microfabricated Biodevices*, Marcel Dekker, New York 2002, pp. 223-269.
- [9] Becker FF, Wang X-B, Huang Y, Pethig R et al. *J. Phys. D: Appl. Phys.* 1994, 27L 2659-2662.
- [10] Becker FF, Wang X-B, Huang Y, Pethig R et al. *Proc. Nat. Acad. Sci. U.S.A.* 1995, 92: 860-864.
- [11] Stephens M, Talary MS, Pethig R, Burnett AK, Mills KI, *Bone Marrow Transpl.* 1996, 18: 777-782.
- [12] Washizu M, Kurosawa O. *IEEE T. Ind. Appl.* 1990, 26: 1165-1172.
- [13] Washizu, M, Kurosawa O. Arai I, Suzuki S, Shimamoto N. *IEEE T. Ind. Appl.* 1995, 31: 447-456.
- [14] Asbury CL, Van Den Engh G, *Biophys J.* 1998, 74: 1024-1030.
- [15] Asbury CL, Diercks AH, Van Den Engh G, *Electrophoresis.* 2002, 23: 2658 – 2666.
- [16] Holzel R, Calander N, Chiragwandi Z, Willander M, Bier FF, *Phys. Rev. Lett.* 2005, 95: 128102 1-4.

- [17] Ramos A, Morgan H, Green NG, Castellanos A., J. Phys. D: Appl. Phys. 1998, 31: 2338–2353.
- [18] Green NG, Ramos A, Morgan H. J. Phys. D: Appl. Phys. 2000, 33: 632-641.
- [19] Hughes MP, in: Goodard WA, Brenner DW, Lyshevski SE, Iafrate GJ (Eds.), Handbook of Nanoscience, Engineering, and Technology, Second Edition, 2nd edition., CRC Press , Florida 2007, pp. 16-1 to 16-32.
- [20] Hirsch FG, Texter EC, Wood LA, Ballard WC et al., Blood 1950, 5: 1017-1035.
- [21] Higuchi Y, Biochem Pharmacol. 2003, 66: 1527-1535.
- [22] Ziegler A, Zangemeister-Wittke U, Stahel RA. Cancer Treat Rev. 2002, 5: 255-271.
- [23] Wu TL, Zhang D, Chia JH, Tsao KH et al., Clin Chim Acta. 2002, 21: 77-87.
- [24] Higuchi Y, Matsukawa S. Free Radical Bio. Med. 1997, 23: 90–99.
- [25] Gautschi O, Bigosch C, Huegli B, Jermann M et al. J Clin Oncol. 2004, 22: 4157-4164.
- [26] Stroun M, Anker P, Lyautey J, et al. Eur J Cancer Clin Oncol 1987, 23:707–712
- [27] Cheng J et al. Nature Biotechnology 1998, 16: 541-546
- [28] Green NG, Morgan H. J. Phys. D: Appl. Phys. 1997, 30: L41-L44.
- [29] Gascoyne PRC, Vykoukal J. Electrophoresis 2002, 23: 1973-1983.
- [30] Cheng J et al. Analytical Chemistry 1998, 70(11): 2321-2326
- [31] Morgan H, Hughes MP, Green NG, Biophys J. 1999, 77: 516–525.
- [32] Ermolina I, Morgan H, J. Colloid Interf. Sci. 2005, 285: 419-428.
- [33] Ermolina I, Milner J, Morgan H, Electrophoresis. 2006, 27: 3939-3948.
- [34] Hughes, MP, J. Colloid Interf. Sci. 2002, 250: 291-294.

Chapter 3:

- [1] Kraeft S-K, Sutherland R, Gravelin L, Hu G-H et al. *Clin. Cancer Res.* 2000, 6: 434-442.
- [2] Guiver M, Borrow R, Marsh J, Gray SJ et al. *FEMS Immunol. Med. Mic.* 2000, 28: 173–179.
- [3] Kramvis A, Bukofzer S, Kew MC. *J Clin Microbiol.* 1996, 34: 2731–2733.
- [4] Lacroix J, Becker HD, Woerner SM, Rittgen W. et al. *Int. J. Cancer* 2001, 92: 1-8.
- [5] Tong Y-K, Lo YMD. *Clinica Chimica Acta.* 2006, 363: 187-196.
- [6] Mu L, Feng SS, *J. Control. Release* 2003, 86: 33-48.
- [7] Liu RH, Yang J, Lenigk R, Bonanno J, Grodzinski, P. *Anal. Chem.* 2004, 76: 1824 – 1831.
- [8] Heller MJ, in: Heller MJ, Guttman A. (Eds.), *Integrated Microfabricated Biodevices*, Marcel Dekker, New York 2002, pp. 223-269.
- [9] Becker FF, Wang X-B, Huang Y, Pethig R et al. *J. Phys. D: Appl. Phys.* 1994, 27L 2659-2662.
- [10] Becker FF, Wang X-B, Huang Y, Pethig R et al. *Proc. Nat. Acad. Sci. U.S.A.* 1995, 92: 860-864.
- [11] Stephens M, Talary MS, Pethig R, Burnett AK, Mills KI, *Bone Marrow Transpl.* 1996, 18: 777-782.
- [12] Washizu M, Kurosawa O. *IEEE T. Ind. Appl.* 1990, 26: 1165-1172.
- [13] Washizu, M, Kurosawa O. Arai I, Suzuki S, Shimamoto N. *IEEE T. Ind. Appl.* 1995, 31: 447-456.
- [14] Asbury CL, Van Den Engh G, *Biophys J.* 1998, 74: 1024-1030.
- [15] Asbury CL, Diercks AH, Van Den Engh G, *Electrophoresis.* 2002, 23: 2658 – 2666.

- [16] Holzel R, Calander N, Chiragwandi Z, Willander M, Bier FF, Phys. Rev. Lett. 2005, 95: 128102 1-4.
- [17] Ramos A, Morgan H, Green NG, Castellanos A., J. Phys. D: Appl. Phys. 1998, 31: 2338–2353.
- [18] Green NG, Ramos A, Morgan H. J. Phys. D: Appl. Phys. 2000, 33: 632-641.
- [19] Hughes MP, in: Goodard WA, Brenner DW, Lyshevski SE, Iafrate GJ (Eds.), Handbook of Nanoscience, Engineering, and Technology, Second Edition, 2nd edition., CRC Press , Florida 2007, pp. 16-1 to 16-32.
- [20] Hirsch FG, Texter EC, Wood LA, Ballard WC et al., Blood 1950, 5: 1017-1035.
- [21] Higuchi Y, Biochem Pharmacol. 2003, 66: 1527-1535.
- [22] Ziegler A, Zangemeister-Wittke U, Stahel RA. Cancer Treat Rev. 2002, 5: 255-271.
- [23] Wu TL, Zhang D, Chia JH, Tsao KH et al., Clin Chim Acta. 2002, 21: 77-87.
- [24] Higuchi Y, Matsukawa S. Free Radical Bio. Med. 1997, 23: 90–99.
- [25] Gautschi O, Bigosch C, Huegli B, Jermann M et al. J Clin Oncol. 2004, 22: 4157-4164.
- [26] Stroun M, Anker P, Lyautey J, et al. Eur J Cancer Clin Oncol 1987, 23:707–712
- [27] Krishnan R, Sullivan BD, Mifflin RL, Esener SC, Heller MJ. Electrophoresis 2008, 29(9): 1765-1774.
- [28] Cheng J et al. Nature Biotechnology 1998, 16: 541-546

Chapter 4:

- [1] Becker FF, Wang X-B, Huang Y, Pethig R et al. J. Phys. D: Appl. Phys. 1994, 27L: 2659-2662.
- [2] Huang Y, Joo S, Duhon M, Heller M, Wallace B, Xu X. Anal. Chem. 2002, 74: 3362.
- [3] Akin D, Li H, Bashir R. Nano Lett. 2004, 4: 257.
- [4] Washizu, M, Kurosawa O. Arai I, Suzuki S, Shimamoto N. IEEE T. Ind. Appl. 1995, 31: 447-456.
- [5] Asbury CL, Diercks AH, Van Den Engh G, Electrophoresis. 2002, 23: 2658 – 2666.
- [6] Holzel R, Calander N, Chiragwandi Z, Willander M, Bier FF, Phys. Rev. Lett. 2005, 95: 128102 1-4.
- [7] Green NG, Morgan H. J. Phys. Chem. B. 1999, 103: 41
- [8] Cheng J et al. Analytical Chemistry 1998, 70(11): 2321-2326
- [9] Cheng J et al. Nature Biotechnology 1998, 16: 541-546
- [10] Ermolina I, Morgan H, J. Colloid Interf. Sci. 2005, 285: 419-428.
- [11] Ermolina I, Milner J, Morgan H, Electrophoresis. 2006, 27: 3939-3948.
- [12] Green NG, Morgan H. J. Phys. D: Appl. Phys. 1997, 30: L41-L44.
- [13] Hughes MP, in: Goodard WA, Brenner DW, Lyshevski SE, Iafrate GJ (Eds.), Handbook of Nanoscience, Engineering, and Technology, Second Edition, 2nd edition., CRC Press , Florida 2007, pp. 16-1 to 16-32.
- [14] Krishnan R, Sullivan BD, Mifflin RL, Esener SC, Heller MJ. Electrophoresis 2008, 29(9): 1765-1774.
- [15] Krishnan R, Heller MJ, J. Biophotonics 2009, 2: 253-261

Chapter 5:

- [1] Editorial, Nat. Nanotechnol., 2007, 2: 451

- [2] Nishiyama N, Nat Nanotechnol., 2007, 2: 203-204
- [3] Ferrari M, Nat. Rev. Cancer, 2005, 5: 161–171
- [4] Sozzi G, Conte D, Leon M, Cirincione R, Roz L. et al. J. Clin. Oncol., 2003, 21: 3902-3908
- [5] Board RE, Knight L, Greystoke A, Blackhall, FH, Hughes A, Dive C, Ranson M. Biomarker Insights 2007, 2:307-319
- [6] Gautschi O, Bigosch C, Huegli B, Jermann M et al. J Clin Oncol. 2004, 22: 4157-4164.
- [7] Wu TL, Zhang D, Chia J, Tsao K, Sun C, Wu J. Clin Chim Acta. 2002, 321(1-2): 77-87.
- [8] Gormally E, Caboux E, Vineis P, Hainaut P. Mutation Research/Reviews in Mutation Research 2007, 635: 105-117.
- [9] Jen J, Wu L, Sidransky D. Ann. N.Y. Acad. Sci. 2000, 906: 8–12.
- [10] Sozzi G, Conte D, Mariani L, Vullo SL, Roz L, Lombardo C, Pierotti MA, Tavecchio L. Cancer Res. 2001, 61: 4675-4678
- [11] Diehl F, Li M, Dressman D. et al. Proc. Natl. Acad. Sci. U.S.A 2005, 102(45):16368–73.
- [12] Stroun M, Anker P, Lyautey J, et al. Eur J Cancer Clin Oncol 1987, 23:707–712
- [13] Duncan R, Nat. Rev. Drug Discov. 2003, 2: 347–360
- [14] Nishiyama N, Kataoka K. Pharmacol. Therapeut. 2006, 112: 630–648
- [15] Mu L, Feng SS. J. Control. Release, 2003, 86: 33-48
- [16] Albrecht DR, Underhill GH, Wassermann TB, Sah RL, Bhatia SN, Nat. Methods 2006, 3: 369-375
- [17] Becker FF, Wang X-B, Huang Y, Pethig R et al. Proc. Nat. Acad. Sci. U.S.A. 1995, 92: 860-864.
- [18] Stephens M, Talarly MS, Pethig R, Burnett AK, Mills KI, Bone Marrow Transpl. 1996, 18: 777-782.

- [19] Asbury CL, Van Den Engh G, Biophys J. 1998, 74: 1024-1030.
- [20] Ramos A, Morgan H, Green NG, Castellanos A., J. Phys. D: Appl. Phys. 1998, 31: 2338–2353.
- [21] Hughes MP, in: Goodard WA, Brenner DW, Lyshevski SE, Iafrate GJ (Eds.), Handbook of Nanoscience, Engineering, and Technology, Second Edition, 2nd edition., CRC Press , Florida 2007, pp. 16-1 to 16-32.
- [22] Cheng J et al. Nature Biotechnology 1998, 16: 541-546
- [23] Cheng J et al. Analytical Chemistry 1998, 70(11): 2321-2326
- [24] Krishnan R, Sullivan BD, Mifflin RL, Esener SC, Heller MJ. Electrophoresis 2008, 29(9): 1765-1774.
- [25] Krishnan R, Heller MJ, J. Biophotonics 2009, 2: 253-261
- [26] Krishnan R, Dehlinger DA, Gemmen GJ, Mifflin RL, Esener SC, Heller MJ. Electrochem. Comm., 2009, 11: 1661-1666
- [27] Ermolina I, Milner J, Morgan H, Electrophoresis. 2006, 27: 3939-3948.
- [28] Green NG, Ramos A, Morgan H. J. Phys. D: Appl. Phys. 2000, 33: 632-641.
- [29] Cui L, Holmes D, Morgan H, Electrophoresis, 2001, 22: 3893-3901
- [30] Morgan H, Hughes MP, Green NG, Biophys J. 1999, 77: 516–525.
- [31] Hirsch et al. Blood 1950, 5(11): 1017-1035.
- [32] Visser KR. Med. & Biol. Eng. & Comput. 1992, 30: 636-640

Chapter 6:

- [1] Editorial, Nat. Nanotechnol., 2007, 2: 451
- [2] Nishiyama N, Nat Nanotechnol., 2007, 2: 203-204
- [3] Ferrari M, Nat. Rev. Cancer, 2005, 5: 161–171

- [4] Mu L, Feng SS. *J. Control. Release*, 2003, 86: 33-48
- [5] Sinha R, Kim GJ, Nie Shuming, Shin DM. *Mol. Cancer Ther.* 2006, 5: 1909-1917.
- [6] Duncan, R. *Nat. Rev. Drug Discov.* 2003, 2: 347–360.
- [7] Nishiyama N, Kataoka K. *Pharmacol. Therapeut.* 2006, 112: 630–648
- [8] Nasongkla N, et al. *Nano Letters*, 2006, 6: 2427-2430.
- [9] Sozzi G, Conte D, Leon M, Cirincione R, Roz L. et al. *J. Clin. Oncol.*, 2003, 21: 3902-3908
- [10] Board RE, Knight L, Greystoke A, Blackhall, FH, Hughes A, Dive C, Ranson M. *Biomarker Insights* 2007, 2:307-319
- [11] Gautschi O, Bigosch C, Huegli B, Jermann M et al. *J Clin Oncol.* 2004, 22: 4157-4164.
- [12] Albrecht DR, Underhill GH, Wassermann TB, Sah RL, Bhatia SN, *Nat. Methods* 2006, 3: 369-375
- [13] Becker FF, Wang X-B, Huang Y, Pethig R et al. *Proc. Nat. Acad. Sci. U.S.A.* 1995, 92: 860-864.
- [14] Akin D, Li H, Bashir R, *Nano Lett.* 2004, 4: 257-259
- [15] Asokan SB, Jawerth L, Carroll RL, Cheney RE, Washburn S, Superfine R, *Nano Lett.* 2003, 3, 431-437
- [16] Vijayaraghavan A et al. *Nano Lett.* 2007, 7: 1556-1560
- [17] Tuukkanen S. et al. *Nano Lett.* 2006, 6: 1339-1343
- [18] Ramos A, Morgan H, Green NG, Castellanos A. *J. Phys. D: Appl. Phys.* 1998, 31: 2338–2353
- [19] Hughes MP, in: Goodard WA, Brenner DW, Lyshevski SE, Iafrate GJ (Eds.), *Handbook of Nanoscience, Engineering, and Technology*, Second Edition, 2nd edition., CRC Press , Florida 2007, pp. 16-1 to 16-32.
- [20] Cheng J et al. *Nature Biotechnology* 1998, 16: 541-546
- [21] Krishnan R, Sullivan BD, Mifflin RL, Esener SC, Heller MJ. *Electrophoresis* 2008, 29(9): 1765-1774.

- [22] Krishnan R, Heller MJ, J. Biophotonics 2009, 2: 253-261
- [23] Krishnan R, Dehlinger DA, Gemmen GJ, Mifflin RL, Esener SC, Heller MJ. Electrochem. Comm., 2009, 11: 1661-1666
- [24] Green MR et al. Ann. Oncol. 2006, 17: 1263-1268
- [25] Hirsch et al. Blood 1950, 5(11): 1017-1035.
- [26] Visser KR. Med. & Biol. Eng. & Comput. 1992, 30: 636-640
- [27] Ermolina I, Milner J, Morgan H, Electrophoresis. 2006, 27: 3939-3948.
- [28] Green NG, Ramos A, Morgan H. J. Phys. D: Appl. Phys. 2000, 33: 632-641.
- [29] Cui L, Holmes D, Morgan H, Electrophoresis, 2001, 22: 3893-3901
- [30] Morgan H, Hughes MP, Green NG, Biophys J. 1999, 77: 516–525.